Jadeitite from Guatemala: New observations and distinctions among multiple occurrences

George E. Harlow[1], Virginia B. Sisson[2], Sorena S. Sorensen[3]
1. Department of Earth and Planetary Sciences, American Museum of Natural History New York, New York, USA;
2. Department of Earth and Atmospheric Sciences, University of Houston, Houston, TX, USA
3. Department of Mineral Sciences, Smithsonian Institution, Washington, DC, USA

gharlow@amnh.org, j_sisson@netzero.net, sorensen@si.edu

Abstract:

In Guatemala, jadeitite occurs as blocks in serpentinite mélange in distinct settings on opposite sides the Motagua fault, the current North American – Caribbean plate boundary. This study expands the known sources north of the fault to a zone over 200 km and describes three distinct sources south of the MF narrowly distributed in a region 11 km across.

Jadeitites north of the fault have been found associated with other high-pressure / low-temperature metamorphic rocks (eclogites, blueschists, and garnet amphibolites) in serpentinites from Saltán, Baja Verapaz to Río Hondo, Zacapa and near Rosario, Izabal. Jadeitite from all "northern" localities is generally quite similar: whitish to gray-green with rare streaks of imperial green along veins, generally coarse grained (mm to cm scale) jadeite, with common albite, white-to-tan mica(s), omphacite, and late analcime and an absence of quartz. These jadeitites are generally granoblastic with considerable Ab+Anl veining and secondary taramitic amphibole, but microcrystalline varieties with fan-spherulitic-to-felted textures can be found. Darker green jadeitite is more common with distance from the fault. Deep-green omphacitite, omphacite-taramite metabasite, albitite, albite-phengite rock, and phengite-dominant rock are commonly found with jadeitite. The complete assemblage indicates formation at 6-12 kb and 300-400°C, however Jd-Omp pairs yield T from ~200 to >500ºC for jadeite crystallization. Garnet-clinozoisite amphibolite and clinozoisite eclogite are also found in the mélange and in some cases with jadeitite; they are the highest-grade HP-LT rocks north of the MF.

The jadeitites south of the MF are sourced from three separate fault slices of serpentinite in the mountains of Jalapa and Zacapa departments and are individually distinctive:

1- Jadeitite near Carrizal Grande is found as alluvial blocks and float in serpentinite with lawsonite eclogites, variably altered to blueschist, and rare schists. Color varies from medium to dark green with late veins of dark-green and/or blue omphacite and translucency surpasses most northern jadeitite. Phengitic muscovite is common, followed by titanite, lawsonite, apatite, quartz, garnet, zircon with rare albite and analcime in late veins and intergranular space. Jadeite grain size is medium to fine (submillimeter), alteration is minor. A larger Jd – Omp gap and lawsonite also suggests T = 300-400, but at high P as indicated by Qtz: P > 12-20+ kbar. Lawsonite eclogites (P = 20-25 kbar, T = 350-450°C) occur with these jadeitites. Likewise in these jadeitites, Jd-Omp pairs yield T from ~200 to ~500ºC for jadeite crystallization.

2- La Ceiba jadeitites are moderate to intense dark green, occasionally lavender to whitish, with late-stage veins of quartz, diopside, cymrite, actinolite, titanite and vesuvianite. A large Jd – Omp gap suggests 300-400°C, but at lower *P* as indicated by Qtz $\pm$ Ab: P = 10-14 kbar. These coexist with omphacite-glaucophane blueschists.

3- La Ensenada jade is whitish and opaque with small green, blue, orange, and mauve streaks and spots. It is a fine-grained jadeite-pumpellyite (Pmp) rock, intensely deformed and veined with orange grossular, omphacite and albite, and contains minor titanite but no quartz. A large Jd – Omp gap and Pmp suggests ~200-~300°C at lower *P* as indicated also by primary Ab and secondary Anl: *P* = 6-9 kbar. The silicates are very low in iron and coexist with pure clinochlore and magnetite, which suggests removal of ferrous iron from silicates by a fluid. The jadeitite occurs with lawsonite-glaucophane blueschists and chloritite.

Important results of this comparison of known jadeitite occurrences in Guatemala are 1) the higher-pressure signatures south of the MF relative to those from north of the MF, with the latter generally showing extensive albititization likely related to being formed and exhumed at different times at different conditions; 2) distinctive differences in *PT* conditions across the northern jadeitite distribution and between the three areas to the south; 3) a record of jadeite crystallization as interpreted from Jd-Omp pairs indicating initial cold (~200ºC) to hotter conditions with a recurrence of this trend in some samples; and 4) a textural uniformity arguing against metasomatism of a protolith but rather crystallization of jadeitite directly from an aqueous fluid.

Keywords: Jadeitite, serpentinite, mélange, HP-LT rock, subduction processes

Introduction:

The jade of the indigenous Middle American cultures of Mexico and Central America is jadeite rock – jadeitite – as well as the material from which jadeite derived its name (Foshag, 1957; Harlow *et al.* 2007). After knowledge of the sources were lost to the original inhabitants of Middle America, it was not until the early 1950s that workshop materials were discovered by Foshag and Leslie (1955) and then boulders by McBirney *et al.* (1967). These led to the eventual recognition that jadeitite was hosted in serpentinite mélanges north of the Río Motagua in central Guatemala (*e.g.*, Hammond *et al.* 1979, Harlow 1994). The river generally follows the Motagua fault zone (MFZ; this zone includes many nearby parallel and sub-parallel faults within the valley), the broad boundary between the North American and Caribbean plates. The location (north versus south) is best referenced to the active strand in the MFZ, the Motagua fault (MF), which has other names locally, such as the Cabañas fault in the central part of the valley, named for the town closest to the epicenter of the 1976 earthquake. The jadeitite-bearing region was demarked as extending between Río La Palmilla and the town of Estancia de La Virgen, a distance of about 14 km (Fig. 1) and was the only described jadeitite source in Central America prior to the year 2000. A resurgence of interest and scientific recognition of a much larger areal distribution awaited the serendipitous recognition by Russell Seitz, an investigator from a 1970s jade sourcing project, of a single piece of jade (jadeitite) at a shop in Antigua Guatemala that closely resembled blue-green Olmec jade (Seitz *et al.* 2001, Taube *et al.* 2004). This discovery combined with severe flooding caused by Hurricane Mitch in 1998, which turned over the boulder fields in drainages south of the Río Motagua, led to a resurgence of interest in jadeitite sources by the authors and others. Over a few years we were shown previously undescribed sources by Guatemalan geologists and local jade hunters (jaderos), including ones traversed by Río El Tambor (Río Jalapa in Jalapa Department) and its tributaries, south of Río Motagua. In addition to the jadeitite, largely overlooked eclogite occurrences were encountered which increased the interest and potential scientific significance among the serpentinite-hosted high-pressure / low-temperature (HP–LT) rocks of the MFZ. Commercial and artisanal exploration for jade and our own field studies over the intervening years have revealed that sources north of the fault are distributed sporadically in serpentinite over at least 110 km E-W and a smaller distribution of sources of 3 distinct clusters of jadeitite sources, within 11 km of one another. Most recently we sampled an area of jadeitites near Rosario, east of Lago Izabal, and 203 km from Saltán the most western source. Although we have mentioned some of these new sources in part in other papers (Seitz *et al.* 2001, Harlow *et al.* 2004a, 2006, 2007), here we describe these jadeitites and jade-like rocks to point out their location-distinctive appearance, mineralogy, and microtextures and inferences for origin among the HP-LT blocks in the serpentinite mélanges straddling the MFZ in Guatemala.

Geological Setting

The boundary between the North American and Caribbean plates in Guatemala is defined by the Motagua fault zone, one of three left-lateral, subparallel strike-slip fault systems: Polochíc (Polochíc–Chixoy), Motagua, and Jocotán (Jocotán–Chamelecón;(see Fig. 1). Tectonic slices of serpentinite mélange containing HP-LT rocks occur adjacent to the MF, both north (regionally the Maya block) and south (Chortís block). These blocks are distinctly different as the basement of the Chortís block contains a significant mafic component, while the Chuacús Series of the Maya block is dominantly quartzofeldspathic. Lithologies on either side of the MF, with the exception of the serpentinites and related rocks, are completely different from each other

(Francis 2005; Alvarado *et al.* 2007; Martens *et al.* 2007a; Francis *et al.* in review), suggesting simple juxtaposition of differing terranes and/or considerable displacement along the MF. The units in the Maya block to the north include the high-metamorphic-grade Chuacús Complex (McBirney 1963; van den Boom 1972; Ortega-Gutiérrez *et al.* 2004; Martens *et al.* 2007b), Paleozoic sediments of the Santa Rosa Group and deformed granites. The Chortís block south of the fault contains the greenschist-facies San Diego phyllite, the amphibolite-facies Las Ovejas complex with felsic and mafic intrusives, and large, relatively undeformed granitoids of uncertain age. There are several granitic intrusions in the Chortís block that are of Late Cretaceous and Early Tertiary age (Donnelly *et al.* 1990). The block also contains the El Tambor "ophiolite complex," recently dated on the basis of radiolaria to be of Late Jurassic age (Chiari *et al.* 2006). Both blocks are mantled with modern arc volcanics to the south and west, further complicating interpretation.

Until recently, the HP-LT belts along the MF had been assigned to a single tectonic (collisional) event in the Late Cretaceous, although all studies noted the strong lithotectonic dichotomy in these terranes (see Donnelly *et al.* 1990). North of the Motagua fault, serpentinite mélange hosts garnet amphibolite, omphacite-taramite metabasite, jadeitite, albitite, and, more recently reported, altered clinozoisite-amphibole-eclogite in the western reaches of the serpentinite mélange (Tsujimori *et al.* 2004; Brueckner 2005). These rocks span a wide range of conditions, from greenschist-blueschist at lower P (200-400°C at ≤1 GPa) to moderate LT eclogite facies of 500-600°C at ~ 2 GPa. In contrast, south of the fault assemblages include lawsonite eclogite, blueschist, and jadeitite in serpentinite matrix that record peak P-T conditions among the coldest and wettest deep subduction trajectories on Earth, to ~2.6 GPa and only ~470 ºC (Tsujimori *et al.* 2006a,b). Compounding the differences, Harlow *et al.* (2004a) reported disparate $^{40}Ar/^{39}Ar$ ages on the mica and Amp from these HP-LT rocks: north of the fault ages range between 77 and 65 Ma, whereas rocks south of the fault yield ages of 125-116 Ma. Subsequent determinations of five Sm-Nd mineral isochrons from eclogites both north and south of the fault have yielded ages of 144-126 Ma (Brueckner *et al.* 2009). The rarely recorded presence of jadeitite, lawsonite eclogite and a tectonic-timing conundrum represent only a small aspect of the complex geology exposed in central Guatemala related to the boundary region between the Maya and Chortís blocks, let alone the North American and Caribbean plates.

Jadeitite: Occurrence and Associations

The jadeitite found north of the MFZ was described by Harlow (1994), so the intent here is to present new observations and interpretations, while only summarizing the generalizations in that paper. Moreover, as jadeitite from south of the MFZ has not been described in detail and is distinctly different from jadeitite found north of the MFZ, a greater portion of the attention is devoted to these. Fundamentally, most of the jadeitite occurrences were discovered by jade hunters (jaderos in Spanish) who have shown them to us. This transfer of information has resulted in the considerable growth in areal distribution presented here. The rocks studied and abbreviations for mineral names are given in Table 1.

The jadeitite occurrences along the MFZ are all sourced within serpentinite-dominant mélange (that is mélange in which serpentinite dominates both as matrix and as broken up blocks–an abundance of mixed sedimentary and HP-LT rocks is not observed). The serpentinites consist predominantly of antigorite, with lesser lizardite (no chrysotile has been observed) with interstitial magnetite, magnesite, Chl, Tlc, pentlandite and low-T Ni-sulfides and occasional

relict Cpx, pseudomorphed orthopyroxene (bastite) or magnesiochromite (Harlow *et al.* 2006b, Bertrand and Vuagnat 1976, 1980). There are subtle differences in the mineralogy of the serpentinite, as a whole, from the north to the south sides of the MF, particularly in the relative abundance of magnesite and Tlc, but otherwise the recorded gross differences are not large (Harlow *et al.* 2006b). The protolith has so far been interpreted as dominantly harzburgite but probably ranges from dunite with rare podiform chromite through harzburgite to spinel lherzolite (Bertrand and Vuagnat 1976, 1980; Harlow *et al.* 2006b); however, further analysis is required. Serpentinization in most samples is complete (no protolithic mineral or textural relics remain) with petrofabrics varying greatly between antigorite fels to highly sheared serpentine "schists." Rare ultramafic relic phases include aluminous augite, chromite and perhaps pentlandite (Tsujimori, personal communication 2007). All features are consistent with serpentinite produced at depth, presumably adjacent to a subduction channel responsible for the HP-LT blocks.

Irrespective of location relative to the MF, jadeitite occurs in small areas, typically extending no more than a few hundred meters, commonly distributed as boulders and cobbles of a dismembered larger body sitting on (and in) serpentinite (Fig. 2). Even more commonly the jadeitite occupies drainages cutting through or down-stream from serpentinite mélange. In some cases these broken blocks are dispersed with other HP-LT lithologies along alignments, which we interpret as faults within the mélanges, or in slumped fields in serpentinite downhill from such a boundary. Boulders can measure up to 5 meters across (*e.g.*, at Quebrada Seca, about 2.5 km SE of Carrizal Grande, south of the MFZ, or Río La Palmilla, north) although meter or smaller sizes are most common. Jadeitite rarely occurs as discrete blocks or veins with contact relationships to serpentinite. Jadeitite blocks in place (although probably with tectonic contacts) are limited to La Ceiba (S.), Quebrada Seca, near Carrizal Grande (S.) and El Ciprés in the Sierra de las Minas (N.) (see Figs. 1 & 3), although the latter has been dismembered by jade extraction (Sorensen *et al.* 2005, 2010).

North of the MF: Fields of jadeitite generally occur in what appear to be distinct fault segments or along boundaries between serpentinite and Chuacús Series basement. The distribution now extends from the western-most occurrence, just south of the town of Saltán, Baja Verapaz department (14.9005° N. 90.5983° W.), to the town of Río Hondo, Zacapa department (15.0444º N. 89.5853 W.), spanning a distance of 110 km (Fig. 1). The newly-visited far-eastern source area is near Rosario, Izabal department (15.6866 N, 88.8998 W), more than 200 km from Saltán. The jadeitites share many characteristics and occur with a limited assemblage of other HP-LT rocks. Most of the jadeitite is massive and whitish to pale gray or pale green (Fig. 4a) and commonly with transecting veins of coarser jadeitite or albitite-like alteration). Blocks of white-to-mauve jadeitite (Fig. 4b) have been found in a quebrada (dry gulch) near Saltán, the western extent to date, and have a distinctive phase assemblage as well as appearance. Mostly medium green jadeitite has been recovered from near Rosario at the eastern limit of occurrences, and this material is not distinctive in terms of phase assemblage compared to the bulk of jadeitite north of the MF. The jadeitite blocks show cataclastic to sheared textures in addition to the veins. Albitization around block margins and fractures post-dating Jd-veining is common; complete replacement of jadeitite by albitite typically occurs toward the boundary of a block with serpentinite host, if contact relationships can be observed. The jadeitite-serpentinite contact zone consists of concentrically foliated blackwall mineralogy (Act + Clc ± Tlc) a few cm to perhaps a meter thick, penetrated by centimeter to decimeter wide bundles of acicular Act aligned radial to

the block. Sorensen *et al.* (2010) have described a complete contact assemblage at El Ciprés, a site in the Sierra de las Minas, documenting not only the transition from jadeitite to albitite to altered ultramafic boundary to serpentinite but also the chemical transport between and through each zone. Rocks that have the same massive appearance as jadeitite but are darker green tend to be dominated by Omp and thus are actually omphacitites. There is an intimate association of jadeitite and albitite north of the MF, which is in part due to the alteration of jadeitite to albitite, but albitite occurs as a distinct rock without apparent replacement texture (Harlow 1994). In addition, albite-phengite rocks, phengite rocks (noticeably dense from high Ba content; Harlow 1995), taramite-omphacite metabasite (Harlow and Donnelly 1989), omphacitite, and garnet-clinozoisite amphibolite or clinozoisite eclogite are commonly associated with the jadeitites. Garnet amphibolite is found only in the eastern extent (as far west as Morazán) and eclogite in the west (as far east as Quebrada de los Pescaditos). Omp inclusions in Grt of garnet amphibolite indicate that some of this lithology is retrograded eclogite. Jadeitite from north of the MF is also distinctive in its mineralogy (below).

South of the MF: Jadeitite has probably been known in this area for a considerable time by some jaderos and jade workshops in Antigua, Guatemala; however, study did not commence until our first visit in 2001. There are three distinct areas in the mountains of Jalapa and Zacapa departments with very small areal distributions, typically of one to several kilometers. They are near the towns of Carrizal Grande, La Ceiba, and La Ensenada (Figs. 1 & 3) and are all within 11 km of one another.

In the Carrizal Grande area, furthest south, the jadeitite occurs mostly as isolated blocks with ill-defined contacts to adjacent serpentinite or in the drainages of several quebradas Up-slope and up-stream limits appear to align with minor fault traces cutting subparallel to the overall serpentinite fault boundary (John Cleary, Ventana mining, personal communication, 2006; see Fig. 3). Jadeitite is generally massive and often contains conspicuous phengitic Ms or Lws phenoblasts. Color is light to medium to medium dark green with occasional dark blue-green veins colored by blue Omp (Fig. 4c; Harlow *et al.* 2004b). Coexisting lithologies include lawsonite eclogite, blueschist-altered eclogite, lawsonitite, glaucophane-omphacite rock, garnet-quartz-phengite schist, and Gph-bearing quartz-mica schist (Tsujimori *et al.* 2006a). Near La Ceiba the jadeitite is tightly confined to a 100 meter wide exposure in serpentinite (no contacts exposed) as blocks to a few meters in size. Smaller blocks litter a quebrada below this exposure. The jadeitite is generally medium to dark green, on occasion intensely green, and fine-grained to microcrystalline but highly fractured (Fig. 4d). In rare cases jadeitite blocks are encapsulated by a diopside-rich rock. Coexisting tectonic blocks in the area are omphacite-glaucophane blueschist and epidote-amphibolite. Finally, near La Ensenada in a serpentinite slice further north, in and around an E-W trending quebrada are dismembered blocks ($\leq$ 3 m across) of a whitish gray jadeitite with green, blue, orange (Grs), and mauve streaks and spots that is a fine-grained jadeite-pumpellyite rock (this material has been sold as *jade lila* or *rainbow jade*). It occurs interlayered with a pale brown chloritite (Fig. 4e), and the associated lithologies is lawsonite blueschist and a partially amphibolitized-chloritized serpentinite. A single other occurrence of this material is found ~3 km east and appears to be in the same fault slice of serpentinite.

Jadeitite: Texture and Mineralogy

Analytical Techniques

Optical and SEM/BSE petrographic and microprobe analysis of thin sections and X-ray diffraction of mineral grains were performed in this study. Electron-microprobe analysis of minerals in thin section to determine concentrations of the major constituent elements (except O) was carried out using a Cameca SX-100 microprobe at AMNH operated at 15 kV, 10 nA sample current for Na-bearing or hydrous silicates and 20 kV, 15 nA for oxides and sulfides, a point beam was used in all cases. Standards included natural minerals and synthetic compounds. The PAP correction scheme according to Pouchou & Pichoir (1991) was employed. Potential interferences between Ba (Lα) and Ti (Kα) were minimized by measuring X-ray counts on a PET crystal and background measured outside the window of both peaks; as long as concentrations are below ~2 wt% of either, there are no overlaps that exceed the detection limit. For all elements the detection limits are <0.01 wt% but "as measured" values are presented here. Examination of amphiboles and micas found no detectable F or Cl, so these elements were not analyzed. No post-processing correction was made for the effect of inferred H_2O content. Estimates of Fe^{2+} and Fe^{3+} were made using an algorithm similar in concept to that of Finger & Burt (1972) to calculate Fe^{3+} from total Fe in which cation charge must sum as close as possible to twice the number of oxygen atoms plus the number of univalent anions (*e.g.*, 6 oxygen in pyroxene), with a maximum permissible sum of cations determined by the crystal's stoichiometry (*e.g.*, four for pyroxene as above; vacancies in large cation sites are permissible– see Harlow *et al.* 2006 for more details). Particularly in the case of iron-rich amphiboles, ferric-ferrous determination by the above technique may lead to poor, particularly somewhat low, totals for the C cations. Typically these totals can be improved by readjusting the FeO-Fe_2O_3 balance; but that has not been done here because the deficiencies are relatively small.

Back-scattered electron (BSE) imaging was carried out on the microprobe and on a Hitachi S-4700 Field Emission Scanning Electron Microscope SEM. Both microprobe and SEM were equipped with either PGT-Imix (prior to April 2007) or Bruker Quantax energy-dispersive X-ray spectrometric (EDS) analyzers. X-ray diffraction identification was carried out on some powdered samples of jade using a Bragg-Brentano diffractometer or on sub-millimeter fragments and sub-millimeter areas on rock surfaces using a Rigaku DMAX/Rapid microdiffraction system employing a 100 μm monocapillary collimator and monochromatized Cu Kα radiation. Patterns were interpreted with Jade 7.0 (MDI) software; although Fe fluorescence degraded the patterns in some cases, the peaks were more than sufficient for assignment of *d* values and phase identification.

North of the MF

The macrotextures (hand samples) are generally granoblastic (grain size from 1 mm to 1 cm) made conspicuous in "monomineralic" masses by cleavage in blocky grains of Jd. Weathering greatly enhances visual aspects of texture and can accentuate areas of Ab and/or Anl from some combination of enhanced solubility and reduced hardness. Increased whiteness (light scattering) is common in the cores of grains or in grain clusters with grain rims more likely to be semitranslucent and greener. Although coarse grain size is typical, microcrystalline zones (Fig. 4f) and whole blocks are also found. Coarse-grained jadeitite is typically opaque while fine-grained material is more translucent. Shearing and brecciation is common, with cementation by both jadeitite and albitite assemblages (Harlow 1994). Veins are common but not always conspicuous because of the near-monomineralic composition and lack of obvious variance in

color and texture. However, very coarsely crystallized veins of jadeite exist, with walls dominated by Jd (crystals to ~20 cm) and central or interstitial white mica and/or green Omp or late-stage alteration infilling (albitite-like), which can be decorated by black sprays of Amp or green fingers or zones of Omp.

Microscopic textures are highly variable, but certain features can be considered typical. Clusters of both solid and 2-phase fluid inclusions are common in the cores of Jd grains that have survived deformational comminution. Omphacite, Ab, Pg, and Ttn are the most common core mineral inclusions. Moreover, in many coarse-grained jadeitites interiors of Jd grains are dense with somewhat large solid, both mono-phase and polyphase inclusions, typically Ab, Anl, Pg, and Omp (Fig. 5a), commonly connected by cleavage cracks. These solid inclusions commonly have associated fluid inclusions voids observed in surfaces by SEM/BSE as well as resolvable two-phase fluid inclusions via optical microscopy. These "lake district" interiors of Jd grains typically have irregular compositional zoning and are commonly surrounded by a cleaner overgrowth of rhythmically zoned Jd before encountering grain boundaries. Narrow boundaries between Jd grains typically contain Anl, Ab, Anl + Ab or least commonly Ab + Ne; these latter two are typically in symplectitic intergrowths (Harlow, 1994). Smaller Omp, Zo (Czo),Ttn, Pg or Amp grains can be included in the granular boundary zone intergrowths. While not as common as the granoblastic or sheared textures, mesh and felted textures of submillimeter prismatic Jd are found, and a few localities yield conspicuous fan-spheroidal clusters of elongate Jd prisms relatively free of anything but two-phase fluid inclusions (Fig. 5b). In retrogressed jadeitites, inter-Jd grain zones resemble albitite with pseudormorphing of Jd by intergrowths of Ab + Omp ± Amp, Pg, preiswerkite (Prs), Apt, Zoi, Ttn, Bnl, Gph, etc. (see Harlow 1994). Sorensen *et al.* (2006) has shown via cathodoluminescence (CL) imaging that deformation textures plus consistent Jd overgrowth along fracture veins are common to most jadeitite, worldwide, including those from north of the MF.

Mineralogy of samples from the originally described areas was presented in Harlow (1994); here we present mineral assemblages of samples not presented in that paper and, now, spanning the entire 200 km east-west extent north of the MF (Table 1). Jadeitite exclusive of secondary veins or alteration consist fundamentally of Jd (>90 vol%, sensu stricto but more altered rocks may only be > 60%) with subsidiary Ab, white-to-tan mica (Pg in most cases, with Ms-Ph and/or Phl in some cases two or all three), Anl, Omp with minor small crystals of Ttn, Zo, Apt and Zrn, which all can be found as inclusions in Jd. Rutile has only been found in one sample in the core of Ttn. Veins and grain boundary alteration consist of Ab + Anl or Ab + Ne, Zo (and Czo), taramitic amphibole, Pg, Phl, Prs, Bnl, Kfs, and Gph. Phengite grains can show barian overgrowths (Harlow 1995). Zircons are generally small (<50 μm long) and vary from euhedral crystals to irregular rounded ones. Their abundance correlates with K-mica abundances, and rare inclusions include holes (presumably fluid) and Omp. As emphasized in Harlow (1994) Qtz is absent from these jadeitites, not as inclusions in Jd, not as a constituent phase of the rocks, nor in alterations of Jd that retain Jd—Jd + Qtz is absent.

One suite of jadeitite samples north of the MF is unique for its late-stage assemblage: lavender jadeitite from near Saltán, which is the western-most known locality (MVE07B-19). The Jd grains form radiating prismatic clusters, although largely broken up by deformation and variably retrograded. Jadeite grains are relatively inclusion free, primarily being small (<20 μm) two-phase fluid inclusions that, on occasion, have adjacent blebs of Kfs, and grain boundaries coated with Ab ± Anl ± Kfs. Allanite-(Ce) with overgrowths of REE-rich Czo occurs as broken

prisms amidst Jd but also with Ab, so it may be either primary or an early secondary phase. Omphacite is absent and Kfs takes its textural place. Phengite occurs intimately with Jd and Ms-Ph grains are partially replaced or infiltrated by Kfs (variably Ba enriched) and Sr-rich Zo-Czo. Extensive Ab retrogression of, selvages on or veining through Jd contains discontinuous stringers of Kfs, laths Sr-rich Zo (sometimes overgrowing Aln), and rare crystals of Pmp. Isolated vesuvianite (Ves) grains, Gph clusters, and boundary selvages of Pmp and stringers of Grs are also associated with the late Ab (Fig. 5c). This is the only recorded occurrence of Pmp north of the MF.

Pyroxene compositions have been measured for a large number of rocks ranging from light-colored through variable green and even lavender jadeitites toward darker green mixed Jd-Omp jadeitites to omphacitites. Representative compositions for Jd and Omp (and pairs) from individual samples are presented in Table 2 (a growing database of compositions, images, and plots can be found at the senior author's research website). Figure 6a presents a sampling of compositions for clinopyroxenes in an individual jadeitite from north of the MF to demonstrate the range measured in a single sample, as well as portray the ranges among several rocks from the western-most, central, and eastern-most sources. The compositional variation is represented as broad lines where there is a continuous variation, both in Jd and Omp. This approach makes it easier to show the fundamental compositional variation among the four primary compositional components: Jd-Di-Hd-Ae. Adjacent Jd-Omp, either as Omp inclusions in Jd grains or immediate contact of Omp overgrowths on Jd, are shown with tie-lines. One important caveat in these data is that, although we have tried to take into account analyses that represent beam overlap between two pyroxenes which yield reasonable stoichiometry, some instances of reported compositions in plots that are actually mixtures, particularly for Omp or Di, cannot be ruled out without a much greater density of data than we have collected for all samples. A few characteristics of compositions and zoning are worth pointing out.

1. Jadeite compositions typically range from nearly pure Jd to perhaps $Jd_{\sim 80\text{-}85}Di_{510}Ae_5Hd_2$, although some samples have a smaller range restricted toward pure Jd and in others Ae is the next most abundant component, rather than Di. The Saltán lavender Jd is distinctive for its very low iron content (<1 wt%) consistent with enabling the Mn chromophore for the lavender color (*c.f.*, Ouyang 2001, Nassau and Shigley 1987), as well as minimal Ca content (Di + Hd ≤ 2 mol%), and no coexisting Omp.
2. Zoning patterns in Jd grains vary considerably, particularly between different samples, but two general patterns are common. Most commonly grains contain relatively Jd-rich crystal cores, with subtle cryptic zoning and cluttered with inclusions as described above, surrounded by overgrowths richer in other components, particularly Di. (Fig. 7A). Somewhat less common are cryptically zoned interiors of variable composition with or without an overgrowth of rhythmically zoned Jd (Fig. 7B). [Superimposed or overprinted on these patterns can be numerous "inclusions" of Ab, Anl, Pg, Omp or some combinations of these, as described above.] These observations are consistent with prior descriptions (Harlow 1994; Sorensen *et al.* 2006) but different, in particular, from the recent description of jadeitite from the Sierra del Convento region, Cuba (Garcia-Casco *et al.* 2009; see discussion).
3. Omphacite is most common as overgrowths on and veins cutting through Jd. In the former case, compositions of contacting Jd and Omp usually approach that of equilibrium pairs (more discussion below), but in the latter case, there is zoning across the Omp vein (Fig. 7C) in which a portion or even all of the vein Omp does not appear to be in equilibrium with adjacent Jd (also discussed below). Omphacite compositions trend away from that potentially in equilibrium with

Jd toward more Di+Hd+Ae-rich compositions.
4. The compositions of Omp inclusions and overgrowths generally overlap in each thin section, although some "Omp" inclusion compositions are much higher in Ae content (Fig. 6a) than is consistent with interpretations of coexisting sodic pyroxenes (Green *et al.* 2007). In addition, most coexisting Jd-Omp compositions do not follow the Green *et al.* (2007) solvus (see discussion below).
5. There is a trend displayed among the three different regional clusters of jadeitite indicating higher Ae component in the compositions of Omp and Jd (trending away from the cores of Jd grains) for the western-most samples that decreases further eastward. In addition, there is a trend toward a smaller Jd-Omp compositional gap in jadeitite from the west as compared to those from further east (Fig. 6a; Table 2).
6. The green color of Jd and Omp is mostly related to iron content, although no study has been carried out to accurately evaluate the ferrous-ferric variation or its impact on color. Chromium has been shown clearly to yield the color in so-called imperial jade (see Harlow et al. 2007), and likely contributes to color in impure Jd and Omp (Table 2, Sorensen *et al.* 2006, Harlow and Olds 1987).

Mica: Representative mica compositions are presented for only the new localities from north of the MF in Table 3, as details of mica composition were presented in Harlow (1995). Paragonite has a nearly ideal end-member composition. Phengitic Ms is less common than Pg in jadeitite north of the MF, with maximum Si atoms per formula unit (apfu) < 7 and Mg/Mg+Fe (MMF) > 0.7. Muscovite (low Mg+Fe) is comparatively rare as inclusions, but is most common in the latest stage of crystallization of lavender jadeitite from near Saltán; Ph occurs with Jd in less altered areas. Phlogopite is less common than either Pg or Ph in jadeitite but increases in abundance with that of Omp in the jadeitite-omphacitite rocks; MMF values range between 0.69 and 0.93 with variation typically limited to <0.04 in single samples. Assemblages and even interlayering of the three micas has been found in several samples (see Table 1). As described by Harlow (1994) Prs occurs as a late-stage alteration of Pg with MMF varying distinctly between different rocks and even different localities, from a rare low of 0.75 to a more common 0.93-0.95.

Amphibole: Representative Amp compositions are presented in Table 4. As also reported by Harlow (1994), all Amp in jadeitite is late-stage taramitic Amp, both magnesian and ferroan, which appears to reflect the composition of the late Omp (late fluid), at least in terms of $MgO/(MgO+FeO_{Total})$ (MMF_T) as ferrous-ferric evaluation is only assessed here by stoichiometry.

Other Calcic Minerals: Grossular **garnet** was described in some of the taramite-omphacite rocks associated with jadeitite north of the MF (Harlow 1994). Grossular (see above) otherwise is only found as a late phase in the lavender jadeitite from near Saltán. A single specimen of jadeitite/omphacitite near Manzanál originally collected by Zenaide Carvalho da Silva (ZC-20, see Silva 1967, 1970) contains Grt somewhat like that of garnet amphibolites in the area but with spessartine-rich rims (Table 5). This sample is the best (and a rare) argument for metasomatic replacement of a metamorphic rock (*e.g.*, pelitic or mafic) by jadeitite, although there is only this relict phase rather than a textural indication. **Pumpellyite-Mg and vesuvianite** are newly described north of the MF from Saltán jadeitite coexisting with Ab, Grs, Sr-rich Zo, Aln, Kfs, and Ph. Vesuvianite has recently been described by Nyunt *et al.* (2009) in jadeitite from the Jade Tract in Myanmar, and the compositional characteristics are very similar to that in Guatemalan

jadeitite, that is, high in Ti (up to ~5 wt% TiO_2) and Na (up to ~2.5 wt% Na_2O; Table 5). We concur with their conclusions of composition influenced by sodic-metasomatic-HP/LT formation, however, whereas Nyunt *et al.* (2009) argue that Ves grew in equilibrium with Jd, textures for Guatemalan jadeitite clearly show Ves to be secondary, in later veins and overgrowth selvages with the phases noted above. Pumpellyite is aluminous but still should be classified as pumpellyite-Mg. For this reason the analyses in Table 5 are normalized to 3 Si cations, which results in ~45-50% Pmp-Al component, and a large cation site (Ca+Na) that contains a small proportion of vacancies (~<0.05 atoms per formula unit). **Lawsonite** compositions are calculated with all iron and manganese as trivalent cations which still leaves the six-fold site deficient when cations are normalized to 4 silicon atoms. Both Czo and Zo are found, generally as late stage phases as described by Harlow (1994), with Al/(Al+Fe+Mn+Cr) ranging from 0.80-0.99. As described in Harlow (1994) Sr can reach significant concentrations in Zo (see Table 5), particularly in the alteration of lavender jadeitite from Saltán, and appears to be concentrated in this calcic phase among those listed above, whether by crystal-chemistry or growth stage in jadeitite evolution/alteration. Allanite–REE-rich Czo/Zo compositions require further study, but appear to be Ce-rich with ~≥ 20 wt% total REE-oxide (0.13 apfu).

South of the MF

Jadeitites from this area are distinct for the three zones recognized at this time. Consequently, we describe them separately.

Carrizal Grande: Jadeitite is generally not so granoblastic, with more columnar or interfingered Jd quasi-prisms, and massive in appearance, with smaller grain size, on average, than north of the MF. Maximum grain size for Jd is generally < 2mm whereas tabular Ph grains can exceed 5mm across. Interiors of Jd grains can contain dense clusters of small inclusions (<10 µm), typically Omp, Ph, Qtz, Lws, 1 or 2-phase fluids as well as Ttn, Zrn, and Apt as crystals, clusters, or blebs. Outside of the cores Jd grains tend to be free of inclusions (Fig. 5d-f), except near the grain boundaries. As observed in BSE images, the interiors of grains typically exhibit subtle, patchy compositional zoning, while rims are rhythmically zoned or nearly unzoned. Most grain boundaries between Jd and other primary minerals do not show interstitial coatings or abundant veining. When Jd rims have inclusions, they typically are enveloped as individual Ph, Ttn, Rt , and/or Zrn grains. Veins, when present, tend to be sharp and cross-cutting and can consist of Omp, Ab, Qtz, and Cym; Qtz veins can be in direct contact with Jd. In jadeitite from Quebrada Seca, Omp veins are common and demonstrate several generations based on zonation across the vein (Fig. 5g) and envelopment of earlier Omp vein fragments by later growths. These Omp veins can color the rock an intense blue-green (desirable as “blue jade”)that is correlated with relatively high TiO_2 content in the Omp (≤ 2.0 wt% see Table 2 and Harlow *et al.* 2004b). Phengite grains are typically zoned by an overgrowth of barian rims (Fig. 5g), but occasionally have a more complex pattern or cryptic internal zoning. These grains are generally free of inclusions, although Ttn and Zrn are most common if encountered, and Ph grain clusters can envelope Jd and other mineral grains. Titanite grains can vary from a few microns to over 1 mm across, and larger ones commonly have a small nucleus of Rt or Zrn (MVE02-8-5) and can include Jd or Ph(MVE07-9). Titanite abundance appears to be correlated with the abundance of Omp as well as the saturation of green color of the rock. Textures of Ttn vary considerably, from larger nematoblasts (to 1 mm), smaller quasi-euhedral crystals, and lacework growths around other phases, such as Jd, Omp, Ph, etc (Fig. 5h). Zircons are generally small (<150 µm long) and vary from well-defined crystals, sometimes in delicate clusters, to rounded blebs;

inclusions observed to date are only cavities, presumably fluid inclusions. Zircon abundance and crystal size appears to be correlated with the abundance of Ph. Allanite has been found in several jadeitites as discrete crystals along Jd-Ph boundaries to ~75 µm maximum dimension and surrounding/invading a monazite grains of similar dimension in two samples.

Late-stage alteration is not as common as observed in jadeitites north of the MF. This is obvious from the generally greater translucency of the jadeitite due to tight grain boundaries lacking refractive-index contrast gaps or coatings. The most common grain-boundary infiltration phases, when observed, are Qtz and Ab, which can be accompanied by Omp or Cym. Quartz infiltrations have been observed in which Jd grains, with somewhat "chewed up" rims, are separated by a Qtz matrix and surrounded by blebs of Omp and Di (Fig. 5i).

La Ceiba: The jadeitite varies from medium- to fine-grained, opaque, granoblastic texture to a darker translucent microcrystalline mesh texture omphacitite however, the latter variety is cut by dense networks of fractures that render the material fragmental (and not suitable for use as gem jade). Jadeite grains have a similar texture as those in jadeitite from the Carrizal Grande area; grain interiors are decorated with blebs of Omp, Qtz and fluid inclusions. Small rounded Zrn inclusions are also common in Jd, but not generally in the areas of the previously mentioned inclusions (Fig. 5j). Zoning in Jd grain interiors is subtle and generally patchy and cryptic, and rims are typically narrow, relatively unzoned with slightly lower Jd content (brighter in BSE). Overgrowth of cryptically zoned core Jd by clean rhythmic purer Jd followed by less Jd-rich, possibly multiple times, is observed in MVE04-15-3 (Fig. 7e). Coarser-grained Omp, Ph, and Ttn fill in around grains of Jd in discontinuous, broken-up veins. Zoning in Omp cores is cryptic but rims or outer regions can be rhythmically zoned. Large Ttn grains (up to several mm) have irregular shape, appear to have numerous Qtz and fluid inclusions (voids in polished section). Late, light-colored veins transect the rock and typically consist of Qtz, Di, Cym, Ves (Fig. 4d; Fig. 5k) and, on occasion, pectolite. Albite appears between grain boundaries of Jd.

La Ensenada: The jadeitite here is noted for its generally pale tan-to-grayish body color decorated by stringers of lavender, blue, emerald-green, and pink, earning it the name "rainbow jade." It consists of dense intergrowths of Jd crystals cut by narrow Pmp-dominant veins, in turn cut by veins of Grs and Ab. Jadeite crystals vary from lathy, generally <300 µm long, to irregular to radial clusters forming a dense mat of Jd. Veins crosscut the Jd and mantle or infill the Jd with blocky Pmp of similar but more equant grain size. The centers of the veins are occupied with Grs ± Ab (Fig. 5l); however, Pmp + Grs ± Ab is also found dispersed as small regions in the jadeitite in what appear to be late-stage veins. Pinkish Grs crystals are commonly intergrown, with individuals ranging from ~100 µm to 1 mm across, and CL reveals oscillatory zoning patterns (Fig. 5m – MVE04-20-1) not evident in BSE or in major elements. Omphacite is minor both as inclusions and overgrowths on Jd. Phengite, Ttn, Apt, Chl, Zrn, and Cln are other minor constituents of this rock type. Light brown chloritite veins cut through some samples and consist of Fe-poor (< 1 wt% FeO_T) Clc plus Omp and Ttn in decreasing abundance with distance from the jadeitite boundary.

Pyroxene compositions: As with the samples from north of the MF, representative compositions are presented in Table 2, and summary plots are provided in Figure 6b, with plots for each of the three distinct source areas south of the MF. The following characteristics are noted:

1. As in the case of northern jadeitite, Jd compositions typically range from pure Jd to perhaps $Jd_{\sim 80\text{-}85}Di_{5\text{-}10}Ae_5Hd_2$, with some dispersion in Di versus Ae content. The La Ensenada Jd, like

the lavender Jd from Saltán, is distinctive for its very low iron content (<1 wt%), but does have minor coexisting Omp and even Di.
2. Zoning patterns in Jd grains among individual jadeitites vary considerably, but the most common is a Jd-rich core, either relatively homogeneous or with cryptic, patchy zoning, particularly when there are abundant inclusions, and a less Jd-rich (more Di+Ae+Hd) rim. In some samples, *e.g.*, JJE01-3-1, well-formed crystals manifest coarse oscillatory zoning (from high-to-low-to-high Jd content) usually terminated by a less Jd-rich rim or an Omp overgrowth (Fig. 5n).
3. The compositions of Omp inclusions and overgrowths generally overlap in each thin section, however, the Jd – Omp gap tends to be larger for coexisting Jd and Omp at the cores of Jd grains than at rims of those grains. And, as with samples from the North, some Omp inclusion compositions are much higher in Ae content (Fig. 6b; Table 2) than is consistent with the Green *et al.* (2007) solvus. Likewise, as with northern jadeitite, coexisting Jd-Omp compositions do not follow their solvus. Finally, there is the unusual Ti-rich compositions (*e.g.*, Table 2) of certain blue vein Omp in samples from the Carrizal Grande area and even in Jd from La Ensenada, which is best characterized by a $NaTi_{0.5}Mg_{0.5}Si_2O_6$ (rather than alumino-buffonite – $CaTi_{0.5}Mg_{0.5}AlSiO_6$) component (Table 2; Harlow *et al.* 2003, 2004b).
4. There are distinct differences in the pyroxene compositional arrays between the three different source areas south of the MF (Fig. 6b). In general, the range of compositions of both Jd and Omp are greatest for Carrizal Grande, intermediate for La Ceiba, and the smallest for La Ensenada. The most straightforward interpretation is a decrease in the maximum temperature of growth (equilibration) of Jd and Omp, in the order listed. Likewise, except for a single sample from La Ceiba (MVE03-77-1), the maximum Ae content for both Jd and Omp varies in the same order, greatest at Carrizal Grande and least at La Ensenada. Finally, at La Ceiba and La Ensenada we found individual jadeitite samples (MVE02-15-10, MVE04-21-7) with late stage veining containing a Di composition separated by a gap from Omp compositions.

Mica: Representative mica compositions are presented for localities from south of the MF in Table 3. Muscovite grains analyzed are usually phengitic, with variable enrichments in Ba similar to values in Ms north of the MF. However, Si apfu is significantly higher than in samples north of the MF, from the highest values at Carrizal Grande (≤7.5), lower at La Ceiba (≤7.2), and lowest at La Ensenada (<6.7) where mica is rare. At La Ensenada, mica is more likely to be Phl, but, if Ms, it is not generally phengitic. Ba substitution for K follows the same mechanisms described by Harlow (1995) in mica north of the MF by which the predominant one ($BaAlK_{-1}Si_{-1}$) lowers Si content of the mica. MMF of Ph varies within and between jadeitite samples from 0.57-0.90 (MVE02-8-5) to a narrower 0.80-0.92 (JJE01-3-4), both samples from Carrizal Grande, with a similarity to those values (but perhaps slightly lower) in coexisting Omp (Jd cannot be well assessed for MMF versus MMF_T). This variability is not clear for jadeitite from La Ensenada, for lack of analyses, although MMF of Phl is high 0.96-0.97 from a single sample (MVE04-20-1).

Amphibole: Representative Amp compositions are presented in Table 4. Gln is a rare late phase in jadeitite and more commonly associated with a rock composed principally of Omph+Gln from the Carrizal Grande area, with composition essentially on the Gln–Ferro-glaucophane join (MMF 0.8-0.9 – see Table 4). Act is found in veins, typically with Qtz or Ab and is near the tremolite-Act join in composition.

Other Calcic Minerals: Grossular **garnet** is common but only in the Pmp-jadeitite from around La Ensenada and is nearly pure end-member Grs. The zoning evident by CL does not manifest itself in microprobe analyses. Otherwise, a single specimen of garnet jadeitite infiltrated with Qtz and Lws from Carrizal Grande (MVE06-17-2) contains Grt somewhat like that in eclogite in the area but with much greater spessartine content (to ~8 wt% MnO, ~1.2 Mn apfu: Table 5). This sample is the best (and a rare) argument for metasomatic replacement of an eclogite by jadeitite, without textural indication. If so, the high Mn content of Grt and high Ae content (to 43 mol%) and low Jd content (4-10 mol%) of minor Omp (if relict) are not typical for local eclogite. **Vesuvianite** is found in late stage veins with Cym and Qtz at La Ceiba. As with compositional characteristics from the sample north of the MF, Ti is high (to >5 wt% TiO_2) and Na (to ~2.5 wt% Na_2O; Table 5). It also contains a small amount of SrO (0.25-0.5 wt%, 0.07 – 0.14 Sr apfu). **Pumpellyite-Mg** is common in Pmp-jadeitite from near La Ensenada. Pumpellyite straddles the boundary between –Al and –Mg types with ~30-50% Pmp-Al and 40-50% Pmp-Mg components. Lawsonite is common in some jadeitites and omphacitites from the Carrizal Grande area, occurring in the mélange with Lws-eclogite. **Lawsonite** compositions are calculated with all iron and manganese, although minor, as trivalent cations, which still leaves the six-fold site slightly deficient when cations are normalized to 4 silicon atoms, as well as the oxide (plus calculated H_2O) and cation totals are somewhat low, even while including Sr content (typically 0.03 – 0.35 apfu; Table 5).

Discussion:

Estimates of crystallization *P-T*:

As nearly monomineralic rocks affected by episodes of growth and some alteration, assessing conditions of crystallization, particularly "peak" *P-T*, can be difficult. We have separated the interpretation into sections on phase assemblage and then Jd-Omp relationships as well as the distinctions between the tectonically distinct environments: north versus south of the Motagua fault in Guatemala.

North of the MF: None of the jadeitite in this region contain Qtz, either as inclusions in Jd or in veins, but all contain Ab, mica and usually Anl, which indicates all formed at *P* less than that of Jd + Qtz stability field unless the phase assemblage represents a fully retrograded one, consistent with the earlier observations by Harlow (1994). The presence of Zo-Czo rather than Lws in the presence of Pg suggests formation at *T* above the reaction Lws + Jd = Zo/Czo + Pg + Ab + H_2O (Fig. 8). These constraints yield *P* = 6-12 kbar and T = 300-450°C; higher temperatures are permissible if the activity of SiO_2 is much below unity (see Fig. 8 Harlow, 1994). The modest Jd – Omp gap (Green *et al.* 2007) yields temperature from 200 to > 500°C for pyroxene pairs, with indications of higher temperatures for samples from the more western localities and lower for ones from the east (see Fig. 6), except for those from Saltán. More discussion of these data are presented below.

Carpenter (1979, 1981) described antiphase domain (APD) structures < 20 nm in size in Omp from a jadeitite that undoubtedly came from the central area north of the MF (presumably Manzanal). These Omp APD textures indicates that the Omp went through the order-disorder transformation soon after the Omp crystallization in *C*2/*c* space group (presumably metastably). But more significantly, the very small APD size is consistent with the low-*T* formation of the jadeitite and a simple cooling history.

Alteration of jadeitite to the albitite assemblage, as described in Harlow(1994), involves both additional SiO_2 (as well as LILE) via a fluid (see Sorensen *et al.* 2010), as well as a down *P*

trajectory below the Jd stability field, usually, into the Zo stability field (T > 350-400, see Fig. 8) and into the greenschist facies (350-450ºC at <7 kbar). Moreover, the symplectitic textures of Ab + Anl and Ab + Ne (also described by Tsujimori *et al.* 2004) are further evidence of fluid involvement in these retrograde reactions.

Oberhänsli et al. (2007) used the method of pseudosections to calculate conditions for bulk compositions of jadeitite from Sorkhan, Iran and elsewhere, including an estimate for a sample north of the MF: R11 called Olmec-Blue containing Jd, Ab, Pg, Anl, Zo, Ttn, and Prs (Harlow 1994). Their analysis yields T = ~500ºC and P = ~ 14 kbar, at the high end of our T estimate and above our P estimate. However, this estimate is defined by the lack of Omp and presence of Zo, whereas jadeitites from north of the MF usually contain primary Omp and late or alteration Zo. The authors state that the presence of Jd + Omp yields Ts below 400ºC in their calculations, more consistent with the results of Harlow (1994) and those presented here. Ultimately, their results are useful but may be difficult to apply to jadeitites north of the MF where bulk composition is strongly affected by alteration and phase assemblages must be deciphered for different stages of the rock history.

The jadeitite from Saltán is singular for samples that contain late-stage Pmp + Grs as well as nearly pure Jd; however, the primary crystallization of the Jd in these lavender-colored rocks provides little indication for initial conditions as inclusions are generally fluids and Jd in contact with Ab has rounded grain boundaries as if in reaction relationship. Omphacite is absent. Another sample from Saltán (MVE07B-19-6) contains Ab and Omp inclusions in Jd and no Pmp or Ves, more like other samples from the western end of the northern suite. Our conclusion is that the lavender samples represent both a different origin condition and composition (low Fe), and the alteration assemblage Pmp + Ab + Grs + Zo/Czo suggests T ~ 350ºC at P 6-8 kbar (*e.g.*, Schiffman and Liou 1980), which is probably colder than jadeitite-albitite conditions found elsewhere north of the MF. Another distinctive aspect of these jadeitites is the late extensive enrichment in both Sr and Ba.

South of the MF: Whereas the phase assemblages for the entire 200 km span of jadeitite north of the MF (except Saltán) are remarkably consistent, those south of the MF clearly group into three distinct clusters based on geography. In jadeitites from the **Carrizal Grande** area, the presence of Qtz inclusions in Jd indicates P > Jd + Qtz stability field They are found together with Lws eclogites with maximum metamorphism estimated at P = 20-26 kbar, T = 350-480°C and blueschist alteration from P ≈ 1.4 GPa and T ≈ 400°C indicating a geotherm of ≈ 5°C/Km, comparable to the coldest geotherms from subduction zones worldwide (Tsujimori *et al.* 2006). Jadeitites at Carrizal Grande are consistent as a phase assemblage with the blueschist trajectory of this interpretation, but not well constrained. In this case, the results of Oberhänsli et al (2007) may provide useful insight, as the assemblages of Qtz-Lws-Jd-Omp-Amp-Pg have a narrow stability field from 350-425ºC and 11-16 kb (their Fig. 4a), although Carrizal Grande samples contain Ph rather than Pg and thus have a different bulk composition Thus, jadeitite formation is estimated as T < 500ºC (those with Lws, < 450ºC) and P = 12-20 kbar in the presence of Lws; without Lws T can only be estimated from coexisting Omph-Jd, which is discussed below. Jadeitites from **La Ceiba** also manifest Qtz inclusions in Jd but contain neither Lws or Zoi/Czoi to further constrain the phase assemblage in *PT*. Compared to Carrizal Grande jadeitites, Jd-Omp pairs at La Ceiba suggest a somewhat lower maximum T of ~450ºC. That plus the lack of coexisting eclogite in the local mélange but presence of glaucophane blueschists argues for somewhat lower P of ~12-16? kbar. In the **La Ensenada** jadeitite the lack of Qtz, intimate Pmp-Jd textures, and large Omph-Jd gap suggests maximum T = <300-350ºC at P > 6 kbar.

Mechanism of formation

Previous work on Guatemalan jadeitite (Harlow 1994) and jadeitite in general (Sorensen *et al.* 2006, Harlow *et al.* 2007) has argued for crystallization from a hydrous fluid, derived from a subduction channel, in fractures in serpentinizing peridotite, presumably the hanging wall (the mantle wedge) of the channel. The fundamental arguments are 1) consistent association with serpentinite with some clear cases of contact (*e.g.*, Myanmar – see Harlow *et al.* 2007), 2) textural evidence for crystallization from a fluid including abundant fluid inclusions and unimpeded crystal growth into open space, 3) little evidence for metasomatic replacement of a protolith in terms of either pseudomorphic textures or relict phases from such a protolith, 4) evidence that high pressure hydrous fluids, such as those derived from the blueschist-to-eclogite transition are mostly saturated with respect to Jd (Manning 1998), 5) reaction zones between jadeitite and serpentinite that represent primary or secondary interactions involving a fluid (Sorensen *et al.* 2010, Harlow *et al.* 2007). This report updating jadeitite information from Guatemala reinforces these observations. Harlow *et al.* (2007) cite one case where metasomatic replacement has been documented–Punta Rasciassa in the Monviso serpentinite of the Western Alps, Italy (Compagnoni *et al.* 2007) and two cases in which jadeitite encapsulates eclogite blocks in a mélange – Kampos mélange, Syros, Cyclades, Greece (Bröcker & Keasling 2006) and Borus mélange, Khakassia (Dobretsov 1963). Among more than 100 jadeitite samples examined in this study only a few might be invoked to show metasomatic replacement, and these are most clearly limited to relict Grt: ZC20 and MVE06-17-2. Interestingly, both samples contain metamorphic garnets that are not likely from any eclogite or garnet amphibolite (metabasite) associated with the mélanges as the Sps content exceeds that in the metabasites. Certainly there are ambiguous cases of Jd nucleation around another mineral like Zrn, uraninite and even Ab, but the minerals are either totally exotic (uraninite) or found within the phase assemblages of jadeitite without clearly exotic compositions so metasomatism is not documented.

Pyroxene Zoning, Pyroxene Pairs and P-T-t Paths:

The evaluation of the solvus in the Jd-Di-Hd-Ae clinopyroxene system by Green *et al.* (2007) has been applied to compositional data compiled on the pyroxenes in this study of jadeitite. Pressure has been uniformly set at 12 kbar as a reasonable average for the pseudobinary evaluations along the (Di+Hd+Ae)-Jd joins, following the example of García-Casco *et al.* (2009). Several implications have been derived.

First, only rare pairs give consistent *T* estimates, which is evident from Fig. 6. Omphacite consistently yields a higher *T* estimate than Jd, typically by 100 to 150ºC. Whereas this could be interpreted as due to disequilibrium at low *T* and problems with the Ae estimate, the consistency among many pairs from different samples and locations argues against this. Given the gentler slope of solvus for Jd compositions and their dominance, we have used them for subsequent discussion.

The second implication is derived from the zoning of Jd crystals with Omp inclusions or overgrowths. The recently described jadeitites from Cuba (García Casco *et al.* 2009) have been interpreted with a considerably different sequence of conditions during growth than for others (Harlow *et al.* 2007). Cores of Jd manifest oscillatory zoning of impure Jd interpreted as forming at higher temperatures, ca. 640ºC, with a change to binary Jd-Omp crystallization (a more Di-rich fluid) at ca. 570ºC on Jd crystal rims. This observation led us to reexamine zoning in Guatemalan Jd and Jd-Omp pairs. Jd-rich cores and Jd-poor rims on Jd rims in most

Guatemalan jadeitite are the reverse of those reported by García-Casco *et al.* (2009) and consistent with those previously reported (Harlow 1994, Sorensen *et al.* 2006, Harlow *et al.* 2007b). Indeed, many jadeitite samples with few exceptions, crystallize with a Jd-rich core, Jd_{100-95}, with an overgrowth extending to perhaps Jd_{85-80} followed by Omp. These final Jd compositions in equilibrium with Omp yield T = 500-580ºC based on the solvus of Green *et al.* (2007). Pure Jd cores alone only demand a fluid that is saturated with respect to Jd and presumably not saturated in other components or phases and thus cannot be used to assess T. However, in numerous samples Omp inclusions in the interior of Jd grains appear to be (nearly) in equilibrium with the adjacent Jd. For these pairs, T is about 200-300ºC for P assumed to be 10-12 kbar and should define roughly the initial growth conditions. Decrease in Jd content with continued grain growth requires higher T, otherwise Omp would form. Ultimately, Jd grain compositions decrease to Jd_{80} followed by Omp compositions that can, with continued crystallization along grain boundaries, evolve to Di>Jd and, in some cases, distinct Di coexisting with Ab. These trends suggest up-T crystallization plus increasing Di-content of the fluid, in part contradictory to our previous interpretation (Harlow et al. 2007).

Zoning within Jd crystals is commonly cryptic in interiors and rhythmic toward the rims. Cryptic zoning is puzzling but may combine aspects of fast crystallization and deformation as many cryptically zoned crystals have fuzzy optical extinction. Rhythmic zoning has been explained as the result of pulses of fluid entering open fractures in preexisting jadeitite that crystallizes more Jd-rich compositions first with depletion leading to compositions higher in other components (Harlow 1994, Sorensen *et al.* 2006).

Studies of jadeitites along with many other HP-LT rock P-T-t-x paths following a clockwise PT history argue that jadeitite formation should follow a down-P, down-T path during exhumation (*e.g.*, Harlow *et al.* 2007, Tsujimori *et al.* 2006a, Sorensen *et al.* 2006, Harlow *et al.* 2003). The composition of coexisting Jd-Omp in the cores of Jd crystals as compared to rims generally argue for either cold primary crystallization followed by hotter late crystallization or composition of Jd controlled strictly by fluid composition with Omp being in disequilibrium, perhaps encapsulated from a dismembered Omph-bearing protolith. The lack of replacement textures (see below) and dissimilarity of Omp compositions to any known mélange lithology make the second explanation less credible. Thus, we prefer the interpretation in which initial jadeitite crystallization is colder (ca. 300ºC) with late crystallization and Omp veining as warmer (perhaps to 500ºC). This implies that the most jadeitite crystallizes in a chilled environment that later experiences warming while the crystallization simultaneously evolves toward more Di (+Hd+Ae) bulk composition. This would appear to be an improbable coincidence, but support for an alternate hypothesis is not compelling. Finally, there are a number of samples that show more than one generation of higher initial Jd content growth followed by decreasing Jd (*e.g.*, MVE04-15-3 – La Ceiba: Fig. 7e; or JJE01-3-1 – Carrizal Grande Fig. 5n). Multiply zoned Jd records a repeat of whatever sequence of events and processes responsible for zoning profiles most jadeitite from Guatemala.

Consequently, crystallization of jadeitite probably should not be viewed as directly connected to some phase of the metamorphism of the subducted slab, such as eclogite or blueschist formation, because jadeitite most likely formed in the hanging wall, or a slice thereof, rather than in the slab. However, Jd veins in some Lws-eclogite from Carrizal Grande (Tsujimori et al. 2005, 2006a), suggest that at least a portion of jadeitite formation postdates that of eclogite and that either the jadeitite-forming fluids were active in portions of the subduction channel or eclogite

had been incorporated into the serpentinizing mélange by the time of jadeitite formation. The interpreted progression of colder to warmer crystallization of Jd unfortunately does not include any pressure information. It is unlikely that the process happens deeper than the transition from static mantle wedge to ductile where it is being dragged down with the plate, roughly at 70-80 km depth (~23-26 kbar; *e.g.*, Grove *et al.* 2009.) So, it is not clear whether the trend tracks heating due to the exothermic serpentinization reactions (see Evans 2004) plus aging of the contact or delamination of mantle wedge slabs via volume increase (from serpentinization) and increased traction or some other process. Cycling of this process might be explained by small scale wedge extrusion −decreasing *P*− with or without delamination of the overlying wedge into the subduction channel that puts colder slab and new fluids adjacent to the serpentinizing mantle. Resolution requires better control of *P*-*T*-t-x interpretation as well as modeling.

Differences between jadeitite from north and south of the Motagua fault

From the descriptions above, it is clear that jadeitite occurrences north and south of the Motagua fault vary in some very distinctive ways. The first to be considered is the tectonic context. South of the MF, eclogite and jadeitite are part of a single tectonic event (collision-exhumation) that spans eclogite crystallization from 144-132 (±~10; Sm-Nd) Ma and thermal closure (Ar-Ar) from 125-116 Ma, whereas North of the MF there are clearly two events defined by mélange eclogite (131-126 Ma; Sm-Nd), more or less equivalent to dates south of the MF, and thermal closure ages from 65 to 77 Ma, equivalent to metamorphic ages (Ar-Ar of mica and amphibole in gneisses and Sm-Nd isochrons for eclogite enclaves, e.g., Martens *et al.* 2007a) from the Sierra de Las Minas, north of the mélange (Brueckner *et al.* 2009). Recent crystallization dates for jadeitite are limited but intriguing. U-Pb dating of Zrn from a single jadeitite in the central zone north of the MF gives 95.1±3.6 Ma (Yui et al. 2010) which was concluded to be a formation date on the basis of inclusions in the zircons. This age is certainly younger than the eclogite date but somewhat older than the Cretaceous event that metamorphosed the Sierra de Las Minas and emplaced the Sierra de Santa Cruz ophiolite. A U-Pb date from a Ph jadeitite (MVE02-8-6) from south of the MF of 153.7±3.5 Ma (Fu et al. 2009) was interpreted as a protolithic relic from the oceanic crust based on its it being older than the eclogite ages. However, we have doubts about this interpretation: the Zrn in this sample contain mineral and fluid inclusions inconsistent with an igneous origin, and being older is not a necessarily a criterion for being relict. Certainly, these dates raise a variety of interesting questions beyond the scope of this paper without more Zrn dating, but it does appear that the difference between the jadeitite north and south of the MF. The presence or lack of albitization , albite-mica rocks, etc. may be related to both temporal and physicochemical differences in the formation events.

The next distinction is the vast areal extent of the northern jadeitite belt, more than 200 km with at least three grouped areas compared to a very limited extent, ~11 km, parallel to and south of the MF. All of the jadeitite north of the MF share the extensive albitization overprint, whereas the narrow extent of jadeitite south of the MF can be readily distinguished among three fault slices by different phase assemblages and apparent *P* and/or *T* of crystallization. Moreover, Qtz inclusions and veins in Jd from two of the three occurrences south of the MF stands in contrast to the total lack of Qtz in any jadeitite from north of the MF. So, clearly the different tectonic events have made a difference, but whether the lack of variability on the north side is due entirely to a possible Cretaceous overprint or to different formational events is not yet clear If the Zrn dating holds, the Cretaceous age is the crystallization date and the alteration is just part of the northern processing.

The lavender-colored Jd in samples from Saltán, north of the MF, and La Ensenada, south of the MF, deserve special mention and attention. The Jd in these samples has compositions among the most rich in Jd component and lowest in iron. Likewise, coexisting Omp (found so far only at La Ensenada), Pmp, and Lws (south only) suggest the lowest crystallization temperatures for jadeitite. The minimal iron in both pyroxene and Clc (La Ensenada) suggest some mechanism for keeping ferrous iron in solution during crystallization which could be related to some redox phenomenon such as that which leads to removal of iron in white bauxites during low-*T* diagenesis (Feenstra 1996, pers. comm. 2004), as well as low-*T*, in general, for the formation of these distinct jadeitite.

Finally, although this paper does not present rock compositions and geochemistry, an obvious difference from the mineralogy between the northern and southern jadeitite is the predominant mica. Jadeitite north of the MF predominantly features Pg with very secondary abundance of Ph and Phl plus alteration Prs. In contrast, Pg (and Prs) are absent in jadeitite south of the MF, whereas Ph is common to abundant. Interestingly, the late barium influx is common in all Guatemalan jadeitite occurrences by the presence of barian K-micas, Cym, Cln, Bnl, and hyalophane. The chemically distinctve mineralogies are suspected to be attributed to the compositional characteristics of the sediments accompanying the subducted slab that sourced jadeitite-forming fluid. This would suggest a decoupling of potassium sourcing, probably from clays and continentally derived sediments, from barium, more likely coming from either oceanic seafloor sediments or carbonates. These and other geochemical issues are being taken up elsewhere.

Conclusion:

The distribution of jadeitite in Guatemala is now known to extend for more than 200 km in serpentinite mélange strung out north of the Motagua fault and in three newly described mélange slices south of the fault. All of the jadeitite from north of the MF is characterized by Jd containing inclusions or veins of Ab + Omp ± Anl ± Pg ± Ne with extensive albitization. Jadeitite from the three known sources south of the MF are distinctive by their mineralogy and associated mélange lithologies: Carrizal Grande jadeitite features Jd with inclusions of Qtz + Omp + Ph, minor veining of Qtz or Ab, a substantial proportion of samples containing Lws, and associated Lws-eclogite; La Ceiba has jadeitite similar to Carrizal Grande minus any Lws and Omp bearing gneisses instead of eclogite; and La Ensenada has distinctive light-colored Pmp-jadeitite with veins of Grs + Ab and contacts with Clc rock in a mélange containing lawsonite-glaucophane blueschist. All evidence points to jadeitite formation from primary crystallization of Jd and other phases from hydrous fluid liberated from the subducted slab and introduced into peridotite/serpentinite of the overriding mantle wedge. The extent of jadeitite in Guatemala is second only to Myanmar and the complexity of the tectonic context is noteworthy: Two collisions are recorded in the HPLT blocks from the northern and southern serpentinite mélanges, one Necomanian and the other Maastrichtian, and it appears jadeitite formed in both events.

Acknowledgements:

We want to thank Carlos Gonzales for field assistance and Eric Sahm and Jamie Newman for analytical and sample processing assistance.. This work was funded by EAR0309320 to GEH,

and EAR0309116 to VBS. This project is part of IGCP Project 546 on "Subduction Zones of the Caribbean." We appreciate constructive reviews by Walter Maresch and Tatsuki Tsujimori.

References:

Alvarado, G.E., Dengo, C., Martens, U., Bundschuh, J., Aguilar, T., & Bonis, S.B., 2007, Stratigraphy and geologic history. In: *Central America: Geology, Resources, and Hazards*. (eds., J. Bundschuh and G.E. Alvarado) Taylor and Francis Group, London, pp. 345-483.

Berman R.G. (1988) Internally-consistent thermodynamic data for minerals in the system K_2O-Na_2O-CaO-MgO-FeO-Fe_2O_3-Al_2O_3-SiO_2-TiO_2-H_2O-CO_2-O. Journal of Petrology 29, 445-522.

Berman, R.G. (1991) Thermobarometry using multi-equilibrium calculations: a new technique, with petrological applications. Canadian Mineralogist 29, 328-344.

Berman, R.G., Brown, T. H. and Perkins, E.H. (1987).GE0-CALC Software for the calculation and display of pressure-temperature-composition phase diagrams. University of British Columbia, Vancouver.

Bertrand, J. & Vuagnat, M., 1976. Etude pétrographique de diverses ultrabasites ophiolitiques du Guatémala et de leurs inclusions. Bulletin suisse de Minéralogie et Pétrologie, **56**, 527-540.

Bertrand, J. & Vuagnat, M., 1980. Inclusions in the serpentinite melange of the Motagua Fault Zone, Guatemala. Archives des Sciences (Société de Physique et D'Histoire Naturelle de Genève), **33**, 321-336.

Bröcker, M. and Keasling, A. (2006) Ionprobe U-Pb zircon ages from the high-pressure/low-temperature melange of Syros, Greece: age diversity and the importance of pre-Eocene subduction. Journal of Metamorphic Geology 24, 615-631.

Brueckner, H.K., Avé Lallemant, H.G., Sisson, V.B., Harlow, G.E., Hemming, S.R., Roden-Tice, M.K., Sorensen, S.S., Tsujimori, T., Francis, A.H., Gehrels, G.E., and Blythe, A.E. (in press) Metamorphic reworking of a high-pressure-low temperature serpentinite-matrix mélange belt north of the Motagua fault, Guatemala: A revised record of Neocomian and Maastrichtian collisions. Earth and Planetary Science Letters.

Brueckner, H.K., Hemming, S., Sorensen, S., and Harlow, G.E., (2005) Synchronous Sm-Nd mineral ages from HP Terranes on both sides of the Motagua Fault of Guatemala: convergent suture and strike slip fault? Eos Trans. AGU Fall 86(52), Fall Meet. Suppl., F1736 (Abstract T23D-04).

Carpenter, M.A. (1979) Omphacites from Greece, Turkey, and Guatemala: Composition limits of cation ordering. American Mineralogist 64, 102-108.

Carpenter, M.A. (1981) Time-temperature-transformation (TTT) analysis of cation disordering in omphacite. Contributions to Mineralogy and Petrology 78, 433-440.

Chiari, M., Dumitrica, P., Marroni, M., Padolfi, L and Principi, G., 2002, Radiolarian biostratigraphic evidence for a Late Jurassic age of the El Tambor Group Ophiolites (Guatemala). Ofioliti 31/2, 173-182.

Compagnoni, R., Rolfo, R., Manavella, F., and Salusso, F. (2007) Jadeitite in the Monviso meta-ophiolite, Piemonte Zone, Italian western Alps. Periodico di Mineralogia 76. 79-89.

Dobretsov, N.L. (1963) Mineralogy, petrography and genesis of ultrabasic rocks, jadeitites,

and albitites from the Borus Mountain Range (the West Sayan). Academia Scientifica USSR (Siberian Branch), Proceedings of the Institute of Geology and Geophysics 15, 242-316.

Donnelly, T. W., Horne, G. S., Finch, R. C. & López-Ramos, E. (1990) Northern Central America; The Maya and Chortís Blocks. In: The Geology of North America, Vol. H, The Caribbean Region, Case, J. E. and Dengo, G., eds. Geological Society of America, Boulder, CO pp. 37-76.

Evans, B. (2004): The serpentinite multisystem revisited: Chrysotile is metastable. *International Geology Review* 46, 479-506.

Feenstra, A. (1996) An EMP and TEM-AEM study of margarite, muscovite and paragonite in polymetamorphic metabauxites of Naxos (Cyclades, Greece) and the implications of fine-scale mica interlayering and multiple mica generations. Journal of Petrology 37: 201-233.

Foshag, W.F. (1957) Mineralogical studies on Guatemalan jade. Smithsonian Miscellaneous Collections 135, No. 5, 60pp

Foshag, W.F., and Leslie, R. (1955) Jadeite from Manzanal, Guatemala. American Antiquity 21, 81-83.

Francis, A.H. (2005) Deformation history of the Maya and Chortís Blocks: Insight to the Evolution of the Motagua Fault Zone, Guatemala [MA Thesis]: Houston, Rice University, 149 pp.

Francis, A.H., Avé Lallemant, H.G., Sisson, V.B., Harlow, G.E., Donnelly, T.W., Chiquin, M., Roden-Tice, M.K., Hemming, S.R., and Brueckner, H.K. (in prep.) Interaction of the North American and Caribbean plates in Guatemala: Part 1. Deformation history and consequences for the exhumation of HP/LT metamorphic rocks. Manuscript under internal review.

Fu, B. Valley, J.W., Kita, N.T., Spicuzza, M.J., Paton, C., Tsujimori, T., Bröcker, M., and Harlow, G.E. (2009) Origin of zircons in jadeitite. Contributions to Mineralogy and Petrology, DOI 10.1007/s00410-009-0453-y

García-Casco, A., Rodríguez Vega, A., Cárdenas Párraga, J., Iturralde-Vinent, M. A., Lázaro, C., Blanco Quintero, I., Rojas Agramonte, Y., Kröner, A., Núñez Cambra, K., Millán, G., Torres-Roldán, R. L., and Carrasquilla, S. (2009) A new jadeitite jade locality (Sierra del Convento, Cuba): first report and some petrological and archeological implications. Contributions to Mineralogy and Petrology 158, 1-16. DOI: 10.1007/s00410-008-0367-0.

Green, E.C.R., Holland, T.J.B., and Powell, R. (2007) An order-disorder model for omphacitic pyroxenes in the system jadeite-diopside-hedenbergite-acmite, with applications to eclogite rocks. American Mineralogist 92, 1181–1189.

Grove, T.L., Till, C. B. Lev, E., Chatterjee, N., and Médard, E. (2009) Kinematic variables and water transport control the formation and location of arc volcanoes. Nature 459, 694-697.

Hammond, N., Aspinall, A., Feather, S., Hazelden, J., Gazard, T., and Agrell, S. (1979) Maya Jade: Source location and analysis. In Earle TK and Ericson JE, eds., Exchange Systems in Prehistory, Academic Press, New York. Chapter 3, 35-67.

Harlow, G.E. (1994) Jadeitites, albitites and related rocks from the Motagua Fault Zone, Guatemala. Journal of Metamorphic Geology 12, 49-68.

Harlow, G.E. (1995) Crystal chemistry of barian enrichment in micas from metasomatized

inclusions in serpentinite, Motagua Valley, Guatemala. European Journal of Mineralogy, 7, 775-789.
Harlow, G.E., and Donnelly, T.W. (1989) Unusual metabasites from jadeitite-bearing serpentinite melange, Motagua Valley, Guatemala (Abs.). Eos, 70, 505.
Harlow, G.E., Hemming, S.R., Avé Lallemant, H.G., Sisson, V.B. & Sorensen, S.S. (2004a): Two high-pressure–low-temperature serpentine-matrix mélange belts, Motagua fault zone, Guatemala: A record of Aptian and Maastrichtian collisions. *Geology* **32**, 17-20.
Harlow, G.E,. Murphy, A.R., Hozjan, D.J., de Mille, C.N. & Levinson, A.A. (2006a): Pre-Columbian jadeite axes from Antigua, West Indies: Description and possible sources. *Canadian Mineralogist* **44**, 305-321.
Harlow, G. E. and Olds, E. P. (1987) Observations on terrestrial ureyite and ureyitic pyroxene. American Mineralogist 72, 126-136.
Harlow, G.E., Price, N.A. & Tsujimori, T. (2006b): Serpentinites of the Motagua fault zone, Guatemala: A mineralogical assessment. *19th General Meeting of the Int. Mineral. Assoc. Program & Abs.* Kobe, Japan, P19-17, 223.
Harlow, G.E., Quinn, E.P., Rossman, G.R., and Rohtert, W.R. (2004b) Blue omphacite from Guatemala. Gem News International section – Gems and Gemology 40, 68-70.
Harlow, G.E., Rossman, G.R., Matsubara, S., and Miyajima, H. (2003) Blue omphacite in jadeitites from Guatemala and Japan. 2003 Annual Meeting, Geol. Soc. Amer., Abstracts with Programs, 35(6), 620 (CD-ROM 254-1).
Harlow, G.E., Sorensen, S.S., & Sisson, V.B. (2007a) Jade. In: *The Geology of Gem Deposits* (ed., L.A. Groat), Short Course Handbook Series 37, Mineral. Assoc. Canada, Quebec, pp. 207-254.
Liou J.G., Maruyama, S. and Cho, M. (1985) Phase equilibria and mineral parageneses of metabasites in low-grade metamorphism. Mineralogical Magazine 49, 321-42.
Liou, J.G., Tsujimori, T., Zhang, R.Y., Katayama, I., and Maruyama, S. (2007) Global UHP metamorphism and continental subduction/collision: The Himalayan model. Int. Geol. Rev. 46, 1–27.
Manning, Craig E. (1998) Fluid composition at the blueschist-eclogite transition in the model system Na_2O-MgO-Al_2O_3-SiO_2-H_2O-HCl. Schweiz. Mineral. Petrogr. Mitt. 78/2, 225-242.
Martens, U., Ortega-Obregón, C., Estrada, J., & Valle, M. (2007a) Metamorphism and metamorphic rocks. In: *Central America: Geology, Resources, and Hazards*. (eds., J. Bundschuh and G.E. Alvarado) Taylor and Francis Group, London, pp. 485-522.
Martens, U., Mattinson, C.G., Wooden, J., Liou, J.G. (2007b) Protolith and metamorphic ages of gneiss hosting eclogite in the Chuacús complex, Central Guatemala. Eos Trans. Amer. Geophys. Union 88(23), Joint Assem. Suppl. Abs. U53A-08.Matsumoto, K., and Hirajima, T. (2005) The coexistence of jadeite and omphacite in an eclogite-facies metaquartz diorite from the southern Sesia Zone, Western Alps, Italy. Journal of the Mineralogical and Petrological Sciences, 100, 70-84.
McBirney A.R. (1963) Geology of a part of the Central Guatemalan cordillera. University of California Publications in Geological Sciences 38, 177-242.
McBirney, A.R., Aoki, K.-I., and Bass, M. (1967) Eclogites and jadeite from the Motagua fault zone, Guatemala. American Mineralogist 52, 908-918.
Nassau, K. and Shigley, J.E. (1987) A study of the General Electric synthetic jadeite. Gems & Gemology 23, 1, 27-35.

Nyunt, T.T., Theye, T., and Massonne, H.-J. (2009) Na-rich vesuvianite in jadeitite of the Tawmaw jade district, northern Myanmar. Periodico di Mineralogia 78(3), 5-18.

Oberhänsli, R., Bousquet, R., Moinzadeh, H., Moazzen M, and Arvin, M. (2007) The field of stability of blue jadeite: A new occurrence of jadeitite from Sorkhan, Iran, as a case study. The Canadian Mineralogist 45, 1705-1713.

Oh, C.W., and Liou, J.G. (1998) A petrogenetic grid for eclogite and related facies under high-pressure metamorphism. Island Arc 7, 36-51.

Ortega-Gutiérrez, F., Solari, L.A., Solé, J., Martens, U., Gómez-Tuena, A. Morán-Ical, S., Reyes-Salas, M. and Ortega-Obregón, C. (2004) Polyphase, high-temperature eclogite-facies metamorphism in the Chaucús complex, central Guatemala: Petrology geochronology and tectonic implications. Inter. Geol. Review 46:5, 445-470.

Ouyang, Q. (2001) Characteristics of violet jadeite jade and its coloration mechanism. Baoshi He Baoshixue Zazhi 3**(**1), 1-6.

Peacock, S.M. (1993) The importance of blueschist → eclogite dehydration reactions in subducting oceanic crust. Geol. Soc. Am. Bull., 105: 684-694.

Pouchou, J.L. & Pichoir, F. (1991): Quantitative Analysis of Homogenous or Stratified Microvolumes Applying the Model "PAP". *In* Electron Probe Quantitation (K.F.K. Heinrich & D.E. Newbury, eds.). Plenum Press, New York, 31-75.

Schiffman, P., & Liou, L. (1980) Synthesis and Stability Relations of Mg-Al Pumpellyite, $Ca_4Al_5MgSi_6O_{21}(OH)_7$. Journal of Petrology 21, 441-474.

Seitz, R., Harlow, G.E., Sisson, V.B., and Taube, K.E. (2001) 'Olmec Blue' and Formative jade sources: new discoveries in Guatemala. Antiquity 87, 687-688.

Silva, Z.C.G. da (1967) Studies on jadeites and albites from Guatemala. M.A. thesis: Rice University.

Silva, Z.C.G. da (1970) Origin of albitites from eastern Guatemala: Boletim dos Servicos de Geologia e Minas (Brazil), no. 22, 23-32.

Sorensen, S., Harlow, G.E. & Rumble, D. (2006a) The origin of jadeitite-forming subduction zone fluids: CL-guided SIMS oxygen isotope and trace element evidence. *Am. Mineral.* **91**, 979-996.

Sorensen, S.S., Sisson V.B., Harlow, G.E., Avé Lallemant, H.G. (2005) Geochemistry of a jadeitite-serpentinite contact, Guatemala. *Geol. Soc. Am. Abs. w/ Program*, 37(5), 125.

Sorensen, S.S., Sisson V.B., Harlow, G.E., Avé Lallemant, H.G. (2010) Element transport and residence sites during subduction zone metasomatism: Evidence from a jadeitite-serpentinite contact, Guatemala. International Geology Review DOI: 10.1080/00206810903211963.

Taube, K.A., Sisson, V.B., Seitz, R., and Harlow, G.E. (2004) The sourcing of Mesoamerican jade: Expanded geological reconnaissance in the Motagua Region, Guatemala. In: Olmec Art and Dumbarton Oaks. Karl A. Taube, Pre-Columbian Art at Dumbarton Oaks, No. 2, Dumbarton Oaks, Washington, 246p; 203-228.

Tsujimori, T., Liou, J.G. & Coleman, R.G. (2004): Comparison of two contrasting eclogites from the Motagua fault zone, Guatemala: Southern lawsonite eclogite versus northern zoisite eclogite. *Geol. Soc. Am. Abstr. Program, Annual Meeting*, **36(5),** 136.

Tsujimori T., Liou J. G., Coleman R. G. 2004 A pictorial introduction to coarse-grained symplectites in low-temperature jadeitite from Guatemala. Journal of Geological Society of Japan, 110, XVII-XVIII.

Tsujimori, T., Liou, J.G., and Coleman, R.G. (2005) Coexisting retrograde jadeite and

omphacite in a jadeite-bearing lawsonite eclogite from the Motagua Fault Zone, Guatemala. American Mineralogist 90, 836-842.

Tsujimori, T., Sisson, V.B., Liou, J.G., Harlow, G.E. & Sorensen, S.S. (2006a) Petrologic characterization of Guatemala lawsonite eclogite: Eclogitization of subducted oceanic crust in a cold subduction zone, in Hacker, B.R., McClelland, W.C., Liou, J.G., editors, Ultrahigh pressure metamorphism: Deep continental subduction, GSA Spec Publication no. 403, 147-168.

Tsujimori, T., Sisson, V.B., Liou, J.G., Harlow, G.E. & Sorensen, S.S (2006b) Very-low-temperature record of the subduction process: A review of worldwide lawsonite eclogites: Lithos, v, 92, no. 3-4, p. 609-624.

van den Boom, G. (1972) Petrofazielle Gliedrung des metamorphen Grudgebirges in der Sierra de Chuacús, Guatemala. Beihefte Geologisches Jahrbuch 122, 5-49.

Yui, T-F., Maki, K., Usuki, T., Lan, C-Y., Martens, U., Wu, C-M., Wu, T-W., & Liou, J.G. (2010) Genesis of Guatemala jadeitite and related fluid characteristics: Insight from zircon. Chemical Geology 270, 45-55.

Figures

Figure 1. Regional map showing the location of jadeitite occurrences along the Motagua Valley of central Guatemala. Serpentinite bodies are differentiated between lizardite-dominant thrust blocks (ophiolitic) andantigorite-dominant HPLT mélange. Late Cretaceous – Early Tertiary granite bodies in the Chortís block are shown with hachures. The area in Fig. 3 is defined by the outlined rectangle in lower portion of the figure.

Figure 2. Broken jadeitite blocks sitting on serpentinite subsurface, Piedra Parada Dos Ríos, El Cimiento Quad. (9.4 km NNW of the mouth of Río La Palmilla, 300 m from that river). The accumulation of smaller boulders at the bases of trees were placed there by jaderos.

Figure 3. Geological map of area of HP-LT sources south of the Motagua fault, showing the general location of Carrizal Grande, La Ceiba, and La Ensenada; Manzanal, the first-described location north of the Motagua fault (Cabañas fault) is also shown. See the box in Fig. 1 for the location of this map. The base map is derived from a revision of an unpublished map by T. Donnelly and coworkers (Sisson *et al.* in prep.). Formation abbreviations: chm – Chuacús marble; chsa – San Agustín formation; Ket – El Tambor fm.; Kti – granite plutons; lom – Las Ovejas marble; Qa – Quaternary alluvium; s – Serpentinite, including mélange lithologies in most cases, but m – mélange, e – eclogite and b – blueschist shown near Carrizal Grande; Tv – Tertiary volcanics.

Figure 4. Photographs of jadeitite hand-samples: **A.** slab of whitish coarse-grained jadeitite: MVE04-44-2, Quebrada de los Pescaditos, 2.3 cm wide; **B.** slab of lavender jadeitite with Pmp at rim: MVE07B-19-1, near Saltán, 3 cm across; **C.** polished slice of jadeitite w/ large Ph grains and veins of blue-green Omp: VM02-1, Quebrada Seca, Carrizal Grande, 15 cm across; **D.** polished jadeitite showing mottled dark green body cut by fractures and veins of Cym and vesuvianite + Cym: MVE02-17-5, La Ceiba, 3 cm across; **E.** Sawn block of Pmp-jadeitite cut by a vein of brown chloritite: MVE03-76-4, Quebrada La Peña, La Ensenada, sawn surface is 20 cm across; **F**. slab of white-green medium-grained jadeitite with zones of translucent blue-greenish microcrystalline texture: MVJ84-10-1, Manzanal, ~14 cm across.

Figure 5. Photomicrographs: **A.** BSE image of jadeitite showing cryptic-zoned grains filled with inclusions of Anl, Ab, Pg, Omp, and now-empty fluid inclusions; rims can be relatively free of inclusions and irregular grain boundaries are decorated with the minerals found in the inclusions: MVE03-82-3, El Mapache; **B.** Photomicrograph (plane light, 2 mm across) of radiating Jd grains: MVE02-39-5, Pica Pica; **C.** BSE image of Ab-Pmp selvage with Grs stringers, Sr-Zo prisms, and Kfs-Pheng intergrowths on a jadeitite: MVE07B-19-1, near Saltán; **D**. BSE image of jadeitite showing Jd with many blebby Omp inclusions and a zone with more abundant fluid inclusion voids and Qtz inclusions: MVE04-14-6, Quebrada Seca; **E.** Close-up of area with Qtz shown in previous image; **F.** BSE image of Jd grains (center) with inclusions of Qtz and Ttn: MVE07-9, Carrizal Grande; **G.** BSE image of blue Omp vein cutting jadeitite; Jd exhibits cryptic zoning and overgrowth of Omp; in vein two generations of Omp are apparent: KT02-3, Quebrada Seca, Carrizal Grande; **H**. BSE image of a latticework-textured Ttn typical of an association with late Omp in jadeitite from south of the MF: JJE01-3-1, Quebrada El Silencio, Carrizal Grande; **I.** BSE image of Ttn-apatite intergrowth and Jd grains surrounded by islets of

Omp + Di in a matrix of Qtz: MVE02-15-10, Quebrada Seca, Carrizal Grande; **J.** BSE image of Jd grains with small inclusions of Qtz, Omp, and fluids toward cores and small zircons (brightest) elsewhere and a large Zrn at center: MVE02-17-5, La Ceiba; **K.** BSE image of a vein cutting jadeitite with Qtz (dark gray) and vesuvianite (light gray) in the center and Cym (white) at the edges: MVE02-17-5, La Ceiba; **L**. BSE image of a jadeitite (dark gray) cut by vein of Pmp (light gray) and Grs (white): MVE04-20-1 La Ensenada; **M.** Cathodoluminescence (CL) image of same area as in previous image with Grs (bright), inclusions of Pmp (black) and Jd (mottled bright)–subtle and sharp zoning of Grs is visible; **N.** BSE image of multiple stages (at least 2) of zoning from Jd-rich-to-Jd-poor (darker to lighter) composition of Jd: JJE01-3-1, Quebrada El Silencio, Carrizal Grande.

Figure 6 Plot of pyroxene compositions (molar components) in jadeitites. **A.** Samples north of the Motagua Fault. A1 – Western most: MVE02-44-1, MVE06-X-1, MVE06-X-2, MVE07-1, MVE07-5, & MVE07B-19-6. A2 – Central zone: MVE02-4-3, MVE02-39-5, MVE02-39-6, MVE07B-3-1, MVE07B-3-2 & MVJ84-9C. A3 – Eastern most: MVR07-23C, MVR07-23D, MVR0724C & MVR07-25C. **B.** Samples south of the MF. B1 – Carrizal Grande: JJE01-3-1, JJE01-3-2; JJE01-3-4, MVE02-8-5, MVE02-8-6 & MVE04-14-6. B2 – La Ceiba: MVE02-15-6, MVE02-15-10, MVE02-17-5, MVE03-77-1. B3 – La Ensenada: 108355, MVE03-76-5, MVE04-20-1, MVE04-20-3 & MVE04-21-7. Broad lines are representative of the zoning in Jd and Omp; individual compositions may scatter more broadly about the line but the width is indicative of the most prominent trend and the range of scatter. However, where the lines will obscure one another, lines may be thinner just for clarity. Fine lines and colored dots represent adjacent compositions of Jd and Omp. Temperature estimates are derived from pseudobinary section solvi calculations (García-Casco et al. 2009) for nearest Jd to Di_{100}, $Di_{90}Hd_5Ae_5$, $Di_{80}Hd_{10}Ae_{10}$, or $Di_{70}Hd_{15}Ae_{15}$ section.

Figure 7 Plot of pyroxene components from microprobe traverses of grains, overgrowths and veins in jadeitite. BSE images show traverse (+ sign at ends) and phase labels. **A.** Traverse across Jd grain with cryptically zoned interior and a more Di-rich overgrowth: MVE04-44-1, Quebrada de los Pescaditos; **B.** Traverse across Jd grain with relatively uniform interior containing inclusions toward diopsidic rim: MVR07-23C, Aldea Las Cruces; **C.** Traverse of a Omp vein in a jadeitite: MVJ84-12-2, Río La Palmilla; **D.** Traverse of Omp overgrowth on Jd MVE02-39-5, Pica Pica; **E.** Traverse of rhythmic overgrowths of Jd-rich and Jd-poorer compositions in MVE04-15-3, La Ceiba.

Figure 8 Plot of P-T grid with estimates for jadeitite formation. Conditions north of the fault (N of MF) are shown in green with the singular conditions at Saltán shown at the lower-left end of the distribution. Conditions south of the fault are shown in blue-green for Carrizal Grande (C.G. – S of MF), an outlined area for La Ceiba (Ceiba), and in pink for La Ensenada (Ensenada). Narrower colored bands show the temperature range inferred from pyroxene compositions alone in the assemblage space consistent with the mineralogy. The area around "Albitite" is the greenschist condition for the albitite/alteration of jadeitites from north of the MF. A facies grid for metabasalts that is a hybridization of Oh & Liou(1998) and Peacock (1993) is shown for reference; facies symbols are ZE – zeolite, PA – pumpellyite actinolite, GS – greenschist, AM – amphibolite, EpA – epidote amphibolite, EpB – epidote blueschist, LwsB – lawsonite blueschist, AmpEC – amphibole eclogite, ZoEC, zoisite eclogite, and LwsEC – lawsonite eclogite.

Reactions are from Harlow (1994) plus Pmp calculations from GeoCalc (Berman *et al*. 1987, Berman 1988, 1991). Reactions defined by an integer are (1) 4 Lws + 2 Anl = Ab + Pg + 2 Czo + 8 W; (2) 4 Lws +2 Jd = Ab + Pg+ 2 Czo + 6 W; (3) 4 Lws + Jd = Qtz + Pg + 2 Czo; (4) 4 Lws + Ab = 2 Qtz + Pg + 2Czo + 6 W; (5) 3 Ab + 4 Pmp = 2 Jd + 6 Czo + Pg + 4 Di + 10 W.

Table 1.	Locality	N.Latitude	W.Longitude	Description	Jd	Omp	Ab	Anl	Wm	Amp	Grt	Pmp	Zo	Lws	Apt	Rt	Ttn	Zrn	Qtz	Chl	Other
NORTH of MF																					
Western Region																					
MVE07B-19-1	Q nr. Saltán	14.884º	90.595º	Lavender jadeitite	x		x		Ms		Grs	x	Sr-Zo				x	x			Kfs
MVE07B-19-4	Q nr. Saltán	14.884º	90.595º	Lavender jadeitite	x		x		Ms, Ph		Grs	x	Sr-Zo				x				Ves, Kfs?
MVE07B-19-6	Q nr. Saltán	14.884º	90.595º	Jadeite metabasite?	x	x	x		Ba-Ph				Czo			?	x			x	
MVE07B-X-2	nr. Saltán	14.884º ?	90.595º ?	Pale-green jadeitite	x	x	x	x													
MVE06-X-1	Pachalum	14.884º ?	90.595º ?	White jadeitite	x	x	x		Prs	Mtar							x	x			Ne, Gph
MVE07-1	El Chol?	14.892º ?	90.549º ?	White jadeitite	x	x	x										x	x			
MVE07-5	El Chol?	14.892º ?	90.549º ?	Yellowish-green jadeitite	x	x	x		Prs				Al				x				
MVE06-4-3	Granados	14.892º	90.549º	White albitized jadeitite		?	x	?	x	Tr							x				
MVE04-44-1	Q. Los Pescaditos	14.852º	90.444º	White jadeitite w/ emerald green zones	x	x	x	x	Pg,Ph,Prs				Czo								Bnl,Ne
MVE04-44-2	Q. Los Pescaditos	14.852º	90.444º	White jadeitite	x	x	x	x	Pg				Czo				x				Ne
MVE04-44-4	Q. Los Pescaditos	14.852º	90.444º	White jadeitite	x	x	x	x	Pg,Prs				Czo				x				Bnl,Ne
Central Region																					
MVE04-30-1	CA 7, Morazán	14.904º	90.169º	White albitized jadeitite	x	x	x	?	Ba-Ph								x			x	Kfs,Cln?
MVE06-13-4	Río Comaja	14.944º	90.056º	Grayish jadeitite	x	x	x	x													
R-18	Guat I (Río Comaja)	14.944º	90.056º	Dark blue-green omphacitite	x	x	x		Ph	?	Sps-Grs-Alm		Al				x			x	Py,Cpy
MVE02-39-5	Pica pica	14.931º	89.961º	Greenish white jadeitite	x	x	x	x	Pg				x			x	x	x			
MVE02-39-6	Pica pica	14.931º	89.961º	Greenish white jadeitite	x	x	x	x	Phl,Ph				Czo								Ne?
MVE07-2	Pica pica	14.931º	89.961º	White jadeitite	x		x	x	Ms,Ph				Zo/Czo				x				Kfs
MVE03-81-3	El Mapache	15.008º	89.863º	Med. green jadeitite	x	x	x	x	Prs	Mtar			x				x				Unk w/ vein
MVE03-82-3	El Mapache	15.007º	89.864º	Med. green jadeitite w/ veins	x	x	x	x	Pg	Mtar											
MVE04-24-4	above Dos Rios	15.020º	89.802º	White jadeitite w/veins	x	x	x	x	Pg	Mtar			Zo								
MVE04-25-6	Piedra Parada	15.012º	89.811º	Green omphacitite		x	x		Phl								x				
MVE07-4	Los Vados, El Jute	14.977º	83.835º	Dark green omphacitite	x	x	x								x						
MVE07-7	Estancia de La Virgen	14.941º	89.885º	Omp-Jadeitite	x	x	x	x		Mtar							x	x			
ZC20	NW Manzanal	14.939º	89.871º	Med. green jadeitite	x	x				Ftar	Alm		Czo,Al				x				
MVJ84-3-4	Manzanal	14.942º	89.852º	White jadeitite	x		x	x													
MVE04-26-2	w Río Uyus	14.941º	89.836º	White-green jadeitite	x	x	x	x	Pg				x				x				
NHMLAC20368	Guat. I	15º	89.8º	Green omphacitite	x	x	x		Pg,Phl								x	x		x	K-Bafs
MVJ87-8-1	Guat. I	15º	89.8º	Green Omphacitite	x	x	x	x	Ph,Pg,Phl				x		x	x	x				Kfs
MVJ87-8-2	Guat. I	15º	89.8º	Light blue-green jadeitite	x																
R-11	Guat. I	15º	89.8º	"Olmec Blue" jadeitite	x		x	x	Pg, Prs				x		x		x				
RSJ00-2	El Ciprés	15.073º	89.796º	Light green jadeitite	x	x	x		Prs?, ?								x				
RSJ00-3	El Ciprés	15.073º	89.796º	Med. Blue-green jadeitite	x	x	x		Pg		Grs						x	x			
RSJ00-6	El Ciprés	15.073º	89.796º	Med. green jadeitite	x	x			Phl,Pg, Prs	Mtar			Czo				x				
RSJ00-7	El Ciprés	15.073º	89.796º	Med. green jadeitite	x	x	x										x	x			
RSJ01-1	El Ciprés	15.073º	89.796º	Pale green jadeitite																	
MVJ84-51-3	N. of Q. Escorpión	14.99º	89.787º	White-green jadeitite vein	x	x	x		Pg	Mtar			x				x				
RSJ01-8	nr Río La Palmilla	14.99º	89.787º	Pale green jadeitite w/ emerald green zones																	
MVJ84-9C-2	Río La Palmilla	14.99º	89.787º	Greenish white jadeitite	x	x	x	x	Pg,Prs	Mtar			Zo				x				
MVJ84-12-2	Río La Palmilla	14.99º	89.787º		x	x	x										x				
MVJ84-44-2	Río La Palmilla	14.99º	89.787º	Green omphacitite		x	x			Ftar					x		x				Cpy
MVE07-10	Río La Palmilla	14.99º	89.787º	Greenish white jadeitite	x	x	x	x													
MVJ84-29-2	Usumatlán	14.962º	89.762º	Bluish gray jadeitite	x	x	x		Pg,Phl	Mtar							x	x			Gph
MVE07B-3-1	Cerro Colorado	14.965º	89.759º	Green micaceous jadeitite	x	x	x		Phl,Ph,Pg				Czo					x			Hm, Br
MVE07B-3-2	Cerro Colorado	14.965º	89.759º	Light green jadeitite w/ red spots	x	x	x	x	Ph				Czo					x			Hm, Br
MVE07-8	Río Teculután	15.044º	89.748º	Dark green omphacitite	x	x	x			Ftar							x				
MVE02-2-5	Panaluya-Río Hondo	15.052º	89.59º	Green white jadeitite	x	x	x	x	Pg	Mtar					x		x	x			Bnl
MVE02-4-3	Panaluya-Río Hondo	15.032º	89.621º	Greenish white jadeitite	x	x	x	x	Pg,Bio				x								
MVE07-3	Río Hondo	15.052º	89.59º	Light green jadeitite	x	x							Czo				?	x			Bnl

Table 1 (cont).	Locality	N.Latitude	W.Longitude	Description	Jd	Omp	Ab	Anl	Wm	Amp	Grt	Pmp	Zo	Lws	Apt	Rt	Ttn	Zrn	Qtz	Chl	Other
NORTH of MF																					
Eastern Region																					
MVR07-25C	Rosario	16.182º	88.861º	Jadeitite-omphacitite	x	x	x	x	Ph,Pg								x	x	?		gersdorfite
MVR07-23C	Aldea Las Cruces	15.532º	88.829º	Med. green jadeitite	x	x	x	x	Pg,Ms,Phl				Czo-Zo				x				
MVR07-23D	Aldea Las Cruces	15.532º	88.829º	Med. green jadeitite	x	x	x	x	Ph,Pg								x	x			
MVR07-24C	Rosario	15.541º	88.829º	Light green jadeitite	x	x	x	x	Pg,Ph,Phl												
SOUTH of MF																					
Carrizal Grande																					
JJE01-3-1	S. Q. El Silencio	14.778º	89.893º	Dark-green Lws-jadeitite	x	x	x	x	Ph,Bio					x		x	x	x	x		
JJE01-3-2	S. Q. El Silencio	14.778º	89.893º	Med. green jadeitite	x	x	x	x	Ph,Bio								x	x	x	x	
JJE01-3-4	S. Q. El Silencio	14.778º	89.893º	Med. green jadeitite	x	x			Ph	Gln						x	x	x	?		
MVE02-8-5	Q. El Silencio	14.779º	89.888º	Light green Ph-jadeitite	x	x			Ph							x	x	x	x		
MVE02-8-6	Q. El Silencio	14.779º	89.888º	Light green Ph-jadeitite	x	x	x		Ph				Al			x	x	x	x		Mon
MVE07-9	Carrizal Grande	14.771º	89.886º	Light green jadeitite	x	x			Ph				x					x	x		
RSJ00-4	Q. del Mico	14.770º	89.882º	"Olmec-Blue" jadeitite	x	x	x		Ph				Czo,Al			x	x	x			Mon
MVE06-17-2	Q. del Mico	14.770º	89.882º	Grt jadeitite	x	x			Ph	Gln?	Alm		Czo	x		x	x	x	x		Gph
MVE03-80-1	Q. del Mico	14.772º	89.878º	Drk-green omphacitite		x, Di	x		Ph						x	x	x	x	?	x	Sr-Cc
MVE04-14-6	Q. Seca	14.768º	89.874º	Med. green jadeitite	x	x	x	x	Ph								x	x	x		Cym,
KT02-3b	Q. Seca	14.77º	89.873º	Blue to blue-green jadeitite	x	x							Al				x	x			Mon
RSJ01-X-1	Q. Seca	14.77º	89.873º	Green & blue-green omphacitite		x											x				
VM02-1	Q. Seca	14.77º	89.873º	Blue-green jadeititew/ blue vein	x	x											x				
MVE02-15-5	Q. Seca	14.77º	89.873º	Lws-omphacitite		x							x	x		x	x	x		x	Ba-Kfs
MVE02-15-6	Q. Seca	14.77º	89.873º	Dark green omphacitite	x	x	x		Ph								x	x	x		Kfs
MVE02-15-10	Q. Seca	14.77º	89.873º	Dark gray jadeitite	x	x, Di	x		Ph	Act			?		x		x	x	x		
MVE02-14-5	Q. del Mico	14.776º	89.868º	Chromian omphacite-glaucophane rock		x	x			Gln, Act											
JJE01-6-1	Río La Puerta	14.777º	89.863º	Dark-green Ph-Lws-jadeitite-omphacitite	x	x			Ph				?	x		x	x	x			
JJE01-6-2	Río La Puerta	14.777º	89.863º	Pheng-Omphacitite		x			Ph				x,al		x	x	x		x	x	Cc?
RSJ00-1	Río Jalapa	14.844	89.821	Speckled Olmec-blue	x	x	x		Ph								x				
JJE01-7-5	Río El Tambor	14.85º	89.815º	Nephrite / Diopsidite		Di				Tr	Grs		Al?								Cm, clay
JJE01-X-3	Río El Tambor	14.85º	89.815º	Med green Lws-jadeitite	x	x	x	x	Ba-Ph	Gln				x	x	x	x	x	x		
La Ceiba																					
MVE03-77-1	La Ceiba	14.772º	89.828º	Dark green jadeite omphacitite	x	x	x		Ph				Al				x		x	x	
MVE03-77-3	La Ceiba	14.772º	89.828º	Dark green jadeite-omphacitite	x	x	x		Ph								x	x		x	Cln,Kfs
MVE03-77-4	La Ceiba	14.772º	89.828º	Dark green jadeite-omphacitite	x	x		x	Bio				Al		x				x		Cym,Hyl,Pect
MVE03-77-5-1	La Ceiba	14.772º	89.828º	Qtz jadeitite	x	x	x		Ph	Act							x		x		
MVE04-15-3	La Ceiba	14.771º	89.826º	Grn-Mauve jadeitite	x	x	x						REE-Czo		x		x	x	x		Cym, Uran
MVE02-17-5	La Ceiba	14.771º	89.826º	Med. Green jadeitite	x	x		x									x	x	x		Cym,Ves
La Ensenada																					
MVE03-76-3a	Qbda La Peña	14.822º	89.815º	brown prt/"Lila" jadeitite		x	x					x					x	x		x	
MVE03-76-3b	Qbda La Peña	14.822º	89.815º	Lavender prt/"Lila" jadeitite	x	x	x		Ba-Ms		Grs	x	Zo?				x	x		x	Cln
MVE03-76-5	Qbda La Peña	14.822º	89.815º	"Lila" jadeitite	x	x	x				Grs	x			x		x				
108353a	Qbda La Peña	14.822º	89.815º	"Rainbow" jadeitite	x	x	x					x			x	x	x	x		x	
108353b	Qbda La Peña	14.822º	89.815º	"Rainbow" jadeitite	x	x	x					x				x	x				
108354	Qbda La Peña	14.822º	89.815º	"Rainbow" jadeitite	x	x						x					x				
108355	Qbda La Peña	14.822º	89.815º	Pale green jadeitite	x		x		Ba-Ph			x					x				
MVE04-20-1	Qbda La Peña	14.824º	89.814º	Mauve/orange jadeitite	x	x	x		Phl		Grs	x			x		x				
MVE04-20-3	Qbda La Peña	14.824º	89.814º	White-Blue jadeitite	x		x		Ph		Grs	x	?			x	x	x			
MVE04-21-7	E of San Diego Rd	14.837º	89.79º	Wh-Or-Grn "Rainbow" jadeitite	x	x,Di	x				Grs						x		x		

JJE = Jalapa (southern) samples; MVJ = (northern) Motagua samples; RSJ = Russell Seitz jadeitite sample; R = Ridinger, Jade S.A.; Locality Guat 1 represents samples acquired from jade companies without specific location other than the central area north of the MF.

Ab - albite; Al – allanite, Amp - amphibole (Act – actinolite, Eck – eckermannite, Ftar - ferro-taramite*, Mtar – magnesiotaramite*, Gln – glaucophane, Hb – hornblende, Tr – tremolite); Anl – analcime; Apt – apatite; Bio – biotite; Bnl – banalsite; Eck – eckermannite, Ftar - ferro-taramite*, Mtar – magnesiotaramite*, Gln – glaucophane, Hb – hornblende, Tr – tremolite); Anl – analcime; Apt – apatite; Bio – biotite; Bnl – banalsite; Br – barite; Cc – calcite/aragonite; Cln – celsian; Cpy – chalcopyrite; Chl – chlorite; Clc – clinochlore; Cm – chromite; Cnc – cancrinite; Cpx – clinopyroxene (Ag – augite; Di – diopside; Hd – hedenbergite; Omp – omphacite); Cpy – chalcopyrite; Cus – mixed Cu sulfides; Cym – cymrite; Czo – clinozoisite; Di – diopside; Gph – graphite; Grs – grossular; Hd – hedenbergite; Hgrs – hydrogrossular; Hm – hematite; Hyl – hyalophane; Ilm – ilmenite; Jd – jadeite; Ko – kosmochlor; Lws – lawsonite; Kfs – K-spar; Kfs – K-spar; Mgt – magnetite; Mon – monazite; Mu – muscovite; Ne – nepheline; Omp – omphacite; Pdy – polydimite; Pg – paragonite; Pnt – pentlandite; Prs – preiswerkite; Po – pyrrhotite; Py – pyrite; Qtz – quartz; Rt – rutile; Tlc – talc; Ttn – titanite; Unk – unknown;
Uran – uraninite; Ver – vermiculite; Ves – vesuvianite; W – H2O Wm – white mica (Pg – paragonite, Ph – phengite, Phl - phlogopite); Zeo – zeolite; Zo – zoisite; Zrn – zircon; ? – Suspected but unsubstantiated mineral due to inadequate data

* The nomenclature of amphiboles is in transition, so we have chosen to explicitly distinguish ferro-taramite (new) from magnesiotaramite (old; actually alumino-magnesiotaramite to become taramite).

Table 2: Representative pyroxene compositions in jadeitite from **north** of the Motagua Fault

	West						Central		East			
	Jd	Jd	Omp	Aug	Jd	Omp	Jd	Omp	Jd	Omp	Jd	Omp
	MVE07B	MVE06	MVE06	MVE07	MVE04	MVE04	MVE07B	MVE07B	MVR07	MVR07	MVR07	MVR07
	19-4	X-1	X-1	1	44-1	44-1	3-1	3-1	23C	23C	23D	23D
SiO_2	59.83	59.48	56.90	54.57	59.65	56.42	57.50	59.84	59.75	56.82	59.75	56.39
TiO_2	0.07	0.08	0.30	0.69	0.03	0.03	0.05	0.05	0.10	0.05	0.04	0.08
Al_2O_3	25.30	22.47	14.12	6.89	24.31	12.26	12.38	23.83	25.21	11.98	24.18	12.24
Cr_2O_3	0.00	0.01	0.00	0.02	0.07	0.00	0.00	0.03	0.00	0.03	0.01	0.03
Fe_2O_3	0.00	0.53	3.87	9.33	0.79	4.11	2.66	0.40	0.00	1.12	0.44	5.90
FeO	0.03	1.17	1.84	0.04	0.00	0.00	0.22	0.18	0.14	2.73	0.67	10.10
MnO	0.00	0.05	0.37	0.32	0.01	0.21	0.10	0.01	0.00	0.00	0.00	0.00
MgO	0.03	1.18	5.37	8.43	0.28	7.29	8.00	0.83	0.03	7.26	0.30	3.51
CaO	0.02	1.61	7.70	12.28	0.49	10.87	11.70	1.02	0.20	12.29	0.70	2.56
BaO	0.01	0.00	0.00	0.00	0.00	0.01	0.07	0.00	0.02	0.00	0.00	0.00
Na_2O	15.40	14.20	10.06	7.47	15.39	8.91	8.46	14.80	15.23	7.89	14.96	8.93
K_2O	0.01	0.00	0.01	0.04	0.02	0.01	0.00	0.00	0.01	0.00	0.01	0.03
TOTAL	100.70	100.77	100.54	100.09	101.04	100.12	101.15	100.99	100.69	100.17	101.05	99.77
Cations per 6 O												
Si	2.000	2.009	1.991	1.970	1.997	1.985	1.995	2.004	1.999	2.004	2.002	2.002
$^{[4]}Al$	0.000	0.000	0.009	0.030	0.003	0.015	0.005	0.000	0.001	0.000	0.000	0.000
Ti	0.002	0.002	0.008	0.019	0.001	0.001	0.001	0.001	0.003	0.001	0.001	0.002
$^{[6]}Al$	0.996	0.894	0.574	0.263	0.957	0.493	0.501	0.940	0.992	0.498	0.955	0.512
Cr	0.000	0.000	0.000	0.001	0.002	0.000	0.000	0.010	0.000	0.001	0.000	0.001
Fe^{3+}	0.000	0.014	0.102	0.254	0.020	0.109	0.070	0.005	0.000	0.030	0.011	0.094
Fe^{2+}	0.001	0.033	0.054	0.001	0.000	0.000	0.006	0.000	0.004	0.080	0.019	0.076
Mn	0.000	0.001	0.011	0.010	0.000	0.006	0.003	0.000	0.000	0.000	0.000	0.000
Mg	0.001	0.060	0.280	0.454	0.014	0.383	0.414	0.041	0.001	0.382	0.015	0.312
Ca	0.001	0.058	0.289	0.475	0.018	0.410	0.435	0.037	0.007	0.464	0.025	0.384
Ba	0.000	0.000	0.000	0.000	0.000	0.000	0.001	0.000	0.000	0.000	0.000	0.000
Na	0.998	0.929	0.682	0.523	0.999	0.608	0.569	0.961	0.988	0.540	0.972	0.615
K	0.000	0.000	0.000	0.002	0.001	0.000	0.000	0.000	0.000	0.000	0.000	0.001
SUM	4.000	4.000	4.000	4.000	4.011	4.010	4.000	4.000	3.996	4.000	4.000	4.000
		Pair		vein	Pair		Pair		Pair		Pair	
Jd (%)	99.6	89	57	25	96	48	50	94	99	50	96	51
Di	0.1	~4	28	44	1.4	38	41	4	0	38	1.5	31
Hd	<0.1	~2	>1	0	0	1	1.6	1	0	8	0.9	7
Ae	0.0	>1.4	10	25	2	11	7	1	0	3	1.1	9
Quad	0.2	8	34	46	1.4	40	43	4	1	46	2.9	38
MMF	0.6	0.64	0.81	0.98	0.98	0.98	0.99	1.0	0.28	0.83	0.45	0.80
MMF_T	0.6	0.56	0.63	0.63	0.77	0.41	0.73	0.89	0.28	0.78	0.33	0.65

MMF= $Mg/(Mg+Fe^{2+})$, $MMF_T = Mg/(Mg+Fe_{total})$

Table 2–continued: Representative pyroxene compositions in jadeitite from **south** of the Motagua Fault

	Carrizal Grande						La Ceiba					La Ensenada	
	Jd	Jd	Omp	Jd	Omp	Bl-Omp	Jd	Omp	Jd	Omp	Di	Jd	Omp
	MVE04	MVE04	MVE04	MVE02	MVE02	KT02	MVE02	MVE02	MVE03	MVE03	MVE02	MVE04	MVE04
	14-6	14-6	14-6	8-6	8-6	3	15-6	15-6	77-1	77-1	15-10	20-1	20-1
SiO_2	59.30	58.88	54.17	59.55	57.13	56.74	58.96	56.66	57.88	54.36	55.12	58.98	56.87
TiO_2	0.03	0.03	0.14	0.02	0.15	1.86	0.08	0.11	0.26	0.05	0.14	0.47	0.09
Al_2O_3	25.13	22.17	8.34	24.48	12.03	9.81	23.67	14.01	18.69	10.06	2.54	25.31	12.84
Cr_2O_3	0.00	0.02	0.01	0.02	0.00	0.00	0.01	0.00	0.03	0.00	0.00	0.00	0.00
Fe_2O_3	0.04	0.21	9.95	0.39	2.59	1.40	0.87	1.30	3.76	5.57	1.82	0.08	0.60
FeO	0.19	1.98	6.72	0.26	0.87	2.44	0.00	0.39	1.48	3.57	4.37	0.00	0.00
MnO	0.05	0.00	0.25	0.09	0.14	0.10	0.01	0.09	0.06	0.12	0.09	0.01	0.00
MgO	0.18	0.82	2.60	0.30	7.99	8.10	0.60	7.07	1.79	6.03	12.83	0.41	9.13
CaO	0.39	2.25	9.42	0.47	11.99	11.63	0.90	10.71	3.12	12.68	20.33	0.57	12.73
BaO	0.01	0.03	0.00	0.00	0.02	0.00	0.03	0.03	0.01	0.00	0.06	0.00	0.00
Na_2O	15.06	13.82	8.89	15.04	8.16	8.12	14.75	8.85	13.09	7.41	2.72	15.17	7.79
K_2O	0.01	0.00	0.00	0.00	0.01	0.00	0.02	0.01	0.01	0.00	0.00	0.03	0.02
Total	100.39	100.22	100.51	100.63	101.06	100.20	99.89	99.22	100.19	99.87	100.02	101.02	100.07
Cations per 6 O													
Si	1.992	2.008	1.994	1.999	1.991	2.006	1.998	1.991	2.002	1.968	2.013	1.972	1.983
$^{[4]}Al$	0.008	0.000	0.005	0.000	0.009	0.000	0.002	0.009	0.000	0.032	0.000	0.028	0.017
Ti	0.001	0.001	0.004	0.000	0.004	0.050	0.002	0.003	0.007	0.001	0.004	0.012	0.002
$^{[6]}Al$	0.987	0.891	0.356	0.969	0.485	0.409	0.943	0.572	0.762	0.397	0.109	0.969	0.511
Cr	0.000	0.000	0.000	0.000	0.000	0.000	0.000	0.000	0.001	0.000	0.000	0.000	0.000
Fe^{3+}	0.001	0.005	0.276	0.010	0.068	0.037	0.022	0.035	0.098	0.152	0.050	0.002	0.016
Fe^{2+}	0.005	0.057	0.207	0.007	0.025	0.072	0.000	0.011	0.043	0.108	0.134	0.000	0.000
Mn	0.001	0.000	0.008	0.003	0.004	0.003	0.000	0.003	0.002	0.004	0.003	0.000	0.000
Mg	0.009	0.042	0.143	0.015	0.415	0.427	0.030	0.370	0.093	0.326	0.699	0.020	0.475
Ca	0.014	0.082	0.372	0.017	0.448	0.440	0.033	0.403	0.116	0.492	0.795	0.020	0.476
Ba	0.001	0.000	0.000	0.000	0.000	0.000	0.000	0.000	0.001	0.000	0.000	0.000	0.000
Na	0.981	0.914	0.635	0.979	0.551	0.557	0.969	0.603	0.877	0.520	0.193	0.983	0.527
K	0.000	0.000	0.000	0.000	0.000	0.000	0.001	0.000	0.000	0.000	0.001	0.001	0.001
Sum	4.000	4.000	4.000	4.000	4.000	4.000	4.001	4.000	4.000	4.000	4.000	4.009	4.007
	core		Pair	Pair		*	Pair		Pair*			Pair*	
Jd (%)	98	89	36	97	48	41	94	57	76	37	11	95	50
Di	0.6	4.2	14	1.5	41	42	3	37	9	33	70	0	46
Hd	0	3.9	22	0.2	2.4	3	0.1	1.4	1.6	13	9	0	0
Ae	0.1	0.5	28	1	6.7	3.7	2.2	38	10	46	5	0.2	1.6
Quad	1	9	36	2	44	46	3.1	3.4	12	15	81	1	46
MMF	0.57	0.42	0.40	0.60	0.93	0.85	0.99	0.96	0.68	0.75	0.84	0.99	1.00
MMF_T	0.55	0.40	0.23	0.43	0.81	0.79	0.58	0.88	0.39	0.55	0.79	0.91	0.98

* $NaTi_{0.5}(Mg,Fe)_{0.5}Si_2O_6$ component = ~10% (KT02-3), 6.4% (Omp-MVE03-77-1), 5.6 & 3.4% (MVE04-20-1)

Table 3: Representative analyses of micas in jadeitite from **north** of the Motagua Fault

	Ph	Ms	Phl	Pg	Ms	Ms	Prs	Ph	Pg
	MVE07-2	MVE02-39-6	MVE02-39-6	MVE04 44-1	MVE07B 19-1	MVE07B 19-1	MVE06 X-1	MVR07 23D	MVR07 23D
SiO2	51.79	43.79	39.26	48.55	48.38	44.67	30.91	51.06	48.30
TiO_2	0.09	0.01	0.27	0.07	0.03	0.04	0.04	0.07	0.04
Cr_2O_3	0.00	0.03	0.01	0.00	0.02	0.00	0.00	0.00	0.00
Al_2O_3	26.43	36.52	18.45	38.66	35.49	35.76	35.19	27.79	39.41
Fe_2O_3*	0.00	0.00	0.00	0.00	0.00	0.00	0.00	0.00	0.00
FeO	1.41	0.14	3.29	0.40	0.02	0.32	2.48	1.31	0.48
MnO	0.03	0.09	0.42	0.00	0.00	0.00	0.50	0.00	0.00
MgO	3.95	0.18	21.63	0.26	0.25	0.72	19.16	3.72	0.35
CaO	0.01	0.26	0.09	0.12	0.00	0.01	0.06	0.00	0.14
BaO	1.34	0.02	0.55	0.19	0.21	3.76	0.03	0.79	0.06
Na_2O	0.27	0.41	0.49	7.37	0.06	0.55	7.52	0.43	6.97
K_2O	10.13	10.36	9.67	0.50	11.43	9.50	0.09	10.73	0.86
H_2O*	4.49	4.36	4.19	4.74	4.56	4.42	4.43	4.51	4.76
Total	99.96	96.17	98.33	100.87	100.45	99.75	100.41	100.41	101.37
Cations for 20 Oxygen and 4 OH*									
Si	6.914	6.023	5.614	6.140	6.359	6.065	4.183	6.785	6.081
$^{[4]}Al$	1.086	1.977	2.386	1.860	1.641	1.935	3.817	1.215	1.919
Ti	0.010	0.001	0.029	0.007	0.003	0.004	0.004	0.007	0.004
$^{[6]}Al$	3.072	3.943	0.723	3.903	3.856	3.787	1.795	3.137	3.929
Cr	0.000	0.004	0.001	0.000	0.002	0.000	0.000	0.000	0.000
Fe^{3+}	0.000	0.000	0.000	0.000	0.000	0.000	0.000	0.000	0.000
Fe^{2+}	0.158	0.016	0.393	0.043	0.002	0.036	0.280	0.146	0.051
Mn	0.003	0.010	0.051	0.000	0.000	0.000	0.057	0.000	0.000
Mg	0.786	0.037	4.611	0.050	0.049	0.146	3.865	0.737	0.066
Ca	0.001	0.038	0.014	0.017	0.000	0.001	0.009	0.000	0.019
Ba	0.070	0.001	0.031	0.009	0.011	0.200	0.001	0.041	0.003
Na	0.071	0.108	0.137	1.807	0.015	0.145	1.972	0.111	1.701
K	1.725	1.819	1.765	0.081	1.916	1.645	0.016	1.819	0.138
Total Cats	13.896	13.977	15.753	13.916	13.855	13.965	16.001	13.997	13.911
OH *	4.000	4.000	4.000	4.000	4.000	4.000	4.000	4.000	4.000
MMF	0.83	0.70	0.92	0.54	0.96	0.80	0.93	0.83	0.56

Representative analyses of micas in jadeitite from **south** of the Motagua Fault

	Ph	Ph	Ba-Ph	Ba-Ph	Bio	Ph	Phl	Ph	Ba-Ph
	MVE02	MVE02	MVE02	JJE01	JJE01	MVE03	MVE04	108355	108355
	8-5	8-5	8-5	X-3	3-2	77-5-1	20-1		
SiO_2	54.25	57.24	54.71	47.31	39.09	54.77	41.07	50.34	46.27
TiO_2	0.28	0.26	0.23	0.25	0.14	0.14	0.02	0.00	0.03
Cr_2O_3	0.00	0.01	0.01	0.00	17.49	0.00	0.00	0.08	0.07
Al_2O_3	24.78	21.07	23.75	27.90	0.00	23.40	17.91	33.09	35.90
Fe_2O_3*	0.00	0.00	0.00	0.00	0.00	0.00	0.00	0.00	0.00
FeO	3.57	1.38	2.09	1.38	15.85	1.86	1.31	0.32	0.15
MnO	0.00	0.03	0.02	0.00	0.25	0.01	0.00	0.01	0.00
MgO	3.27	6.49	4.96	3.67	13.03	5.15	23.54	1.35	0.43
CaO	0.00	0.02	0.00	0.03	0.07	0.00	0.16	0.00	0.01
BaO	0.21	0.48	1.50	6.98	0.09	1.03	0.06	0.12	2.31
Na_2O	0.13	0.00	0.05	0.19	0.10	0.12	0.15	0.06	0.22
K_2O	10.16	9.72	9.15	8.66	9.36	9.64	9.97	10.27	9.97
H_2O*	4.56	4.62	4.56	4.35	4.04	4.55	4.27	4.59	4.48
Total	101.21	101.31	101.03	100.71	99.50	100.66	98.46	100.22	99.85
Cations for 20 Oxygen and 4 (OH)*									
Si	7.135	7.435	7.191	6.529	5.796	7.214	5.765	6.583	6.192
$^{[4]}Al$	0.865	0.565	0.809	1.471	2.204	0.786	2.235	1.417	1.808
Ti	0.027	0.025	0.022	0.026	0 .016	0.014	0.002	0.000	0.003
$^{[6]}Al$	2.976	2.659	2.869	3.066	0.852	2.846	0.729	3.684	3.854
Cr	0.000	0.001	0.001	0.000	0.000	0.001	0.000	0.008	0.008
Fe^{3+}	0.000	0.000	0.000	0.000	0.000	0.000	0.000	0.000	0.000
Fe^{2+}	0.393	0.150	0.230	0.159	1.965	0.204	0.154	0.035	0.017
Mn	0.000	0.004	0.002	0.000	0.031	0.001	0.000	0.001	0.000
Mg	0.641	1.256	0.971	0.755	2.880	1.011	4.926	0.263	0.086
Ca	0.000	0.003	0.000	0.004	0.011	0.000	0.024	0.000	0.001
Ba	0.011	0.024	0.077	0.377	0.005	0.053	0.003	0.006	0.121
Na	0.033	0.000	0.012	0.052	0.028	0.030	0.040	0.016	0.057
K	1.705	1.610	1.535	1.524	1.770	1.619	1.785	1.714	1.702
Total Cats	13.786	13.733	13.721	13.965	15.559	13.780	15.663	13.727	13.850
OH *	4.000	4.000	4.000	4.000	4.000	4.000	4.000	4.000	4.000
MMF	0.62	0.89	0.81	0.83	0.59	0.83	0.97	0.88	0.84

MMF= $Mg/(Mg+Fe^{2+})$

* OH is calculated to fill univalent anion site and H_2O is back calculated from the conversion of ions to wt%.

Table 4: Representative amphibole compositions in jadeitite from Guatemala

	Tar	Tar	Ftar	Ftar	Gln	Gln	Act	Act	Act
	MVE03	MVE07	ZC-20	MVJ84	JJE01	MVE02	MVE02	MVE02	MVE03
	81-3	7	39-6	44-2	3-4	14-5	14-5	15-10	77-5-1
SiO_2	42.57	43.00	43.12	41.07	59.24	59.96	57.08	57.44	58.66
TiO_2	0.26	0.67	0.47	0.51	0.03	0.00	0.01	0.01	0.09
Cr_2O_3	0.00	0.00	–	0.00	0.00	0.03	0.00	0.02	0.08
Al_2O_3	20.17	19.34	15.28	16.34	11.61	11.88	0.31	0.26	3.37
Fe_2O_3	3.62	0.00	2.64	4.04	1.20	0.02	0.03	0.00	0.00
FeO	5.25	10.91	15.01	16.71	3.68	3.98	5.16	5.78	7.03
MnO	0.37	0.16	0.59	0.28	0.08	0.07	0.34	0.06	0.10
MgO	11.35	9.24	7.22	5.29	13.01	13.41	20.61	20.39	16.48
CaO	7.33	6.70	6.50	7.03	0.30	0.17	12.98	12.81	10.20
BaO	0.00	0.00	–	0.02	0.02	0.02	0.03	0.00	0.00
Na_2O	6.44	6.72	5.98	5.49	7.47	7.26	0.35	0.13	2.07
K_2O	0.36	0.40	0.74	0.84	0.05	0.03	0.04	0.14	0.11
H_2O*	2.10	2.06	2.01	1.98	2.22	2.24	2.14	2.15	2.18
TOTAL	99.82	99.20	99.54	99.60	98.92	99.06	99.09	99.18	100.37
Cations for 22 O + 2(OH)*									
Si	6.073	6.253	6.442	6.221	7.989	8.036	7.987	8.027	8.077
$^{[4]}Al$	1.927	1.747	1.558	1.779	0.011	0.000	0.013	0.000	0.000
$^{[6]}Al$	1.464	1.567	1.132	1.138	1.835	1.876	0.039	0.042	0.547
Ti	0.028	0.073	0.052	0.058	0.003	0.000	0.001	0.001	0.009
Cr	0.000	0.000	0.000	0.000	0.000	0.003	0.000	0.002	0.008
Fe^{3+}	0.389	0.000	0.297	0.461	0.122	0.002	0.004	0.000	0.000
Fe^{2+}	0.626	1.327	1.875	2.117	0.415	0.446	0.604	0.675	0.810
Mn	0.045	0.020	0.074	0.035	0.009	0.008	0.040	0.007	0.012
Mg	2.415	2.003	1.607	1.195	2.616	2.680	4.299	4.248	3.382
SUM C	4.966	4.990	5.037	5.004	4.999	5.015	4.986	4.975	4.769
SUM C-	0.000	0.000	0.037	0.004	0.000	0.000	0.015	0.000	0.000
Ca	1.121	1.044	1.040	1.141	0.043	1.946	0.025	1.918	1.505
Na	0.913	0.967	0.923	0.855	1.953	0.068	1.888	0.035	0.553
SUM B	2.034	2.010	2.000	2.000	1.996	2.014	1.928	1.954	2.058
Na	0.867	0.926	0.808	0.757	0.000	0.028	0.000	0.000	0.000
K	0.065	0.074	0.140	0.163	0.009	0.008	0.004	0.025	0.019
SUM A	0.932	1.001	0.948	0.920	0.009	0.036	0.004	0.025	0.019
TOTAL	15.932	16.001	15.948	15.920	15.005	15.036	14.968	14.981	14.923
OH *	2.000	2.000	2.000	2.000	2.000	2.000	2.000	2.000	2.000
MMF	0.79	0.60	0.46	0.36	0.86	0.86	0.88	0.86	0.81
MMF_T	0.70	0.60	0.43	0.32	0.83	0.86	0.88	0.86	0.81

MMF= $Mg/(Mg+Fe^{2+})$, $MMF_T = Mg/(Mg+Fe_{total})$

* OH is calculated to fill the univalent anion site, and H_2O is back calculated from the conversion of ions to wt%.

Table 5: Representative analyses of other calcic minerals in jadeitite **north** of the Motagua Fault

	Garnet			Vesuvianite	Pumpellyite	Zo	Zo	Czo	Aln
	MVE07B 19-1	ZC-20	ZC-20	MVE07B 19-4	MVE07B 19-1	MVE07B 19-4	MVE07B 19-1	MVE07B 19-1	MVE07B 19-1
SiO_2	39.42	36.22	36.40	34.43	37.48	38.78	38.01	34.79	30.94
TiO_2	0.30	0.07	0.15	1.55	0.22	0.28	0.27	0.09	0.27
Al_2O_3	21.84	21.13	20.27	17.95	26.44	32.43	31.22	25.96	18.29
Cr_2O_3	0.00	–	–	0.00	0.03	0.00	0.01	0.08	0.20=Y_2O_3
Fe_2O_3	0.74	1.36	1.13	–	–	0.23	0.75	5.41	26.62=LREE‡
FeO	0.17	17.42	22.39	1.50	2.34	–	–	–	9.55
MnO	0.48	12.55	2.98	0.00	0.08	0.00	0.00	0.10†	0.00
MgO	0.03	1.23	0.56	0.27	2.50	0.00	0.02	0.03	0.30
CaO	36.32	9.30	13.61	29.34	22.76	23.42	20.30	12.57	11.58
SrO	0.02	–	–	–	0.05	2.53	7.18	17.63	0.02
BaO	0.00	–	–	0.03	0.00	0.00	0.05	0.16	–
K_2O	0.01	0.01	0.01	0.00	0.50	0.02	0.02	0.00	–
Na_2O	0.00	0.06	0.01	1.05	0.04	0.00	0.00	0.03	–
H_2O*	–	–	–	3.64	6.65	1.94	1.90	1.75	1.56
TOTAL	99.33	99.34	97.53	89.76	99.09	99.64	99.73	98.62	99.84
Normalize	24 O	24 O	24 O	18 Si	3 Si	25 O	25 O	25 O	25 O
$^{[4]}$Si	5.977	5.855	5.950	18.	3.	5.979	5.997	5.967	5.935
$^{[4]}$Al	0.023	0.145	0.050	0.	0.	0.021	0.003	0.033	0.065
SUM Tet	6.000	6.000	6.000	18.	3.	6.0	6.0	6.0	
Ti	0.034	.009	.018	0.609	0.013	0.032	0.031	0.012	0.039
$^{[6]}$Al	3.880	3.879	3.855	11.060	2.494	5.872	5.803	5.215	4.069
Cr	0.000	–	–	0.000	0.002	0.000	0.001	0.011	0.071=Y_2O_3
Fe3+	0.085	.165	.140	–	–	0.027	0.089	0.698	1.829=LREE‡
Fe2+	0.022	2.355	3.061	0.657	0.157	–	–	–	1.532
Mn	0.061	1.718	.413	0.000	0.005	0.000	0.000	0.014†	0.000
Mg	0.006	.295	.136	0.211	0.298	0.000	0.006	0.007	0.086
Ca	5.900	1.610	2.384	16.436	1.952	3.869	3.432	2.311	2.380
SrO	0.001	–	–	–	0.002	0.226	0.657	1.753	0.002
Ba	0.000	–	–	0.000	0.000	0.000	0.003	0.011	–
Na	0.003	.019	.004	1.065	0.076	0.007	0.005	0.000	–
K	0.000	.002	.002	0.000	0.004	0.000	0.001	0.007	–
Total	15.991	16.053	16.013	48.043	8.004	16.032	16.027	16.039	16.008
OH*				12.701	1.551	2	2	2	2
H_2O*						0	0	0	0

Calcic minerals in jadeitite **south** of the Motagua Fault

	Garnet			Vesuvianite			Pumpellyite		Lawsonite	
	MVE06	MVE06	MVE04	MVE03	MVE02	MVE02	MVE03-	MVE04	JJE01	JJE01
	17-2	17-2	20-1	77-4	17-5	17-5	76-5	20-1	X-3	6-1
SiO_2	37.07	37.06	39.57	36.49	37.73	37.86	38.26	37.90	38.07	37.39
TiO_2	0.37	0.09	0.17	4.51	3.92	5.89	0.03	0.01	0.05	0.89
Al_2O_3	0.03	0.00	22.32	17.86	18.61	17.62	26.36	25.95	31.50	30.67
Cr_2O_3	20.56	20.98	0.00	0.00	0.04	0.01	0.01	0.00	0.00	0.03
Fe_2O_3	0.58	0.49	0.03	–	1.63	1.60	–	–	0.10	0.42
FeO	26.84	30.39	0.00	1.87	0	0	0.52	0.13	–	–
MnO	7.79	1.29	0.02	0.09	0.06†	0.08†	0.02	0.00	0.00	0.00
MgO	0.62	1.04	0.07	0.36	0.58	0.35	3.93	4.50	0.00	0.01
CaO	6.41	8.56	37.61	31.94	31.42	30.56	22.96	23.77	17.30	17.03
SrO	–	–	0.00	–	0.26	0.30	–	0.00	0.32	0.66
BaO	0.03	0.05	0.00	0.00	0.00	0.0	0.00	0.00	0.02	0.00
Na_2O	0.19	0.04	0.02	2.01	2.71	3.08	0.47	0.09	0.01	0.00
K_2O	0.00	0.00	0.00	0.00	0.01	0.03	0.00	0.00	0.00	0.00
H_2O*	–	–	–	2.53	3.18	3.18	7.19	6.84	11.41	11.21
TOTAL	100.49	99.98	99.83	97.67	100.00	100.39	99.75	99.18	98.78	98.31
Normalize	24 O	24 O	24 O	18 Si	18 Si	18 Si	3 Si	3 Si	4 Si	4 Si
$^{[4]}Si$	5.981	5.961	5.960	18.	18.	18.	3.	3.	4.	4.
$^{[4]}Aliv$	0.019	0.039	0.040	0.	0.	0.	0.	0.	0.	0.
SUM Tet	6.000	6.000	6.000	18.	18.	18.	3.	3.	4.	4.
$^{[6]}Si$	0.000	0.000	0.000	–	–	–	–	–	–	–
Ti	0.045	0.011	0.019	1.672	1.406	2.105	0.002	0.001	0.004	0.072
$^{[6]}Al$	3.890	3.940	3.922	10.382	10.465	9.874	2.436	2.421	3.901	3.867
Cr	0.004	0.000	0.000	0.000	0.017	0.005	0.001	0.000	0.000	0.003
Fe^{3+}	0.071	0.059	0.003	–	0.587	0.574	–	–	0.008	0.034
Fe^{2+}	3.620	4.089	0.000	0.769	0	0	0.034	0.008	–	–
Mn	1.064	0.175	0.003	0.039	0.023†	0.029†	0.002	0.000	0.000	0.000
Mg	0.148	0.249	0.017	0.267	0.414	0.247	0.459	0.530	0.000	0.002
Ca	1.108	1.475	6.070	16.882	16.059	15.568	1.929	2.016	1.947	1.952
Sr	–	–	0.000	–	0.071	0.083	–	0.000	0.020	0.041
Ba	0.002	0.003	0.000	0.000	0.000	0.000	0.000	0.000	0.001	0.000
Na	0.060	0.011	0.007	1.924	2.509	2.837	0.073	0.013	0.003	0.000
K	0.000	0.000	0.000	0.000	0.007	0.017	0.000	0.000	0.000	0.000
Total	16.011	16.014	16.042	49.935	49.340	49.340	7.936	7.990	9.884	9.972
OH*	–	–	–	8.329	9.494	9.483	1.761	1.611	4	4
H_2O*	–	–	–						2	2
	core	rim								

* OH and H_2O calculated from stoichiometry or charge balance; H_2O wt% back calculated from stoichiometry; † Fe or Mn is recalculated as trivalent. ‡ LREE = La_2O_3 (3.33 wt%, 0.236 apfu) + Ce_2O_3 (10.47, 0.735) + Nd_2O_3 (6.16, 0.422) + the unmeasured estimated as 1/3 of the measured (calculated as Eu_2O_3: 6.66, 0.436).

Figure 1

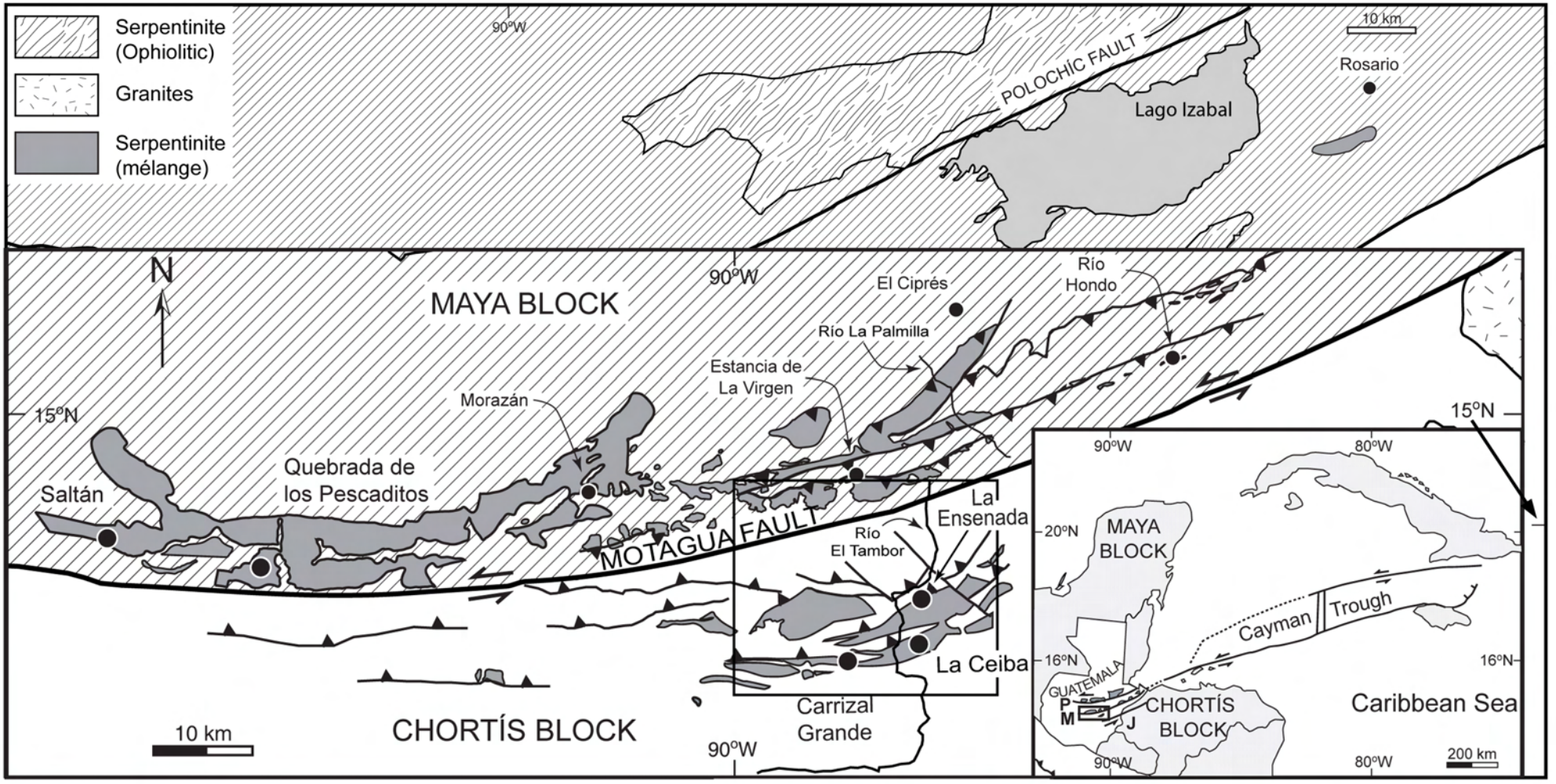
Serpentinite (Ophiolitic)
Granites
Serpentinite (mélange)
90°W
10 km
Rosario
POLOCHÍC FAULT
Lago Izabal
N
MAYA BLOCK
90°W
El Ciprés
Río Hondo
Río La Palmilla
Estancia de La Virgen
Morazán
15°N
15°N
Quebrada de los Pescaditos
Saltán
MOTAGUA FAULT
La Ensenada
Río El Tambor
La Ceiba
Carrizal Grande
CHORTÍS BLOCK
10 km
90°W
90°W
80°W
20°N
MAYA BLOCK
Cayman
Trough
16°N
16°N
GUATEMALA
P
M
J
CHORTÍS BLOCK
Caribbean Sea
90°W
80°W
200 km

Figure 2

Figure 3

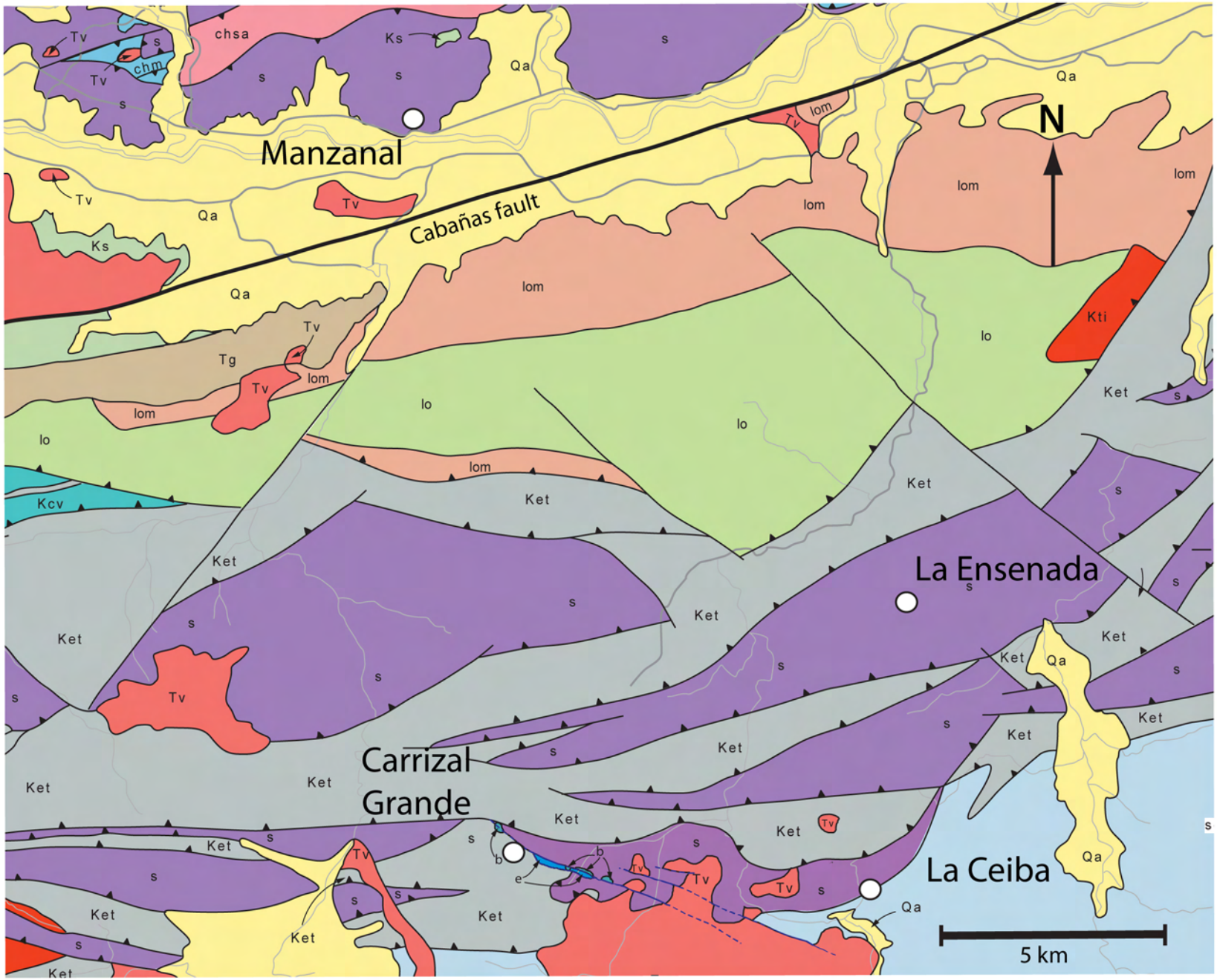
Manzanal
Cabañas fault
N
La Ensenada
Carrizal Grande
La Ceiba
5 km
14º50´
90º00´
89º45´
Tv
chm
chsa
Ks
Qa
Tg
lom
lo
Kcv
Kti
Ket
s
b
e

Figure 4

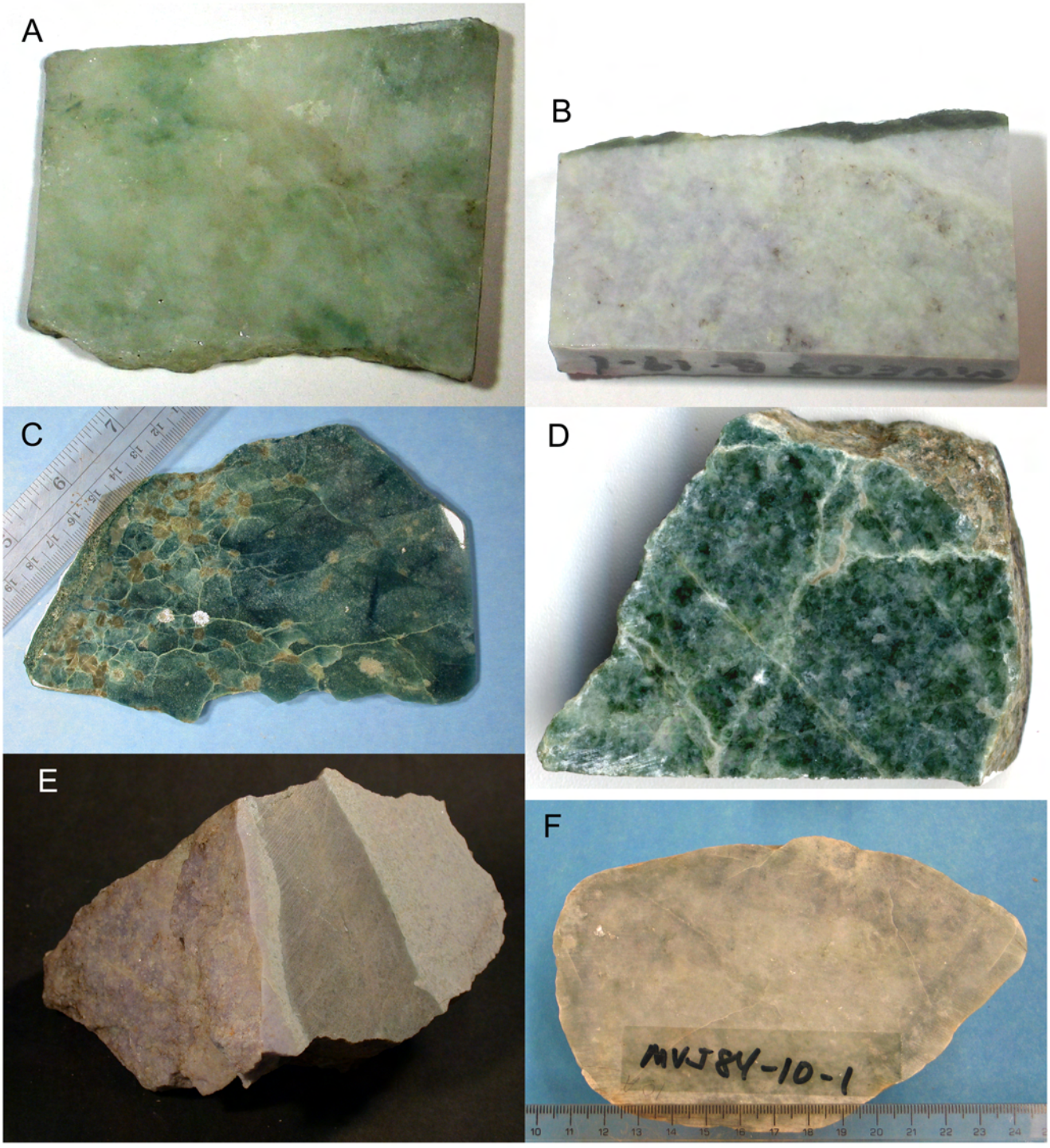

Figure 5 contin.

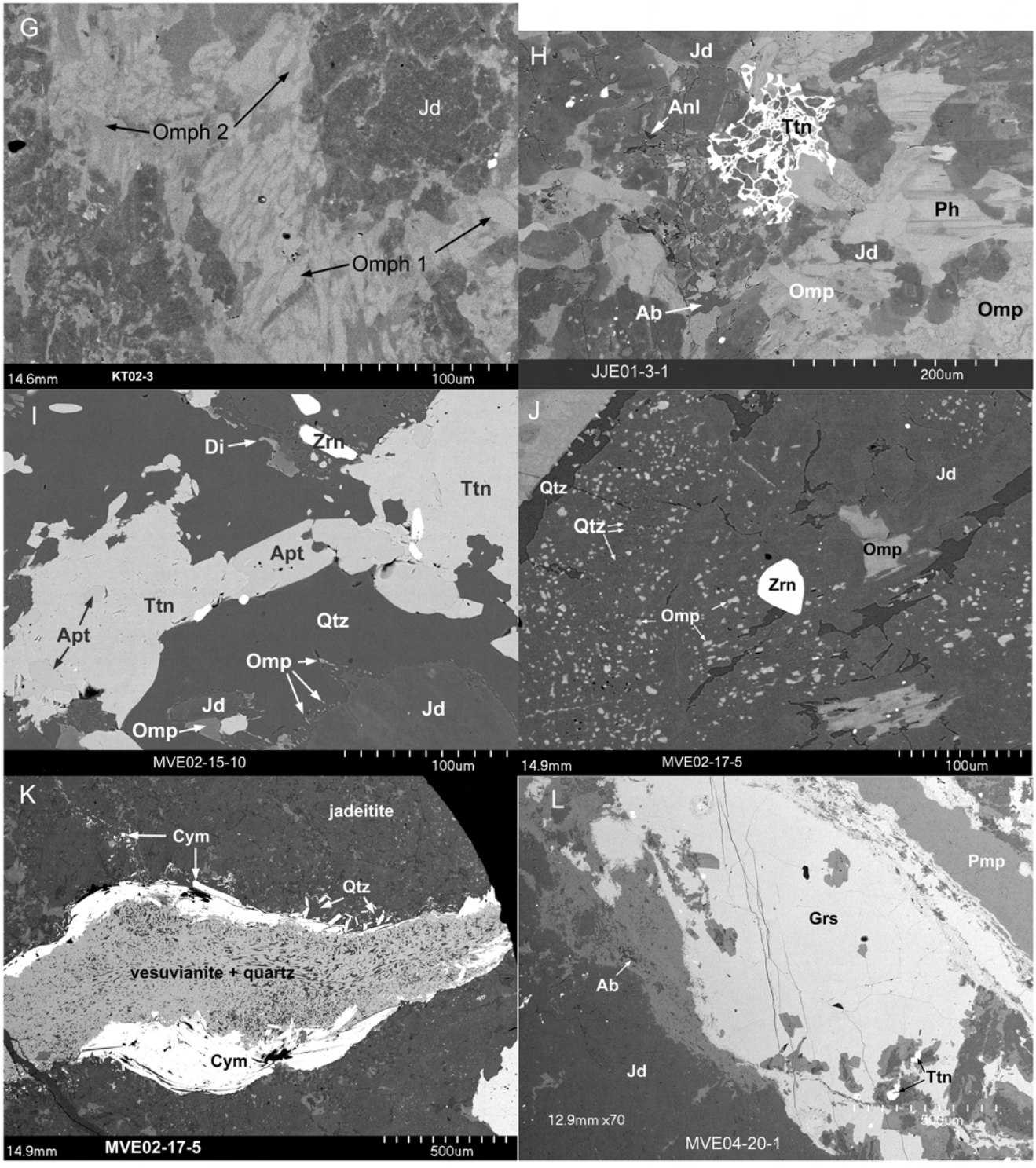

Figure 5 contin.

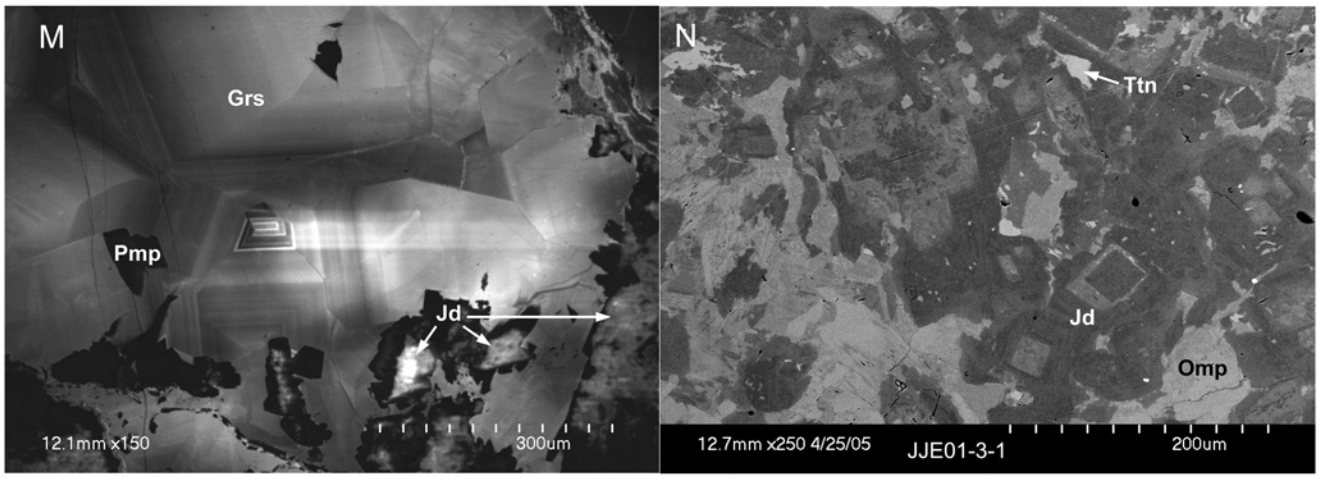

Figure 5

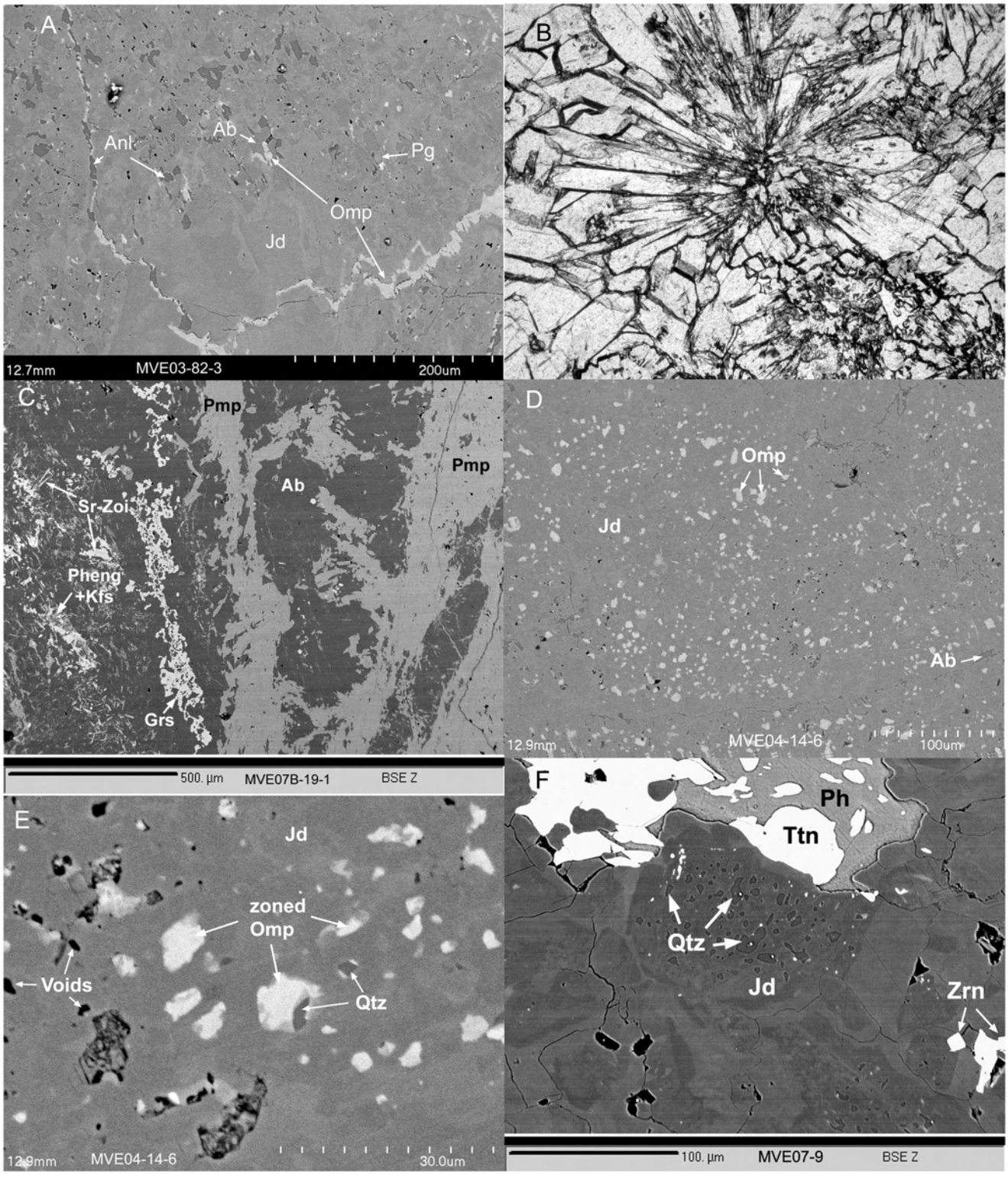
A
Anl
Ab
Pg
Omp
Jd
12.7mm
MVE03-82-3
200um
B
C
Pmp
Pmp
Ab
Sr-Zoi
Pheng
+Kfs
Grs
500. µm
MVE07B-19-1
BSE Z
D
Omp
Jd
Ab
12.9mm
MVE04-14-6
100um
E
Jd
zoned
Omp
Voids
Qtz
12.9mm
MVE04-14-6
30.0um
F
Ph
Ttn
Qtz
Jd
Zrn
100. µm
MVE07-9
BSE Z

Figure 6a1

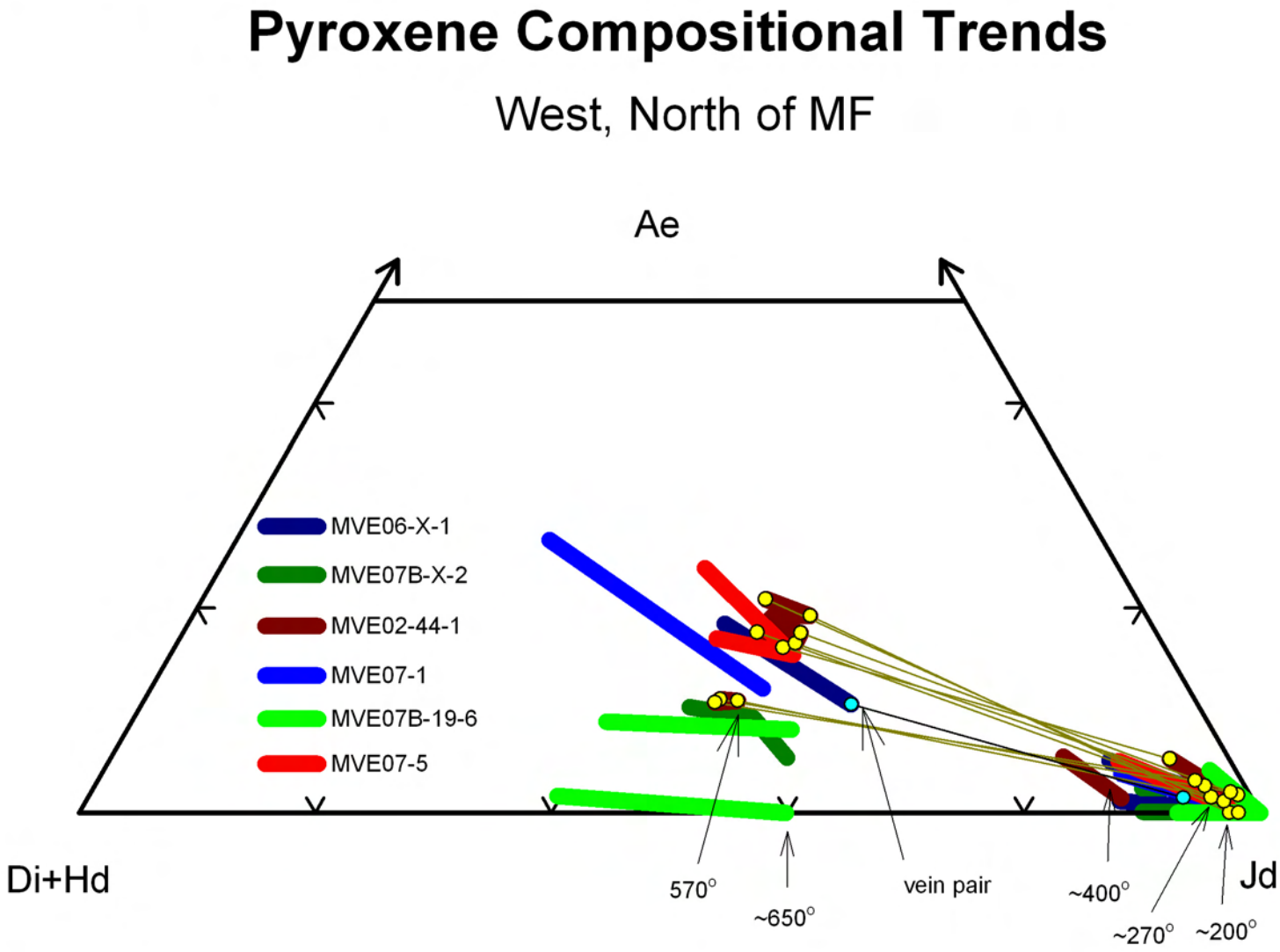
Pyroxene Compositional Trends
West, North of MF
Ae
MVE06-X-1
MVE07B-X-2
MVE02-44-1
MVE07-1
MVE07B-19-6
MVE07-5
Di+Hd
Jd
570°
~650°
vein pair
~400°
~270°
~200°

Figure 6a2

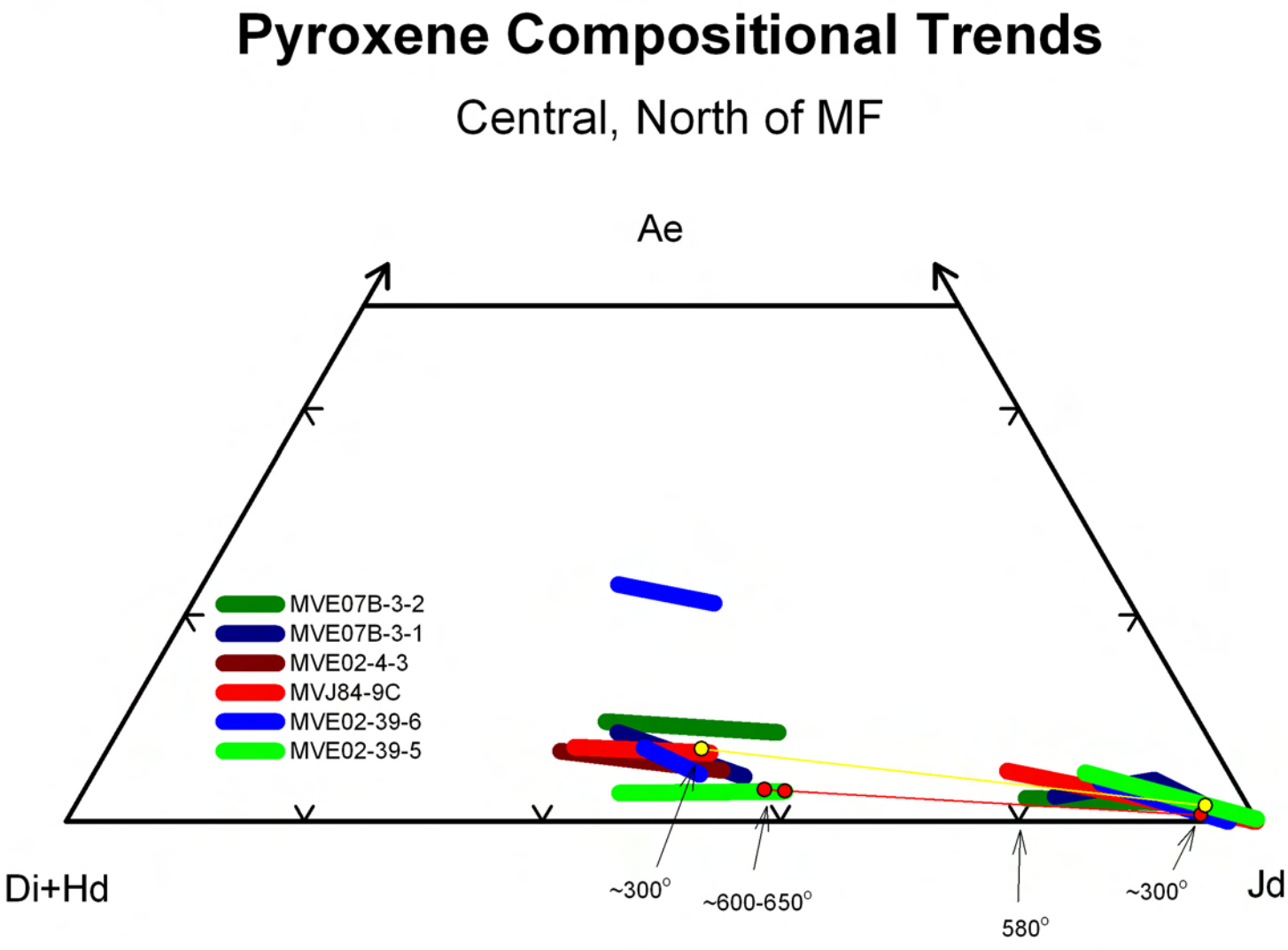
Pyroxene Compositional Trends
Central, North of MF
Ae
MVE07B-3-2
MVE07B-3-1
MVE02-4-3
MVJ84-9C
MVE02-39-6
MVE02-39-5
Di+Hd
~300°
~600-650°
580°
~300°
Jd

Figure 6a3

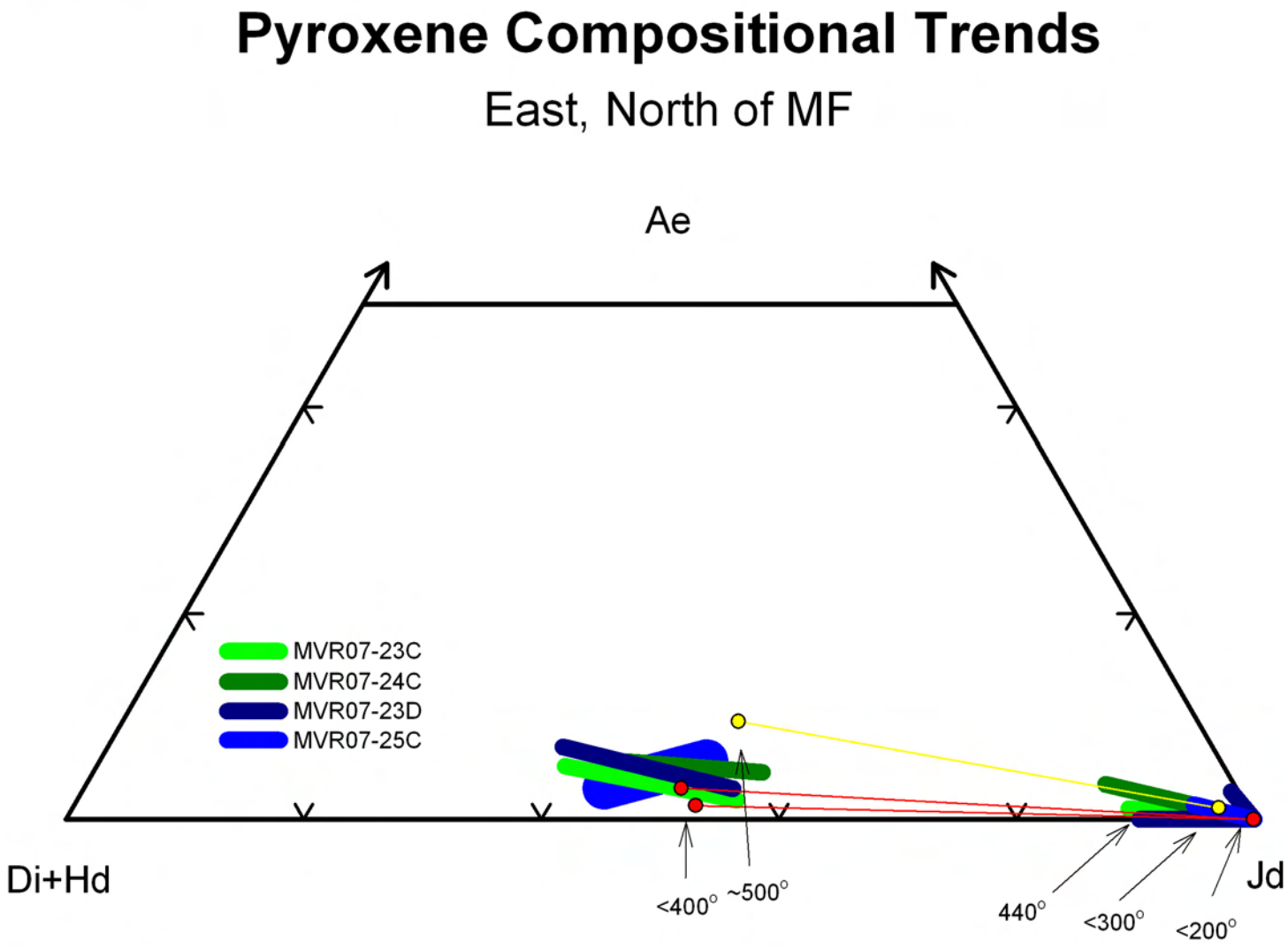
Pyroxene Compositional Trends
East, North of MF
Ae
MVR07-23C
MVR07-24C
MVR07-23D
MVR07-25C
Di+Hd
Jd
<400°
~500°
440°
<300°
<200°

Figure 6B1

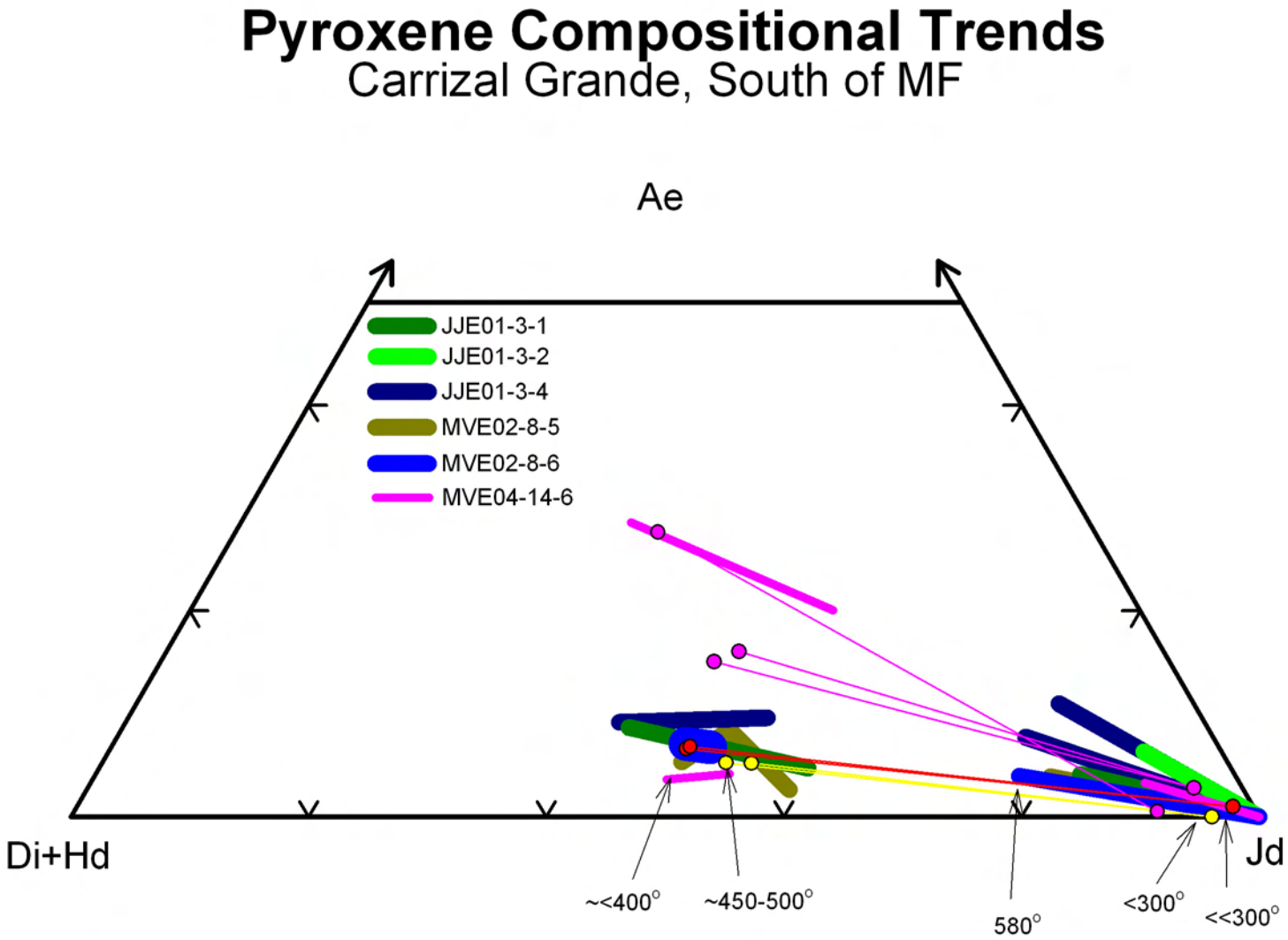
Pyroxene Compositional Trends
Carrizal Grande, South of MF
Ae
JJE01-3-1
JJE01-3-2
JJE01-3-4
MVE02-8-5
MVE02-8-6
MVE04-14-6
Di+Hd
Jd
~<400°
~450-500°
580°
<300°
<<300°

Figure 6B2

Pyroxene Compositional Trends

La Ceiba, South of MF

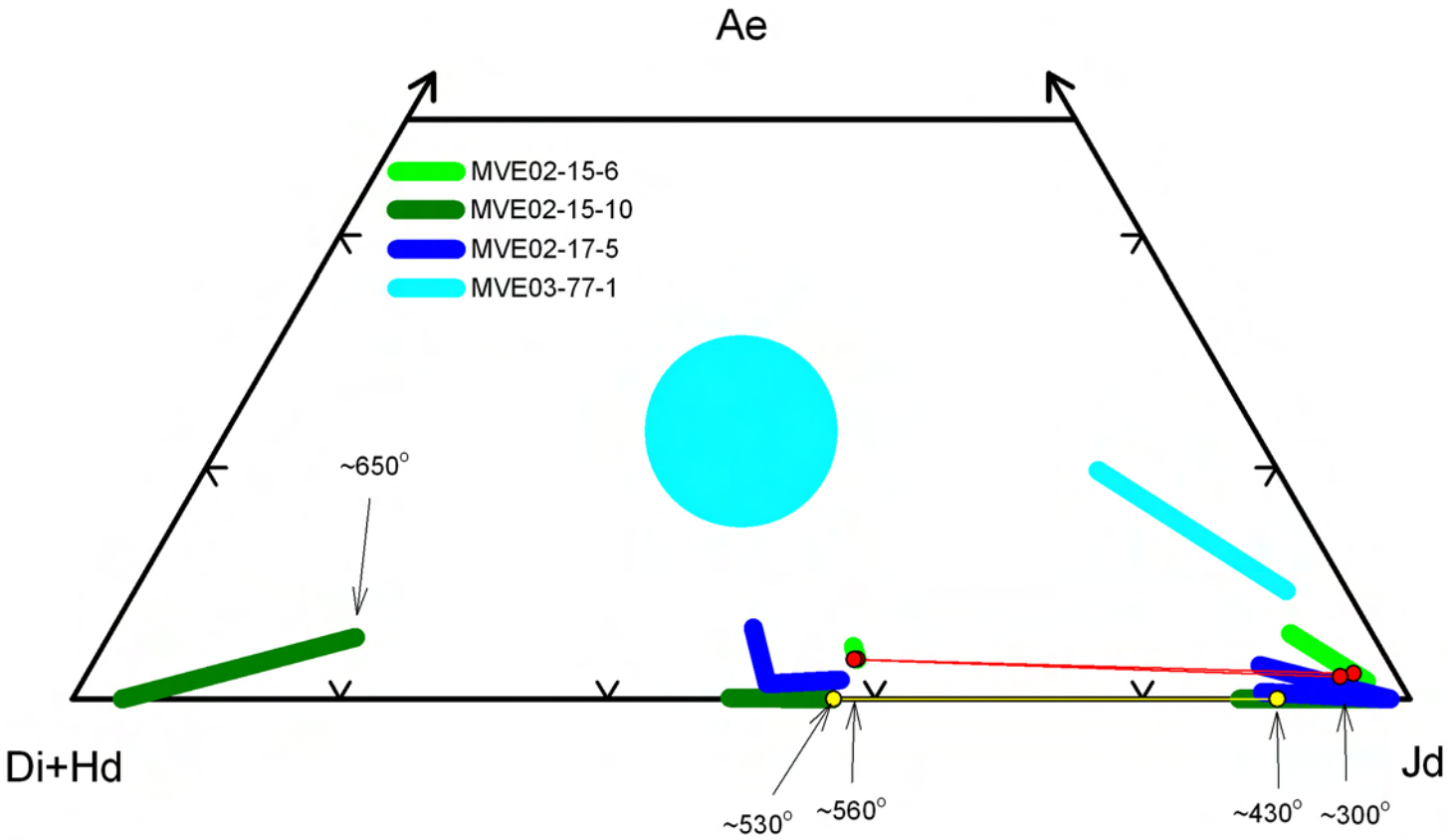

Figure 6B3

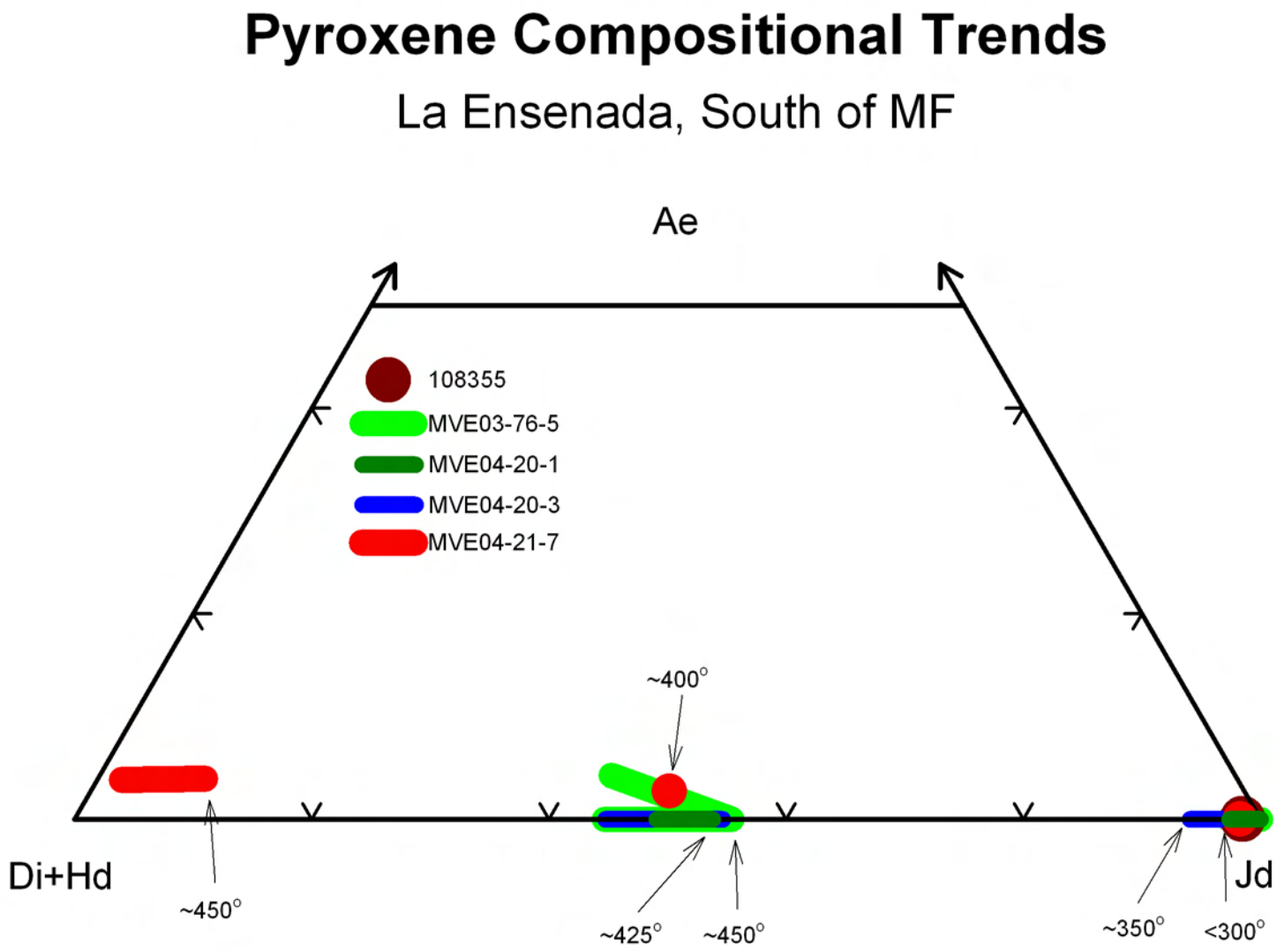
Pyroxene Compositional Trends
La Ensenada, South of MF
Ae
108355
MVE03-76-5
MVE04-20-1
MVE04-20-3
MVE04-21-7
~400°
Di+Hd
~450°
~425°
~450°
~350°
<300°
Jd

Figure 7

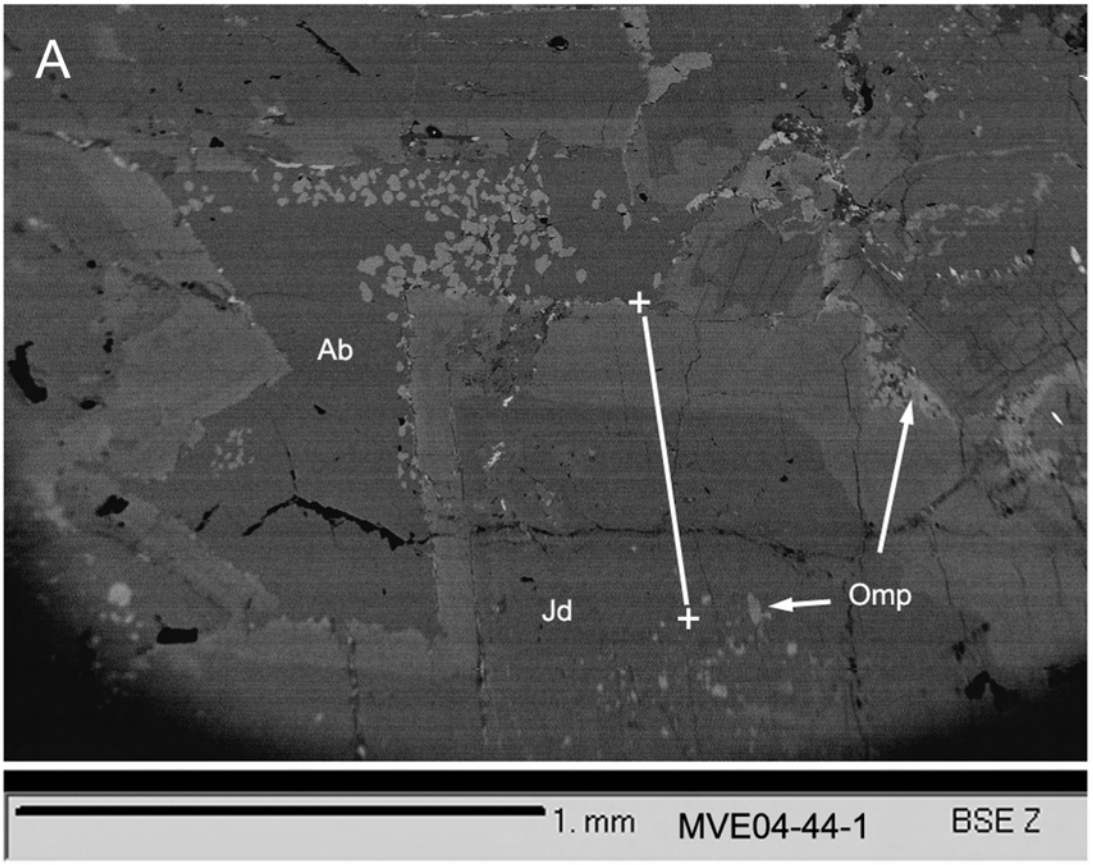
A
Ab
Jd
Omp
1. mm
MVE04-44-1
BSE Z

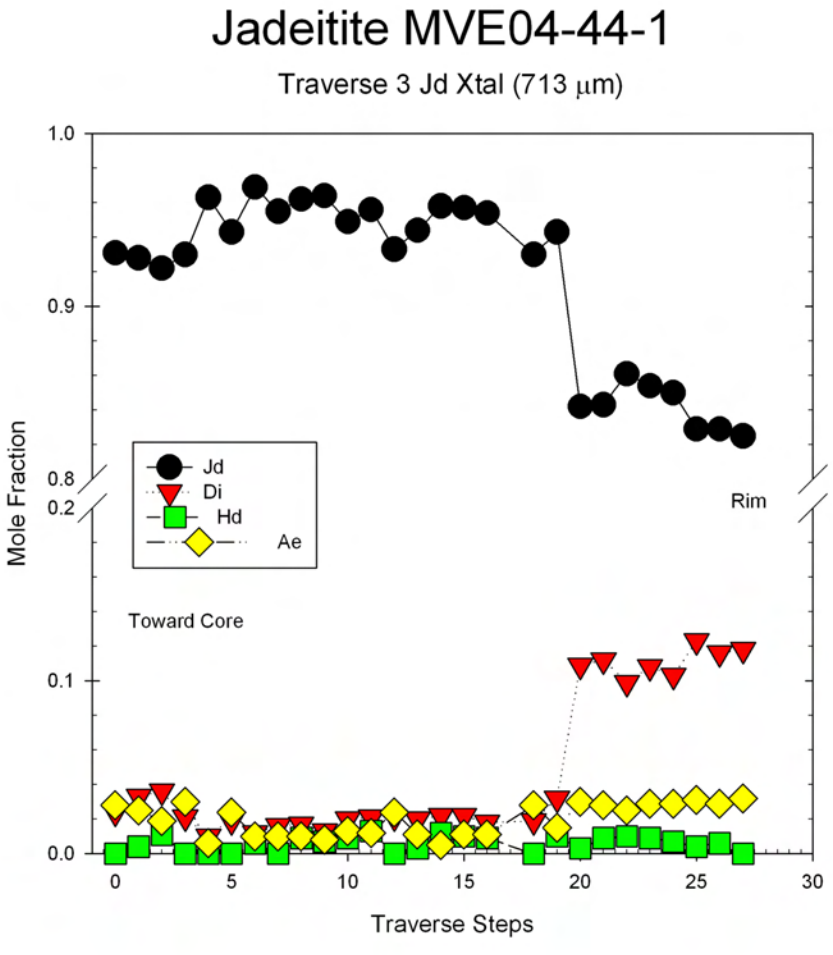
Jadeitite MVE04-44-1
Traverse 3 Jd Xtal (713 μm)
Mole Fraction
Traverse Steps
Jd
Di
Hd
Ae
Rim
Toward Core
1.0
0.9
0.8
0.2
0.1
0.0
0
5
10
15
20
25
30

Figure 7 (contin.)

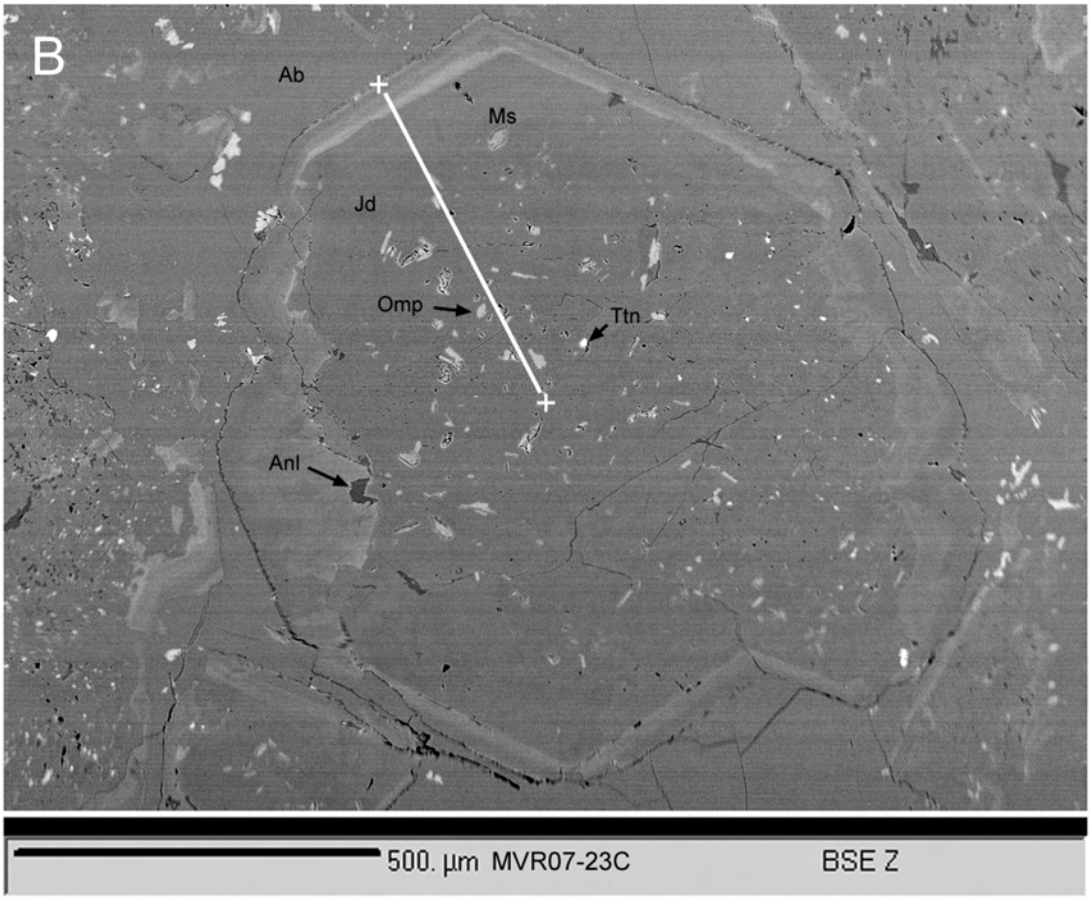

Jadeitite MVR07-23C

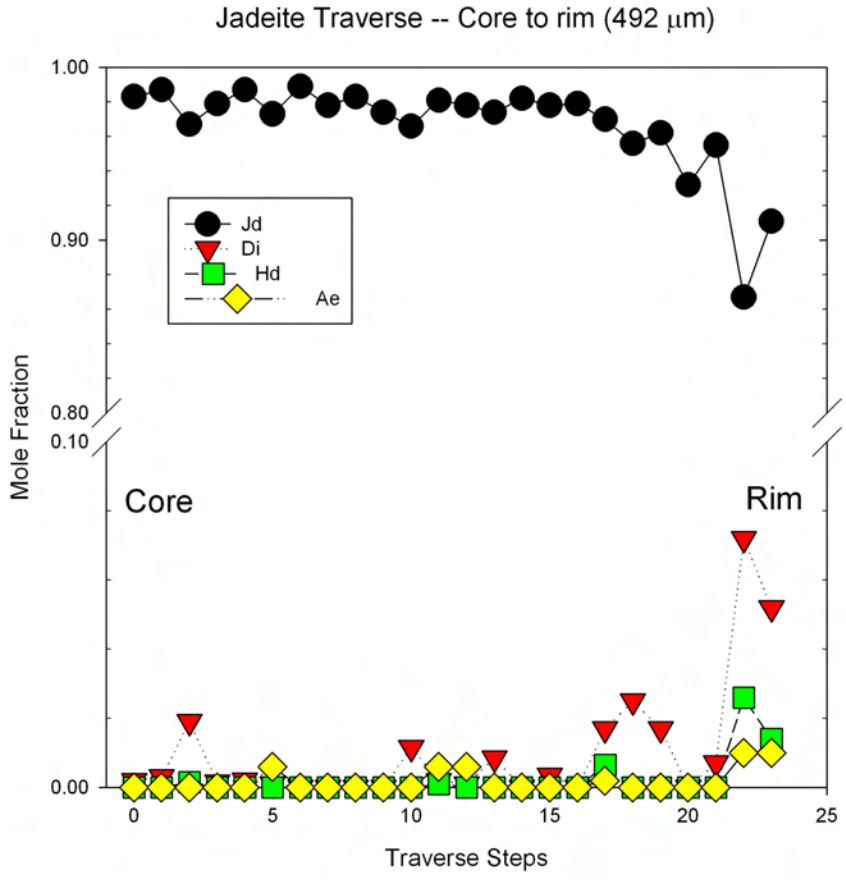

Figure 7 (contin.)

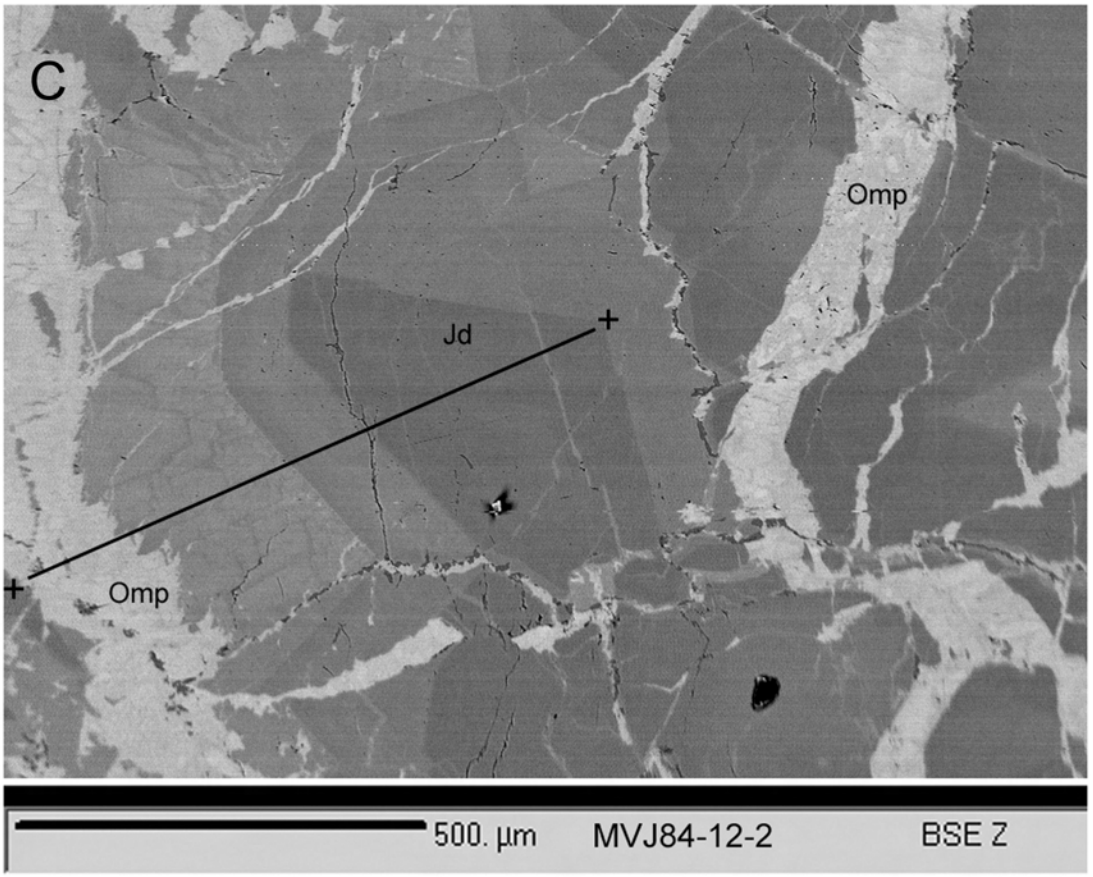

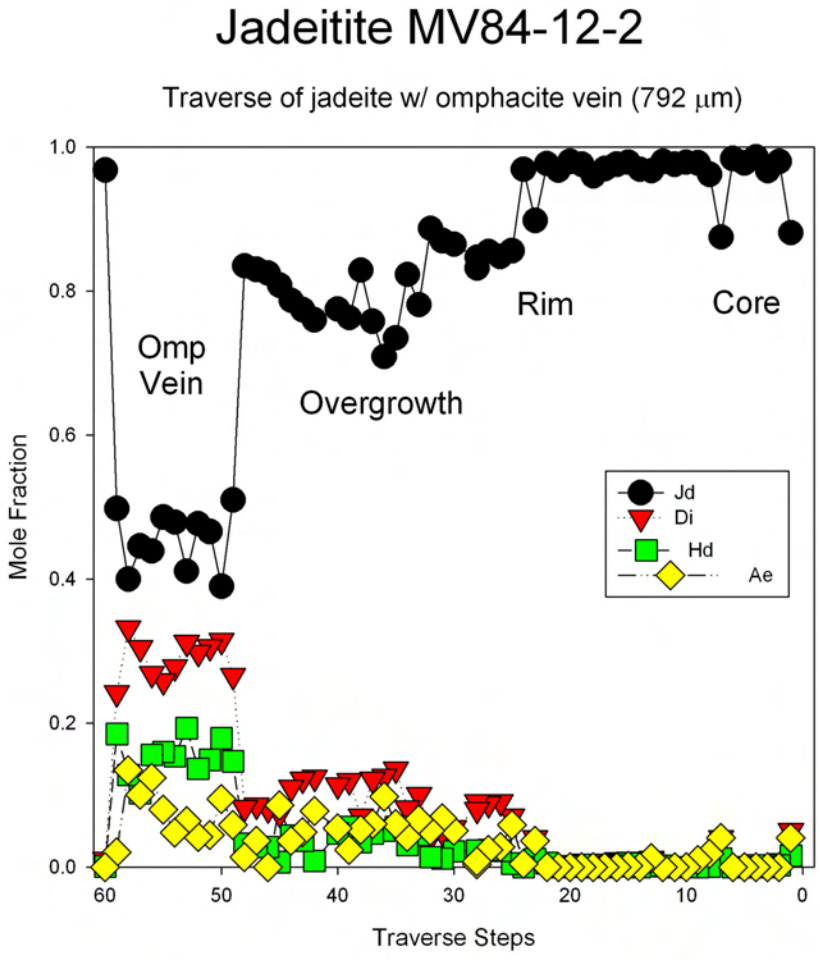

Figure 7 (contin.)

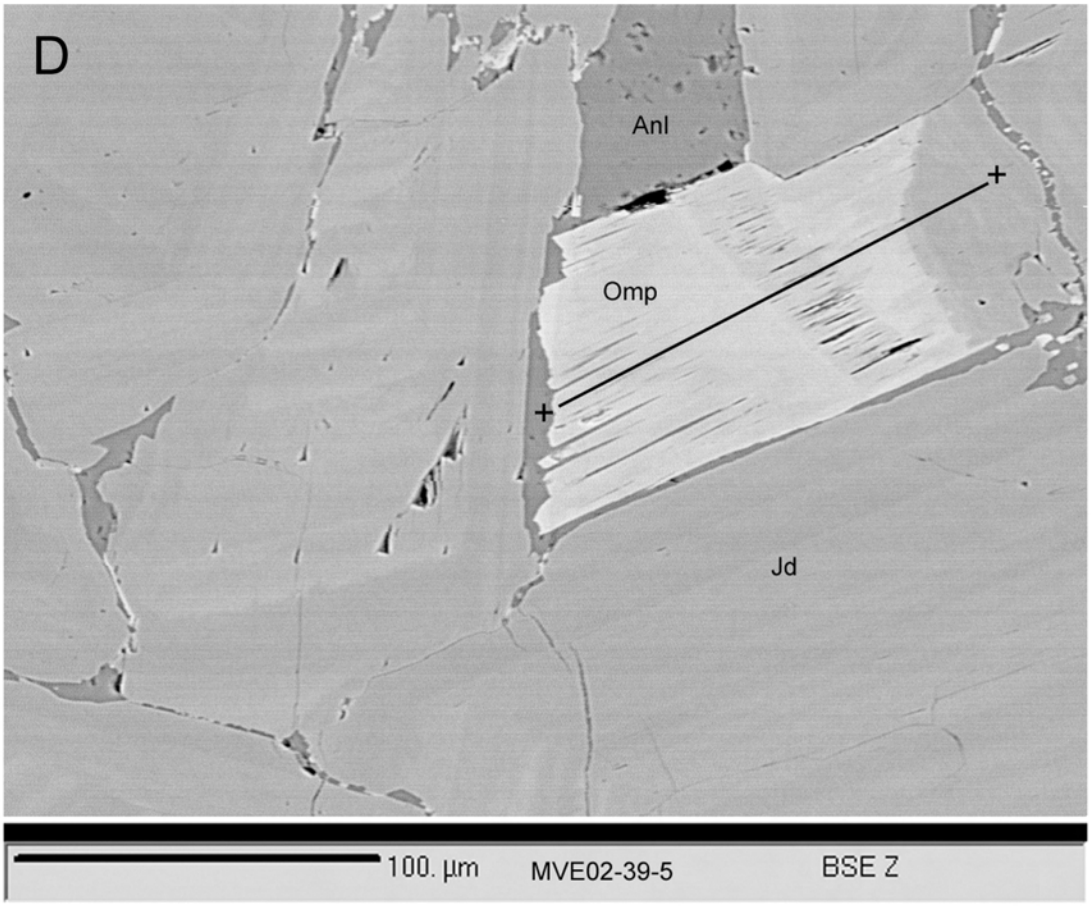

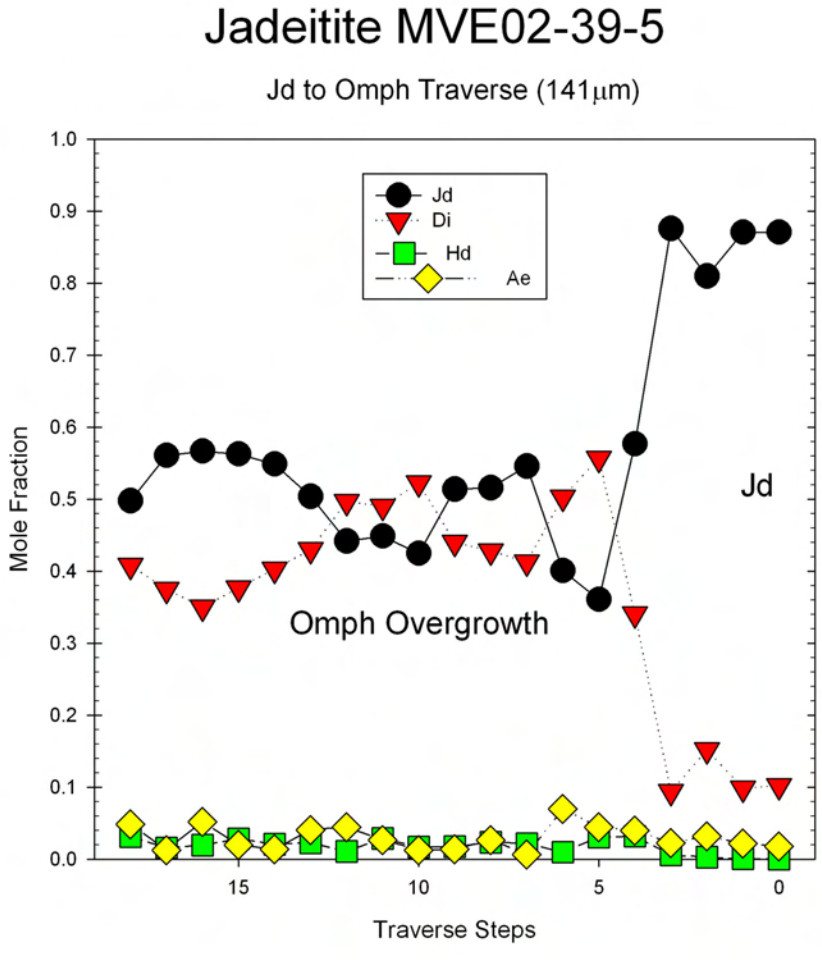

Figure 7 (contin.)

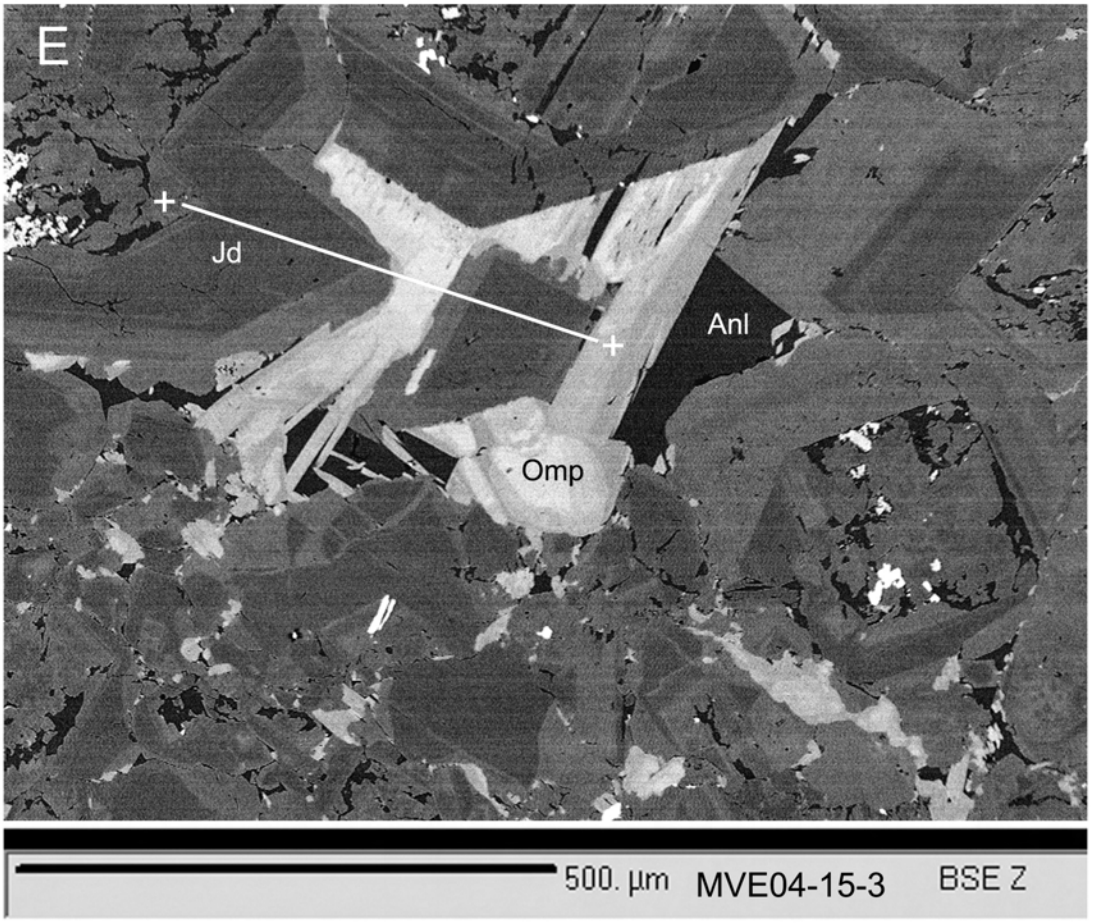

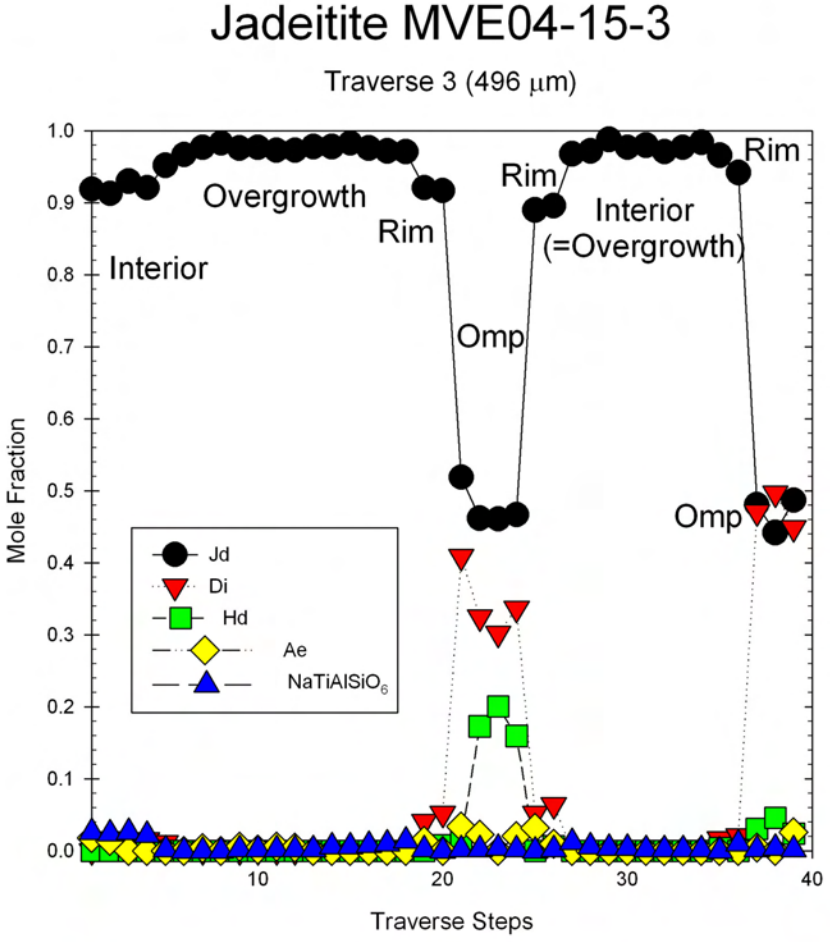

Figure 8

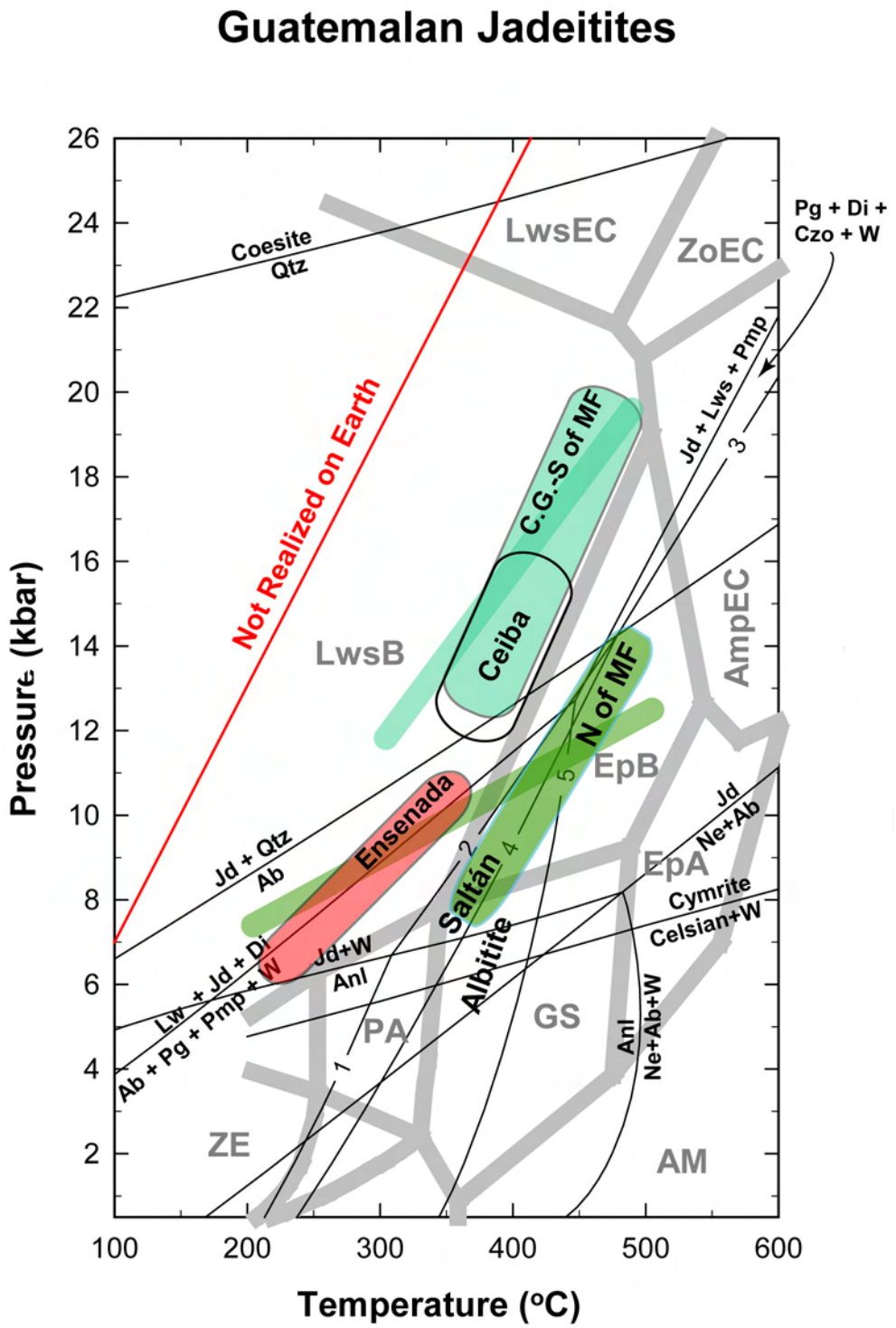
Guatemalan Jadeitites
Pressure (kbar)
Temperature (°C)
26
24
22
20
18
16
14
12
10
8
6
4
2
100
200
300
400
500
600
Coesite
Qtz
Not Realized on Earth
LwsEC
ZoEC
Pg + Di +
Czo + W
Jd + Lws + Pmp
3
C.G.-S of MF
Ceiba
LwsB
AmpEC
N of MF
EpB
5
Ensenada
Jd + Qtz
Ab
Jd
Ne+Ab
Saltán
2
4
EpA
Cymrite
Celsian+W
Albitite
Lw + Jd + Di
Ab + Pg + Pmp + W
Jd+W
Anl
PA
GS
Anl
Ne+Ab+W
1
ZE
AM